Applications of brewster angle microscopy to adsorbed species at the air/water interface

Allison Jane Wigman

Applications of Brewster Angle Microscopy to Adsorbed Species at the Air/Water Interface.

Allison Jane Wigman

Department of Chemistry,

University of Durham,

Durham.

Submitted in partial fulfilment of the requirements for the degree of Doctor of Philosophy, University of Durham.

May 2000.

TABLE OF CONTENTS

List of Figures.

List of Tables.

ABSTRACT

This thesis describes the design and construction of a Brewster Angle Microscope (BAM) to investigate monolayer films at the air/water interface.

A Schiff base coordination polymer, Cu(II) 5,5'–methylenebis(N-hexadecyl-salicylideneamine (poly(CuMBSH)), was initially investigated using the BAM equipment. This material is being developed as the active material in vapour sensing devices produced by the Langmuir Blodgett (LB) method. Transfer of the monomer (MBSH) to the substrate was found to be poor but poly(CuMBSH) had a good deposition ratio (>0.95). The film was polymerised at the air/water interface by injecting a solution of Cu(II) ions into the subphase. BAM was able to record the polymerisation of MBSH to poly(CuMBSH) in real time. Qualitative image analysis indicates a reordering of the material at the interface and a decrease in film thickness. The technique of BAM clearly displays the change in structure between the monomer film and the polymer film and that the poly(CuMBSH) film is homogenous at the micron level.

Poly(para-phenylenevinylenes) PPV derivatives are presently being examined as potential LED devices. One method used to produce such devices is the LB method. BAM was used to investigate ordering of the monolayer prior to deposition. Results by the Physics and Engineering department indicated that if subphase contained water that had been left to stand for several days film transfer was improved. A range of BAM experiments were conducted with varying subphases to determine the cause of this effect.

A new technique of determining the surface excess concentration was developed in this work which is known as Brewster Reflectivity (BAR). The reflectivity of simple surfactants; sodium dodecylbenzenesulfonate, Cetyltrimethylammonium bromide, tetradecyltrimethylammonium bromide and dodecyltrimethyl-ammonium bromide at concentrations above and below the critical micelle concentration (CMC) were correlated to surface excess. This is a new, simple, non-invasive method for probing the surface excess using intrinsic properties of the system.

DECLARATION

The work described in this thesis was carried out in the Chemistry Department of the University of Durham between October 1995 and September 1998. This thesis is the work of the author except where acknowledged by reference and has not been submitted for any other degree.

STATEMENT OF COPYRIGHT

ACKNOWLEDGEMENTS

There are so many people to thank for their help in this work, friends old and new whose help has made this thesis possible. I can only name a few people here but I can honestly say that everyone was very supportive.

Of course I am very grateful to my supervisor, Dr Andy Beeby, for the great food, amusing stories and the wise words of wisdom. You still have to tell me who that person was?!

I am indebted to the Beebettes of lab CG7; Claire, Catherine, Ian (the honorary woman) and Allison for their patience, laughter, chocolate and letting me ask all those daft questions!

My thanks goes to the technical staff of Durham; Joe, Bill, Ray, Gordon, Neil and Jim for their excellent work and always finding a supply of materials for me! Likewise to Simon for the CMC dye work and the secret stash of Twirl bars!

To the folks at Bristol; Dr Julian Eastoe, James and Esther were very helpful both in and out of the lab during my visits - thanks. I am grateful to Professor Michael Petty & Dr Ifor Samuel for the samples and the advice. Also to Jason Wilde for the poetry and beer during the Asilomar conference!

I have been incredibly lucky to have had funny, long-suffering and caring housemates during my time in Durham; John "Plughole" Naylor, Emma "Do I need a passport for Scotland?" Stubbs, Michelle "Sheepy" Felton, Claire "Thank you again!" Stanley, Pete "Chef" Devasagayam, Catherine "Mackham" Barret, Allison "Library" Jones, Susan "Mountaineer" Campbell, Andy "Crewe" Brown, Carrie "Sleeping" Allison, Terry "Smelly meat" Finn. The credit goes to you for surviving!

Yet again I must thank Allison again for ferrying me around after I broke my leg, I know I wasn't the easiest of patients!! Dave, Allison, Michelle, Simon, The Steely and Claire - I really appreciated all those walks and caving trips, next time *I* want the bacon sandwich in bed though! Susan my sincere apologies for

technical ascent of Great Gable, I hope that one day you will recover! Many thanks to Woodsy for the excellent cooking, fine wine, music and adding a little culture!

This list of acknowledgements would not be complete without thanking my parents for their unending support. Also to Jessica, Ian and Christina for their continued friendship. I mustn't forget Wendy "Nappy" Coppenrath, Trevor "Wee? Sporran" Babbs, Frédéric "I don't believe it" Lanoë and Dorotheé "Zee little French" Davenet for not "squeezing" me whilst writing up and working.

Chapter 1 INTRODUCTION

Thin films are ubiquitous and can be found in applications ranging from engine lubricants to the layers of phospholipid on the eye. Detailed studies of the structures of thin films and their uses have only been realised this century and their potential applications have yet to be fully achieved. The first recorded study of a thin film was by Benjamin Franklin in 1774.[1] He dropped a teaspoon of olive oil onto the surface of Clapham Common pond and noticed that it calmed the water and spread out "perhaps half an acre," simple calculations show this film to be one molecule thick. After this experiment he carried a small amount oil in the upper hollow joint of his bamboo cane so that he could repeat the experiment whenever the opportunity arose, a true scientist!

Many sailors had noted the calming effect of oil on stormy water, during the later half of the nineteenth century there was much discussion as to whether ships should carry oil to pour overboard. The oil spreads out across the surface to form a thin film over a large area which has the effect of damping the waves. John Shields attempted to get a patent for his design that would spread oil from valves at harbour entrances and performed trials in Aberdeen harbour.[2]

More recently fatty acids (e.g. cetyl alcohol) have been spread across reservoirs and have been shown to reduce evaporation by up to 40%.[3] The insoluble condensed monolayers are enclosed within floats and are physically self-healing in order to maintain full surface coverage. They allow oxygen to diffuse through the water surface which enables aquatic life to function as normal and being natural products they cause no known environmental damage.

Just over a hundred years after the Clapham pond experiment the studies of thin films began to gain momentum. Gibbs published his analysis of thermodynamics of adsorption and surface tension in 1878. At the same time Lord Rayleigh was studying the motion of waves and during his experiments he noted that contamination from soap had a marked effect on the motion of water jets. It was the fatty acid in the soap that caused the calming effect, he then

went on to study these materials. Although we take it for granted that, given sufficient area, a film of oil will spread out to form a monomolecular layer (a monolayer) this was a point of some dispute among scientists at that time. Such studies at the time were at the forefront of knowledge as atoms and molecules were a new concept and the molecular dimensions were unknown. Rayleigh was convinced that the films were monolayers but he had not devised an experiment that would prove his theories, that was until January 12, 1891 when he received a letter from Agnes Pockels. She had performed surface experiments on her kitchen table using "homely appliances." She simply used a tin trough filled to the brim with water and used another strip of tin to compress the film by scraping it across the surface and a button to measure the surface pressure! Rayleigh then sent the letter to Nature which they published in 1891.[4] Agnes Pockels was the first to publish pressure-area isotherms which are so familiar to surfactant scientists today, she was also the first person to introduce the method of depositing a film on the surface by dissolving the material of interest into a spreading solvent, this allows an even distribution of the material across the surface and is discussed in section 1.2.

At the turn of the century Irving Langmuir was working for the General Electric Research Laboratory in New York, where he studied the electrical properties of gases as well as surface science. Langmuir was the first person to transfer monolayer films from the air/liquid interface on to solid substrates. In 1915 he published his theory of the adsorption thin films, many of these concepts, both theoretical and experimental, have stood up to the test of time and are still in use today. In 1932 he was rewarded with the Nobel Prize for his contribution to surface science.

Katharine Blodgett joined General Electric in 1919, the first woman to join their research staff and the first woman to obtain a doctorate from the Cavendish Laboratory, Cambridge.[2,5] She worked with Langmuir looking at the deposition of multilayer films of fatty acids on to solid substrates. Films deposited by the methods developed by Blodgett are known as Langmuir-Blodgett (LB) films (see section 1.2) these are used to produce materials for use in gas sensors,[6] light emitting diodes[7] and a variety of other state of the art electronic devices.[8]

It was in the 1970's that Hans Kuhn studied energy transfer in multilayers systems with a view to positioning molecules and creating efficient electronic devices. His group was able to show that stable LB films with sufficiently few defects could be produced allowing applications in everyday electronics. [9]

The content of this thesis is concerned with the investigation of thin films oriented at the air/water interface using the technique of Brewster Angle Microscopy (BAM). This is described in detail in chapters 2 and 3. BAM is in principle a simple technique, the incident light approaches the surface at the Brewster angle of the clean (free from surface active materials) subphase. This results in a minimum of the intensity of the reflected light from the surface. A material with a different refractive index to that of the subphase will therefore reflect light as its Brewster angle is different. This reflected light can be magnified and then imaged using a CCD camera. The images observed consist of bright regions which correspond to areas of material on the subphase. These are seen due to their contrast with the low reflectivity (dark background) of the subphase. The images reveal structure of the film on a macroscopic (micron) scale. The technique is sensitive to film thickness and to the orientation of groups of molecules at the interface. Quantitative analyses of BAM images are currently under investigation.[10,11] Using BAM, impurities are not introduced to the interface, unlike fluorescence microscopy. All that is required of the material of interest is that it has a different refractive index to that of the subphase.

The study of thin films at the air/liquid interface is important in ascertaining the physical orientations of many known groups of surface active chemicals. For example, simple biological membranes can be effectively modelled in 2 dimensions using various techniques to give a better understanding of interactions occurring in the body.[12,13]

The industrial applications of LB films are well documented, these typically include biosensors[14] and other electronic devices as mentioned above. Efficient devices require that the molecules are well aligned throughout the film. It is generally accepted that the layers deposited on to the substrate retain the structure of the monolayer.[9] Therefore the study of LB film forming materials at

the air/liquid interface is essential in optimising the alignment within the monolayer in order to produce high quality LB films.

1.1 THEORY OF MONOLAYERS

The materials described in the above experiments are oriented at the air/liquid interface and are known as surfactants, (***surf***ace ***act***ive ***a***ge***nts***) the oldest known surfactant is soap. The surfactant must be amphiphilic, that is the molecule will have a hydrophobic (Greek for water fearing) region and hydrophilic (water loving) region. Alkyl carboxylic acids are widely studied materials at the air/water interface but a certain length of chain is required for the surfactant to be insoluble, the hydrophobic hydrocarbon chain has to be greater than 12 carbons in length otherwise it is dragged into the subphase by the hydrophilic –COOH headgroup.[2,9]

A Langmuir monolayer is a sheet of amphiphiles one molecule thick, the head groups are locked in the aqueous subphase and the hydrophobic tails are directed into the other phase that is usually air. Other interfaces are important but they are more difficult to study. Another type of monolayer that is often discussed is the Gibbs monolayer, the only difference between the two types of film is the solubility of the amphiphile.[2] A Langmuir monolayer is formed from insoluble materials and so they can be compressed and a pressure-area isotherm is recorded. However in a Gibbs film molecules move freely between the surface and the bulk and the surfactants can dissolve and pass under the compression barrier when the surface is compressed, therefore pressure-area isotherms cannot be used to study Gibbs films. Methods such as ellipsometry,[15] neutron reflectivity,[16] X-ray scattering[17] or the new technique discussed in chapter 6 must be used to study Gibbs monolayers.

Unsaturated fatty acids are the building blocks of phospholipids which appear in many biological systems, such as cell membranes, hence they have been widely studied.[18] The fluid coating the lungs contain the surfactants dipalmitoylphosphatidylcholine (DPPC) and palmitic acid which stop the lungs from collapsing on breathing out. Premature babies are often born without

these surfactants, this is known as respiratory distress syndrome (RDS). Lung surfactants have been studied using fluorescence and Brewster Angle Microscopy to understand their behaviour and develop synthetic compounds that mimic this behaviour.[12,19]

1.1.1 The Interface.

In the liquid phase molecules are subjected to short range forces of attraction, in the bulk phase the molecules are attracted in all direction to approximately the same degree. However at the interface there in a net pull into the bulk, therefore a surface has a tendency to contract, see Figure 1.1.[20]

Figure 1.1. Forces of attraction in a liquid.

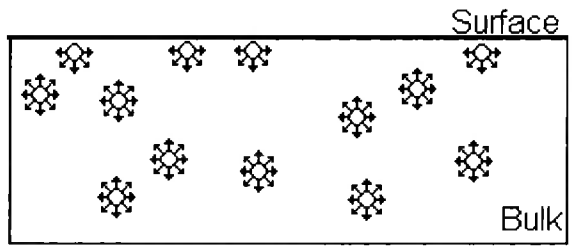

The work required to increase the area of a surface isothermally and reversibly by a unit amount is known as the surface free energy or the surface tension, γ and usually has units of mN/m, the surface tension is a sum of the dispersion (Van der Waals) and hydrogen bonding forces see Equation 1.1.

$$\gamma_0 = \gamma_w^d + \gamma_w^h \qquad \textbf{Equation 1.1}$$

γ_0 = The surface tension of a clean liquid surface,

γ_w^d = dispersion force,

γ_w^h = hydrogen bonding contribution.

When a surfactant is spread at the air/liquid interface the surface tension of the system is changed. The change in the surface tension due to the added surfactant is defined by equation 1.2 below as the surface pressure (Π). However Π is not a pressure in the true physical sense but a change in surface tension.

$$\Pi = \gamma_0 - \gamma = \Delta\gamma \qquad \textbf{Equation 1.2}$$

Π = Surface pressure (mN/m),

γ_0 = Surface tension of the pure subphase (mN/m),

γ = Surface tension of the subphase and the film (mN/m).

Water has a particularly high surface tension (72.8 mN/m) due to the large degree of hydrogen bonding. When surfactant is added to water the amount of hydrogen bonding is reduced and so the surface tension decreases resulting in an increase in the surface pressure (Equation 1.2). The surface pressure can be measured simply using a variety of methods, one of which (the Wilhelmy plate) is described below.

1.1.2 Measuring the Surface Pressure.

Monolayers are studied by spreading the material over a water subphase which is contained in a Langmuir trough, these are discussed in section 3.3. A moveable barrier can be used to decrease the area of the film and the surface pressure increases as the monolayer goes through a gas phase, various liquid phases to a solid phase. The surface pressure is usually measured using a Wilhelmy plate. In its simplest form this consists of a strip of chromatography paper or a platinum plate just touching the film surface suspended from an (electronic) micro-balance, the plate is pulled into the bulk by the surface tension of the subphase.

Figure 1.2 The Wilhelmy Plate.

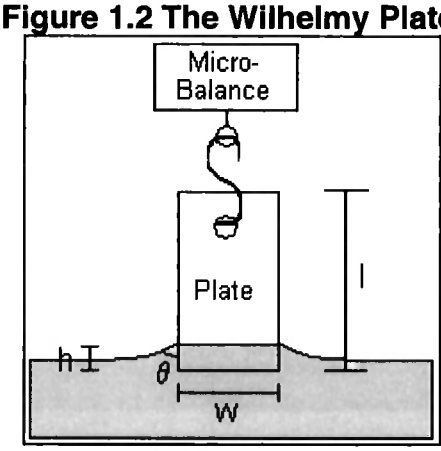

The downwards forces acting on the plate are surface tension and gravity but the buoyancy of the displaced water acts upwards, see equation 1.3.

$$F = \rho_P glwt - \rho_L glwh + 2\gamma(t + w)\cos\theta \qquad \textbf{Equation 1.3}$$

Where:

F = force acting on the plate, g = gravity,
l = length of the plate, w = width of the plate,
t = thickness of the plate, ρ_p = density of the plate,
ρ_L = density of the liquid, θ = the contact angle,
γ = surface tension of the liquid, h = depth the plate is submerged.

The plate is manually lowered until it is just touching the clean subphase and the balance is zeroed before use, this effectively removes the first two terms of equation 1.3. The contact angle is taken to be 90° if the plate is completely wetted. The plate thickness is significantly less than the width of the plate, the plates are usually 1 cm in width, i.e. w>>t, thus equation 1.3 reduces to:[2]

$$\frac{\Delta F}{2w} = \Delta\gamma = \Pi \qquad \textbf{Equation 1.4}$$

Equation 1.4 can then be related to equation 1.2 so that the Wilhelmy balance may be used to measure the surface pressure of a spread film.

1.1.3 Spreading a Monolayer.

A limited number of materials will spontaneously spread over a clean water surface to form a uniform monolayer but the vast majority of materials will not. In order to produce homogeneous films of these materials a solution is prepared in a good spreading solvent such as chloroform. In some cases materials are not soluble in such solvents and then a mixture of solvents are used such as chloroform and methanol.[19] The spreading solvent must be able

to dissolve the material of interest, usually 0.1-1 mg/ml, it must not dissolve into the subphase and it must evaporate fairly rapidly so that it does not interfere with the monolayer but not too rapidly that the concentration cannot be accurately determined. A syringe is generally used to deposit the solution dropwise onto the surface of the subphase, usually this is to sub-monolayer coverage. The ability of the solvent to spread across the surface is determined by the forces of cohesion and adhesion. That is the forces of attraction between the solvent and the subphase (adhesion) have to be greater than that of the solvent/solvent attraction (cohesion).[20]

Figure 1.3 Cohesion and adhesion.

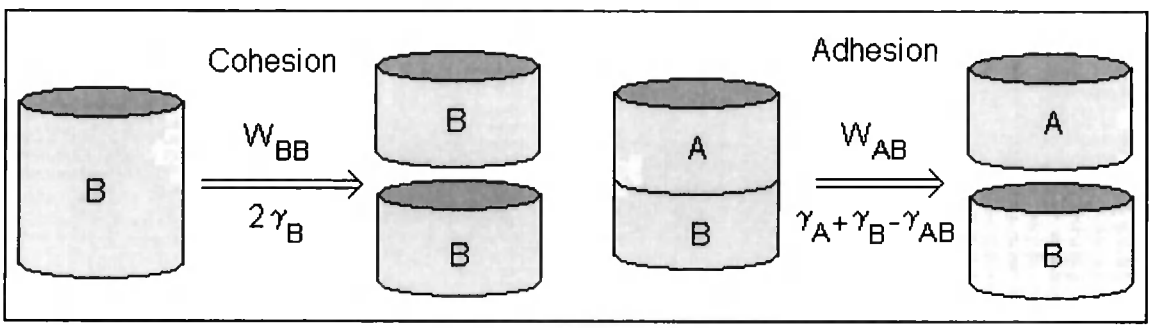

The spreading coefficient is the difference between these forces, see equation 1.5.

$$S_{A/B} = W_{AB} - W_{BB} \qquad \textbf{Equation 1.5}$$

Relating this to the surface tension yields:

$$S_{B/A} = \gamma_A - \gamma_B - \gamma_{AB} \qquad \textbf{Equation 1.6}$$

Where:

$S_{A/B}$ = the spreading coefficient of B over A,

γ_A = the surface tension of A,

γ_B = the surface tension of B,

γ_{AB} = the surface tension of B on A.

If $S_{A/B}$ is positive then there is a decrease in the free energy and spreading will be spontaneous, thus a liquid of low surface tension will spread over one of a high surface tension.

After initial spreading of the monolayer the solvent becomes mutually saturated with the subphase and so the surface tensions change accordingly. See equation 1.7.

$$S_{B(A)/A(B)} = \gamma_{A(B)} - \gamma_{B(A)} - \gamma_{AB} \qquad \textbf{Equation 1.7}$$

Where:

$S_{A(B)/B(A)}$ = the final spreading coefficient,

$\gamma_{A(B)}$ = the surface tension of A when mutually saturated with B,

$\gamma_{B(A)}$ = the surface tension of B, when mutually saturated with A.

For the case of benzene the final spreading coefficient becomes negative and so after rapid spreading it will contract to form small drops, known as lenses, on the water surface. Clusters of the film material are formed and so a homogeneous film is not produced. Care has to be taken in the choice of solvent as some solvents are stabilised by surface active materials such as amylenes (in the case of chloroform) which greatly affects the film formation and surface tension.

1.1.4 Isotherms.

Once a uniform monolayer has been spread it is compressed and a pressure-area isotherm is recorded. This is a plot of surface pressure versus the area per molecule of the surfactant. Such isotherms are analogous to the three-dimensional p-V isotherms as gas, liquid and solid phases are observed.

Figure 1.4 General Isotherm.

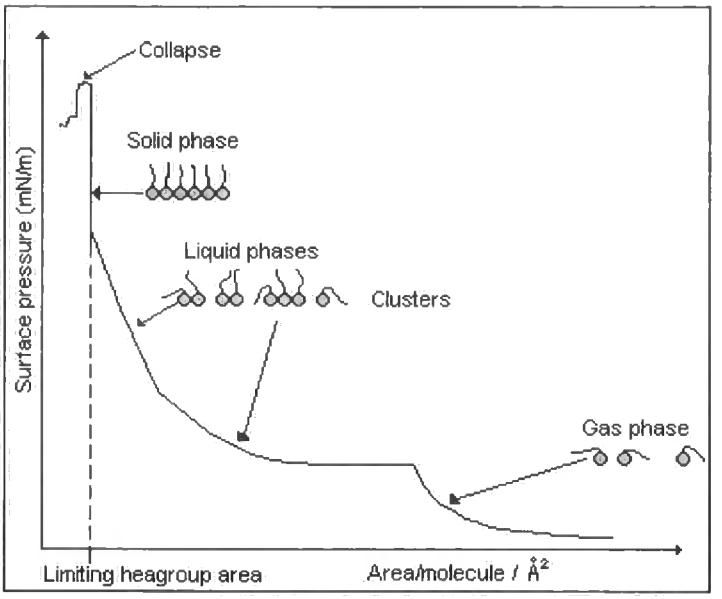

The various phases of the film during compression are observed as a change in gradient of the isotherm, see Figure 1.3. In the gas phase the molecules move independently i.e. Van der Waals' forces are negligible, however the molecules are still anchored by their head groups to the surface and so are not lost into the gas phase. The effective volume of the molecule is that of the tail length as it is lying along the surface. The gas phase occurs at a low surface pressure (<1 mN/m) and so may not be observed by the apparatus. In the limit of very low pressure films a 2D equivalent of the gas law holds, see equation 1.8

$pV = nRT$ Ideal gas law for 3D systems,

$\Pi\left(\frac{A}{nN_A}\right) = kT$ 2D equivalent where nN_A is the total number of molecules at the surface.

$\Pi A' = kT$ Gas law for gaseous films. **Equation 1.8**

Where:

p = pressure (N/m^2), V = volume (m^3),

n = number of moles, R = gas constant,

T = temperature (K), Π = surface pressure (N/m),

A' = area per molecule (m^2), k = Boltzman constant ($J\ mol^{-1}$),

N_A = Avogadro's number (mol^{-1}), A = area of the surface (m^2).

The 2D liquid phase can generally be split into sub-phases (although these are not always observed), the liquid expanded (LE or L_1) and the liquid condensed (LC or L_2) phases. The difference between these two phases is small (as seen with the small phase transition), and is determined by the freedom of motion of the chains which is referred to as the effective volume. In the liquid-expanded phase some part of the hydrocarbon tails may lie along the water surface and this sweeps out the effective volume. There is little interaction between surfactant molecules and they have little effect on the surface tension of the water.[21] In the liquid-condensed phase molecules are closely packed together and the hydrocarbon tails are steeply oriented towards the surface, see Figure 1.3. The gradient of the liquid expanded phase is approximately 10 times lower than that of the liquid condensed phase which means that the compressibility has decreased by a factor of 10. The various monolayer phases that can be observed are shown in the phase diagram in Figure 1.5 below.

Figure 1.5 Pressure - Phase diagram.

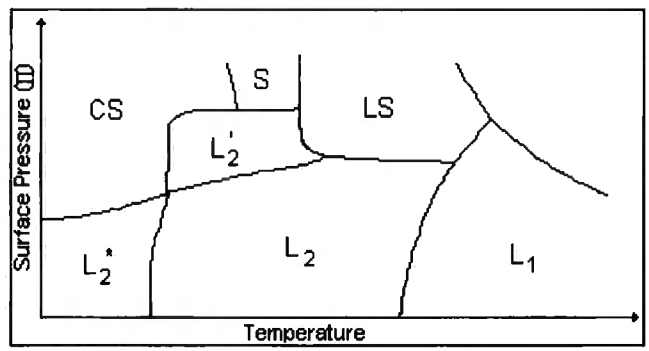

The abbreviations in the above diagram are explained below:

Table 1.1 Liquid crystal phases.

Phase	Properties
L_1	Liquid expanded
L_2	Tilted with respect to the normal but the molecules are free to rotate.
L_2' ⎫ L_2^*	Tilted towards next nearest neighbour
⎭ S^*	Tilted herringbone structure, usually found at high Π and low temperature.

Table 1.2 Liquid crystal phases continued.

LS	The molecules are tilted normal to the surface in a hexagonal unit cell, the chains are free to rotate about their axis.
S	The rotation of the molecules is restricted, the molecules are packed in a rectangular unit cell.
CS	A 2D phase with long range order.

If the monolayer is further compressed after reaching the solid phase, molecules will be ejected from the monolayer and it will collapse. The multilayers formed during the collapse are permanent and the film will not return to form a monolayer when the barrier is opened. The collapse is not usually uniform, there will be large areas of monolayer interspersed with lines of collapsed film. If a tangent is drawn along the solid phase to the x axis the limiting headgroup area can be determined, this is the area that each headgroup occupies on the water surface as shown in Figure 1.3.

If the film is kept below the collapse pressure (π_C) the elasticity of the monolayer can be studied. In the liquid phases long-chain fatty acids can form clusters (also known as islands) on the surface due to the attraction between hydrocarbon chains. This means that the surface pressure remains low and constant at large surface areas and then as the film is compressed the surface pressure rises rapidly due to the clusters being brought together. Hence when the barrier is opened the reverse process occurs and the surface pressure falls rapidly. This behaviour is observed upon recompression of compounds which have formed multilayers on first compression, these compounds do not relax back to their original monolayer state after the film has been allowed to expand,[22] see Figure 1.6.

Figure 1.6 Compression/Expansion Cycles of Films.

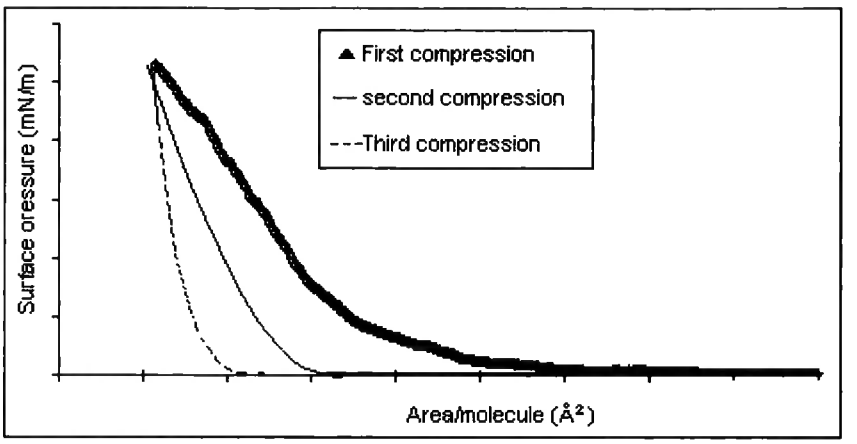

Reda *et al.*[23] studied poly-petptides at the air/water interface using pressure/area isotherms coupled with the techniques of ellipsometry and Brewster Angle Microscopy. They discovered that after 8 compression and expansion cycles the film became rigid due to the formation of helical rods at the interface. The compounds used for LB films are usually polymers and these form a film consisting of large rigid islands. These are often compressed and expanded several times to produce uniform films with no regions of the water surface uncovered, a process known as annealing.[1] When this has been achieved successive compression and expansion cycles cause little or no change in the pressure-area isotherm.

The rate at which the surfactant is compressed affects the shape of the isotherm. The collapse pressure is dependent on the rate of compression, high molecular weight polymers may take hours to reach equilibrium and so must be compressed very slowly.[2]

1.1.5 Structural Changes of the Amphiphile.

There are several factors that influence the film forming abilities of surfactants. These are the geometry of the molecule, the temperature, the pressure and the subphase. The changing structure of isotherms due to structural differences of the monolayer is described below, the behaviour of fatty acids is used as a general example.

1.1.5.1 Geometry

Adding a double bond to the molecule will cause a change in the packing of the molecules; oleic acid, elaidic acid and stearic acid all have 17 carbons, they only differ from each other by their geometry. The shapes of the molecules are illustrated in Figure 1.7 below.

Figure 1.7 Geometry and Isotherms.

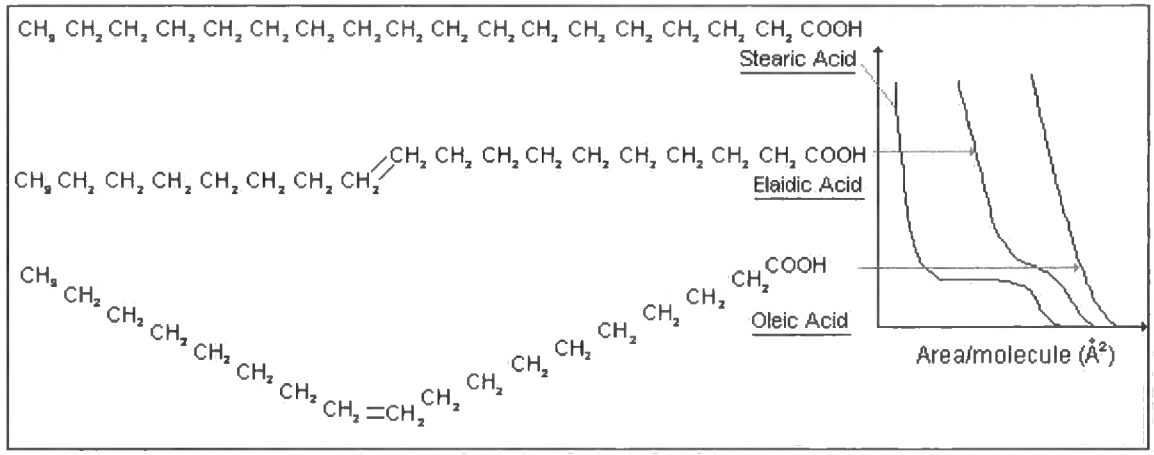

The change in the geometry of the acids is reflected in the resulting isotherms. Molecules with a double bond in the alkyl chain are not able to pack as closely due to steric hindrance, they are less condensed as there are less Van der Waals' interactions. The effect of adding a double bond also affects the melting point of the molecules. Thus, the melting point of oleic acid is considerably lower than that of stearic and elaidic acids due to the less efficient packing.

Adding a methyl group has a similar effect, again the film becomes more expanded and the transition between phases at higher pressure are no longer distinct. As with the double bond, the effect is greatest when the group is added at the centre of the molecule.

1.1.5.2 Changing the Tail Length.

Lengthening the tail of the fatty acid appears to reduce the liquid-condensed phase, it increases the Van der Waals' forces and so increasing the chain

length by one CH_2 group has a similar effect as reducing the temperature by 5-10 K.[24] However the head group area should remain approximately the same as in the solid phase the chains are oriented vertically.

Traube's rule gives a rough guide for the trend. It states that for a homologous series of surfactants the concentration required to reduce the surface tension decreases by a factor of about 3 with every additional CH_2 group. For example docosanoic acid ($C_{21}H_{43}COOH$) has four more CH_2 groups than stearic acid ($C_{17}H_{35}COOH$), the concentration for an equal lowering in the surface tension is expected to be approximately 12 times lower. The longer the hydrocarbon tail then the more the molecule tends to adsorb due to increasing hydrophobicity and hence lower the surface tension.

1.1.5.3 Temperature Dependence.

As stated above, increasing the chain length has a similar effect as decreasing the temperature. Increasing the chain length increases the Van der Waals forces of attraction, this means that there is greater cohesion between molecules. Decreasing the temperature decreases the thermal motion of the molecules and hence reducing the area the film. Again analogies to 3D systems can be drawn, as the temperature is increased the molecules goes from an isotherm showing a solid phase, through intermediates that have both solid and liquid phases until the isotherm is observed for the surfactant displaying only the gas phase. Pressure-temperature graphs (phase diagrams) are used to predict the shape of the curve, a typical phase diagram is shown above in Figure 1.5.

1.1.5.4 Ion Concentration of the Subphase.

The interactions that occur in the film are due to the polar interactions of the head group (proportional to $1/r^2$ where r is the intermolecular separation) and the Van der Waals' forces between the hydrocarbon chains that vary as $1/r^6$ and $1/r^{12}$. Therefore by changing the pH of the subphase and hence the ionisation of the headgroup the polar forces will be changed. Fatty acids are

weak acids and can act as ligands to metal ions therefore small changes in the subphase will have a marked effect. For example if a fatty acid monolayer is spread over cadmium chloride subphase then the cadmium ions will link two molecules together as the headgroups will become carboxylate ions and bind to the metal ion. Oleic acid forms much more expanded films than stearic acid, there is some debate as to whether there is bonding between the double bond and the subphase. For example if the subphase contains potassium permanganate the surfactant may also be attacked at the double bond causing the acid molecules to lie flat on the surface of the subphase, thus a more expanded subphase is observed.[25]

As mentioned above polymer films have been increasingly investigated for use in electronic devices. Such materials are difficult to handle as they do not dissolve in common spreading solvents. To overcome this problem pre-cursors which are easily soluble in suitable solvents are spread over a subphase containing ions. These ions initiate the polymerisation process which can then be monitored using the technique of BAM see chapter 4.[6,26]

1.2 LANGMUIR-BLODGETT FILMS

The study of monolayer films is needed to understand the behaviour of molecules at an interface so that they may be engineered to meet specific requirements. An example of these requirements is in the production of films that have been transferred onto solid substrates, these are known as Langmuir-Blodgett (LB) films after their inventors (see above). An LB trough (a trough with a dipping well) is required for this purpose and the substrate which is hydrophilic (e.g. silicon, glass, chromium or quartz) is held perpendicular to the surface and slowly dipped in and out of the subphase. The surface pressure must be kept constant during this process (the software controlling the trough keeps the surface pressure at a pre-determined value). Dipping speeds vary from μms^{-1} to mms^{-1}, the requirement is that the dipping speed must not be greater than the water drainage of the film.[9] The fabrication of quality electronic devices depends on the production of perfectly aligned layers. The film is usually compressed to a condensed layer as they are uniform (at larger surface

areas small clusters are often observed at the surface). Films may also be deposited by lowering a substrate horizontally onto the surface, this is known as Langmuir-Schaefer deposition and is less common. By changing the initial dipping direction and the substrate LB films may be built up with X, Y or Z type layering, these are shown in Figure 1.8 below. Films hundreds of layers thick can be built up in this manner.

Figure 1.8 LB film Deposition

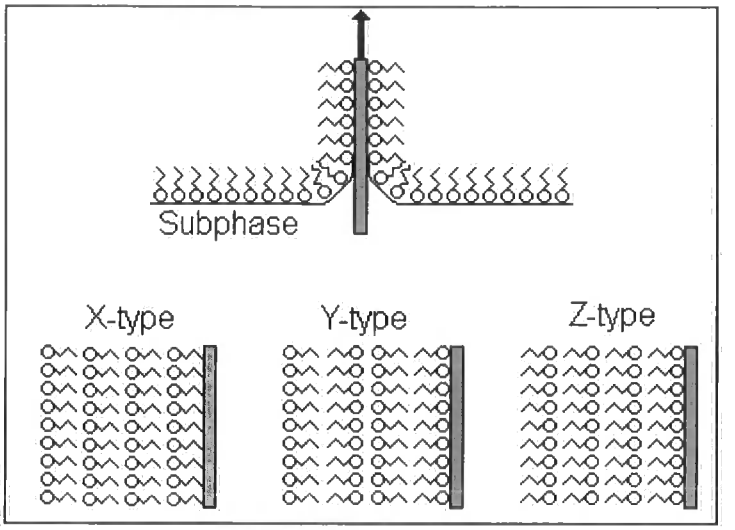

LB films have many uses such as vapour sensors (see chapter 4) and light emitting polymer displays for the next generation of televisions (see chapter 5). The deposited layers normally retain the structure of the monolayer and near perfect layers are required for these devices, therefore molecules must be designed that have excellent electrical or optical properties, bind easily to hydrophilic substrates and also form uniform monolayers for good transfer. BAM is an excellent technique to study monolayers prior to deposition allowing any defects in the film can be easily visualised. BAM has been used to study monolayer flow, see section 2.2.4. This is an important process in deposition to study any changes that occur when the substrate is removed from the subphase, being able to fully control this process will allow optimisation of structure of the transferred films.[27,28]

The quality of film production is measured by the transfer ratio:

$$\tau = \frac{A_L}{A_S} \qquad \textbf{Equation 1.9}$$

Where:

τ = deposition ratio,

A_L = decrease in the area occupied by the monolayer on the water,

A_S = the area coated by the substrate.

Values outside the region $0.95 < \tau > 1.05$ infer poor film homogeneity.

The lack of thermal stability of LB films has delayed their widespread application, however materials have been deposited that polymerise when irradiated with UV light.[29] These crosslinked polymer films retain their structural ordering but the thermal stability of the films is greatly enhanced. Polymers are also being directly deposited onto substrates to produce stable LB films (see chapters 4 and 5).

1.3 ALTERNATIVE TECHNIQUES.

A brief outline of some of the other techniques available to study the properties of monolayers is given below. Currently there are three general categories by which monolayers are studied, these are shown in Figure 1.9 below:

Figure 1.9 Surface Studies.

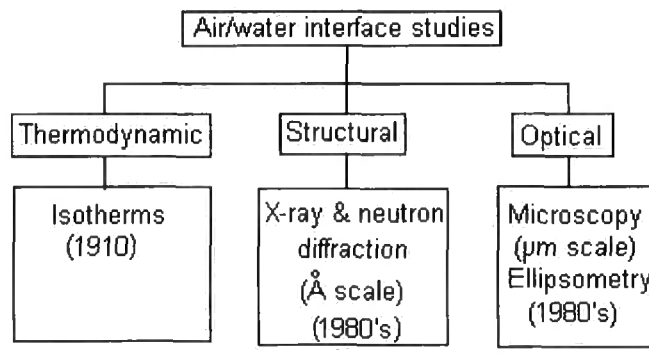

A single technique does give a complete picture of the system, results are often ambiguous therefore most research groups use a combination of these techniques. Isotherms (discussed in section 1.1.4) are often difficult to interpret, some of the changes are often subtle and could be due to impurities rather than structural reordering. As new techniques are introduced they permit new information about the monolayer to be obtained. For example Overbeck *et*

al. identified a new phase transition of even chain length fatty acids using the technique of Brewster angle microscopy (BAM), this phase transition could not be observed in the corresponding isotherms.[30]

1.3.1 Fluorescence Microscopy.

During the last decade the study of monolayers has generally been carried out by adding a fluorescent dye to the monolayer, such as NBD hexadecylamine, in approximately 1% mol. concentration.[31] The contrast between the surfactant molecules and the dye is observed by illuminating the dye with a high intensity laser or UV lamp and imaging the resulting fluorescence by a digital camera. The method exploits the fact that the dye will have different solubilities in different coexisting phases.

Fluorescence microscopy visualises the coexistence of phases, crystal growth and fusion of domains, information previously only obtained from isotherms, this led to the assumption that monolayers were uniform.[32] The technique requires an isotropic distribution of molecules otherwise there is no contrast between the dye and the surfactant molecules. Polarisation fluorescence microscopy (PFM) is now commonly used and allows the molecular orientation to be determined. This is accomplished by using linearly polarised incident radiation and adding an analyser (a polariser between the film and the detector). The added dye means that the dye/surfactant interaction is observed and not the surfactant/surfactant interaction, the assumption has to be made that the dipole moment of the chromophore is parallel to the sample molecules. It is the tilt of the chromophore which is measured and not the amphiphile itself but there is always some uncertainty on the relative orientation of the chromophore.[35] Chromophores have been added to surfactant molecules (e.g. 12-NBD stearic acid) but changing the structure of the molecule may change the behaviour of the molecule.[33]

The intensity of the emitted fluorescence is related to the azimuthal tilt (the rotation of the molecule about its molecular axis see Figure 1.10) of the dye molecule.[34]

Figure 1.10 Molecular orientation.

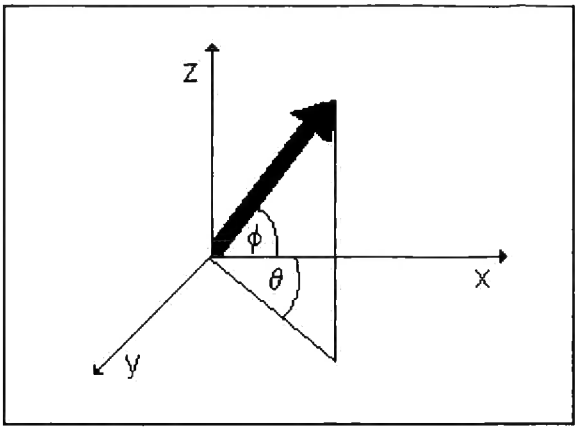

Therefore fluorescence microscopy is particularly good for the liquid-expanded to liquid-condensed phase transition where the azimuthal tilt angle of the molecules changes see Table 1.1. Phase transitions where the molecules become vertically aligned with respect to the surface are observed as a loss in contrast in the image as the tilt azimuth is undefined.[37] Also this means that a change in the molecular tilt with a constant azimuthal tilt cannot be observed using PFM.[36]

In certain cases the addition of the fluorescent dye has shown to affect the monolayer phase transitions. Tsao *et al.* reported that the liquid expanded phases of methyl esters exhibited dendritic structures when cooled with a probe dye present, however these structures were not observed by other techniques.[35] Rivière *et al.* found that the dye (NBD hexadecylamine) caused the phase boundary of alkonoic acids to be 1 mN/m lower than without the dye.[36] Experiments are often performed with different dye concentrations to determine whether the dye affects the phase transitions.[37] Fluorescence microscopy method is the most closely related to BAM as it directly images the surface on the micron scale allowing long range order and textures of films to be studied.

1.3.2 Ellipsometry.

The reflectivity of a surface differs in phase and amplitude for *s* and *p* polarised incident radiation. As circularly polarised incident radiation travels through the film it induces electrical vibrations which re-radiate in the form of the reflected radiation. In an anisotropic film the *s* and *p* polarised emitted radiation will be unequal resulting in an elliptically polarised beam and the technique of ellipsometry compares the resulting changes in reflectivities. The difference in phase of the radiation upon reflection is defined as Δ and the ratio of *p* to *s* amplitudes is defined as $\tan\psi$.[38] From this data information concerning the film thickness, roughness and refractive index may be determined. The analysis of ellipsometry data is complex but commercial ellipsometers come with computer software to performs these calculations. A typical experimental set-up used for ellipsometry is shown in Figure 1.11.

Figure 1.11 Ellipsometry set-up

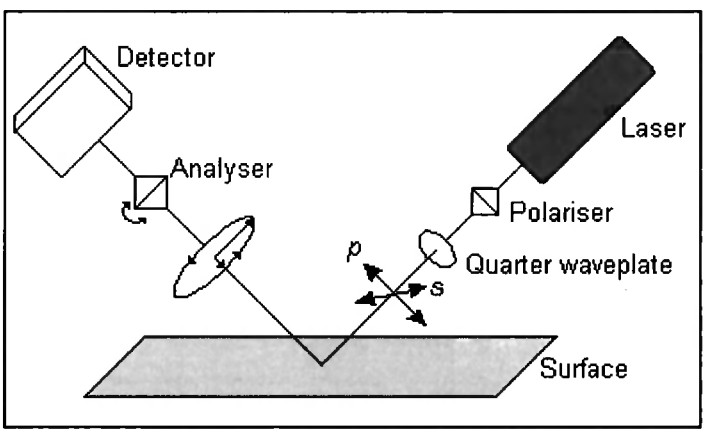

The radiation source is usually a laser with a polariser followed by a quarter wave plate to produce a circularly polarised beam at the surface. An analyser is then used to measure the ellipticity (the phase shift between *s* and *p* polarised radiation) of the reflected signal. Ellipsometry of films is performed in real time at the air/water interface or on films that have been deposited on to solid substrates, it is a non-invasive technique with a high sensitivity to the molecular surface density and the surface anisotropy.

Problems occur with assumptions that must be made for analysis, e.g. that the film is non-absorbing, also the value of the refractive index (n) or film thickness (d) is required.[39] The spatial resolution of ellipsometers is limited to the beam diameter (~1 mm) but by sequentially scanning across the image higher resolutions (10 μm) have been reached at the expense of a greatly increased data acquisition time.[40] Ellipsometric measurements are often performed close to the Brewster angle of the substrate, the reflectivity of the *p* polarised radiation is minimal and so the ratio of *s* to *p* polarised light is high. Therefore the introduction of a thin film at the Brewster Angle has a much greater affect on the ellipticity of the reflected signal making the technique more sensitive at this angle.

Ellipsometry experiments at the air/water interface are possible[41] but the ability of ellipsometry to characterise monolayer films at the air/water interface has been recently called into question.[23,29] A small error in the selected value of the refractive index results in a large error in the determined film thickness. Motschmann *et al.*[42] state that ellipsometry cannot be used to quantitatively characterise monolayers at the air/water interface. They concluded that the changes in phase and amplitude of the reflected signal are extremely small and strongly coupled to other film properties. This in turn means that ellipsometry alone cannot be used to determine the refractive index and the film thickness. However, the film thickness, anisotropy and roughness may still be qualitatively related to ellipticity, thus the homogeneity of monolayers during compression may be studied.[23]

Beaglehole designed an imaging ellipsometer, using a CCD camera he was able to record images a layer of oil on a mica substrate, these images were of dimensions 0.7 x 0.5 mm^2 with a resolution of 3 μm per pixel.[43] The quality of the images were hampered by the lack of fast frame-grabbers available at the time. At thicknesses of less than 50 $Å^2$ the image merged into random noise and substrate variations. The experiment took a considerable amount of time, as a delay of 220s between rotations of the analyser was required (the time needed to record 30 frames).

1.3.3 Second Harmonic Generation

Second harmonic generation (SHG) is an extremely sensitive surface technique, it involves measuring the second harmonic signal generated by the film when illuminated by a higher power laser (typically a Nd:YAG laser at 1064 nm). As it is a second order non-linear technique the material of interest must be asymmetric. A surface layer is by its nature asymmetric but the bulk medium is centrosymmetric and so a minimal signal is recorded from the bulk thus the technique offers good contrast. The ratio of the intensity parallel and perpendicular to the surface is recorded, using this information the tilt angle of molecules can be continuously studied, over a range of surface pressures.[44] SHG does have the advantage over other techniques in that it can detect the polar ordering of molecules. The conversion efficiency of the fundamental to the second harmonic is low, at most 25%, and so a high power laser is required. To achieve the high powers required a pulsed laser is used e.g. a femtosecond or picosecond laser which delivers typically 10^9 W pulses at the surface. However this may cause damage to the film or thermal fluctuations in monolayers at the air/water interface. To obtain the information on the molecular ordering knowledge of some characteristic values of the molecules are required i.e. the non-linear polarisabilities and the 2^{nd} order molecular susceptibility tensors. These values often difficult to calculate and a high degree of accuracy is required.[45] The resulting SHG signal may be greatly enhanced if the wavelength of the fundamental is near to an absorption band of the thin film.

The SHG signal from the surface is an average from the illuminated area. To study the surface region in more detail Florsheimer *et al.*[46] recorded the second harmonic signal as an image using a microscope objective and a CCD camera. This meant that different reflectivities across the laser footprint (2 mm) could be observed. The experiment consisted of a trough with a hole was cut in the base, a window was inserted and the film was illuminated from beneath through the window. A Nd:YAG laser (20 mJ, 100 ps, 20 Hz) was used as the radiation source, a filter was used to remove this fundamental after passing through the film so that it did not damage the camera. The material (2-docosylamino-5-nitropyridine (DCANP)) had a absorption band near the fundamental

wavelength giving a resonance enhancement of the SHG signal. The efficiency of conversion was such that one laser pulse created a second harmonic signal of sufficient intensity to create an image, therefore images were created in real time and ultra fast processes could be recorded. Other materials that do not have a absorption band near to the fundamental would require higher power incident radiation which is likely to damage the material of interest.

1.3.4 X-ray and Neutron Scattering.

X-ray studies can determine the positional order, size of the primitive cell and the tilt angle of the molecules in different phases. When the incident radiation is the same order as the spacing between layers (~0.1 - 5 nm for most LB films) interference between successive layers of the material occurs. The maxima in the interference patterns are described by Bragg's law:

$$n\lambda = 2d\sin\theta \qquad \textbf{Equation 1.10}$$

Where:

n = the order of reflection,
λ = the incident wavelength,
d = the spacing between layers,
θ = the angle of incidence.

Figure 1.12 X-ray diffraction.

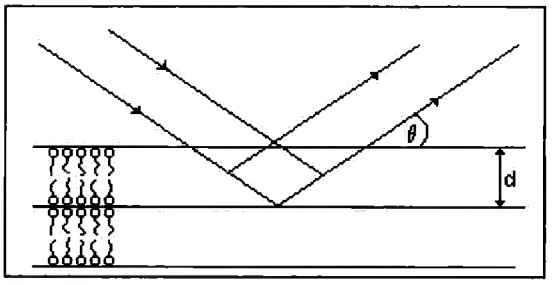

Equation 1.11 defines the scattering vector in X-ray and neutron scattering.

$$Q = \frac{4\pi}{\lambda}\sin\theta \qquad \text{Equation 1.11}$$

Q = the scattering vector,

λ = the wavelength of the incident radiation,

θ = the angle of incidence.

Using X-rays (λ = 0.154 nm) the required angle of incidence is approximately 1° for a typical LB film. There is good agreement between d-spacing values and theoretically calculated chain lengths for Y-type deposited salts of fatty acids. However the d-spacing is often less than twice the molecular length suggesting that the molecules are tilted with respect to the substrate or interdigitated, this method alone cannot determine the structure.

The introduction of synchrotron X-ray sources allows monolayers at the air/water interface to be studied due to the high intensity of the source and the tunable incident wavelength.[47,48] Specular reflectance recorded as a function of incidence angle yields information on the electron density distribution along the surface normal. The thickness, density and surface roughness can be extracted from this data. In-plane diffraction of the evanescent waves (incident below the critical angle for internal reflection) gives the molecular arrangement of the chains with respect to the surface normal. The incident angle is typically 0.1° and the beam penetrates < 10 nm. The illuminated area varies from 1 to 50 cm^2 to allow a relatively large area to be studied. X-ray reflection is less effective for studies of soluble surfactants where the molecules are not as closely packed. The contrast between film and the subphase is small and neutron reflectivity is preferred where the contrast can be enhanced.

Neutron scattering may also be used to study deposited multilayers as well as monolayer films at the air/water interface. The surfactant is deuterated, however some hydrocarbon surfactants have sufficiently high neutron densities to be detected without deuteration. The first studies of films at the air/water interface were performed by Thomas and co-workers in 1989.[49] The water subphase is deuterated such that it does not reflect the incident neutrons (null reflecting water (NRW)) meaning that the signal comes from the surfactant

layer only, thus there is good contrast between the surfactant layer and the subphase. It has been shown that deuteration does influence the surface structure.[50] Progressively deuterating fragments of the surfactant molecules allows the thickness of individual parts of the layer to be calculated, the scattering of the remainder of the molecule is adjusted to zero.[51] Using isotopic labelling resolutions down to 2 Å may be achieved which is of the order of two methylene groups. Lu *et al.* were able divide cetyltrimethylammonium bromide into 5 separate regions to study the chain conformation in the monolayer.[52]

These scattering techniques allow determination of microscopic structures of the phases of monolayers but the results are often difficult to interpret and structural models are required to perform the calculations. Information obtained by these techniques is on the Ångstrom scale and this is extremely useful to determine molecular orientation but information on macroscopic scales (using microscopy) yields information which is advantageous when looking at long range order or for tears in the film that would hinder uniform film production. The use of shared resources for the reflectivity experiments is expensive and time consuming.

This thesis describes the design and construction of a Brewster Angle Microscopy experiment at Durham University. During this development process three polymers were investigated. The first material, poly(Cu (II) 5,5'–methylene-bis(N-hexadecylsalicylideneamine) (poly(CuMBSH)), is used in vapour sensing devices and is described in chapter 4. BAM was used to study the polymerisation of the monomer, MBSH, to poly(CuMBSH) at the air/water interface. BAM shows the differences in structure of the monomer and polymer prior to deposition. The two other polymers studied in this work were derivatives of phenylenevinylenes (PPV's) and have potential uses as light emitting diodes. Improved transfer of the polymer PPV's to the substrate was found to occur when the polymers had been left to age on the water surface. BAM was used to determine the effect of this ageing process on the films, the BAM PPV experiments are described in chapter 5.

A new technique called Brewster Angle Reflectivity (BAR) was also developed in Durham. Chapter 6 describes the design of the equipment, its potential

applications and experiments that prove that this novel technique can be calibrated to measure the surface excess concentration of soluble surfactants.

---

1 Gaines, G. L. Jr. *Introduction to Insoluble Monolayers.* Interscience Publishers, New York (1966).

2 Roberts, G. G. Ed. *Langmuir-Blodgett Films.* Plenum Press, New York. (1990).

3 LaMer, V. K. *Science* **148**, 36 (1965).

4 Pockels, A. *Nature*, **43**, 437. (1891).

5 McMurray, E. J. Ed. *Notable Twentieth Century Scientists.* Gale Research Inc. (1995).

6 Wilde, J.N., Wigman, A. J., Nagel, J., Öertel, U., Beeby, A., Tanner. B. and Petty, M. C. *Acta Polymer.* **49**, 294 (1998).

7 Cimrova, V., Remmers, M. Neher, D. and Wegner, G. *Adv. Mater.* **8**, 146. (1996).

8 May, P. *Physics World* **8**, 52. (1995).

9 Petty, M. C. *Langmuir-Blodgett Films, An Introduction.* Cambridge University Press, UK. (1996).

10 Hosoi, K., Ishikawa, T., Tomioka, A. and Miyano, K. *Jpn. J. Appl. Phys.* **32**, L135 (1993).

11 Tsao, M-W., Fischer, Th., and Knobler, C. M. *Langmuir*, **11** 3184 (1995).

12 Lipp, M. M., Lee, K. Y. C., Zasadzinski, J. A. and Waring A. J. *Chemtech* **27**, 42 (1997).

13 Birdi, K. S. *Lipid and Biopolymer Monolayers at Liquid Interfaces.* Plenum Press, New York. (1989).

14 Zasadzinski, J. A., Viswanathan, R., Madsen, L., Garnaes, J. and Schwartz, D. K. *Science* **263**, 1726 (1726).

15 Beaglehole, D. *Physica*, **100B,** 163 (1980).

16 Simister, E., Thomas, R. K., Penfold, J., Aveyard, R., Binks, B. P., Fletcher, P. D. I., Lu, J. R. and Sokolowski , A. *J. Phys. Chem.* **96**, 1383 (1992).

17 Thomas, R. K. and Penfol, J. *Current Op. Colloid Interface Sci.* **1**, 23 (1996).

18 Mingotaud, A-F., Mingotaud, C. and Patterson, L. K. *Handbook of Monolayers*, Vol 1 & 2. Academic Press, San Diego. (1993).

19 Weidemann G., and Vollhard, D. *Thin Solid Films* **264**, 94. (1995).

20 Shaw, D. J. *Introduction to Colloid and Surface Chemistry.* 4th edition, Butterworth-Heinemann, Bodmin, UK. (1992).

21 Roberts, G. *Langmuir-Blodgett Films.* Plenum Press, New York. (1990).

22 Xue, Q., Yang, K., Chen, X., Zhang, Q. *Supramolecular Sci.* **5**, 587 (1998).

23 Reda, T., Hermel, H. and Höltje, H-D. *Langmuir* **12**, 6452 (1996).

24 Petty, M. C. *Langmuir-Blodgett Films: An Introduction.* Cambridge University Press, Cambridge, UK. (1996).

25 Braude, E. A., and Nachod, F. C. *Determination of Organic Structures by Physical Methods.* Academic Press, New York. (1955).

26 Uredat, S. and Findenegg, G. H. *Colloids Surfaces* A: Physiochem. Eng. Aspects **142**, 323 (1998).

27 Kurnaz, M. L. and Schwartz, D. K. *Phys. Rev. E.* **5**, 3378, (1997).

28 Kurnaz, M. L. and Schwartz, D. K. *J. Rheol.* **41**, 1173 (1997).

29 Adamson, A, W. and Gast, A. P. *Physical Chemistry of Surfaces.* 6th edition, Wiley, New York (1997).

30 Overbeck, G. A. and Mobius, D. *J. Phys. Chem.* **97**, 7999. (1993).

31 Hénon, S. and Meunier, J. *Rev. Sci. Instrumen.* **62**, 936. (1991).

32 Hosoi, K., Ishikawa, T., Tomioka, A. and Miyano, K. *Jpn. J. Appl. Phys.*, **32**, L135. (1993).

33 Kurnaz, M. L. and Schwartz, D. K. *J. Rheol.* **41**, 1173 (1997).

34 Ruiz-Garcia, J., Qiu, X., Tsao, M.-W., Marschall, G., Knobler, C. M., Overbeck, G. A. and Mbius, D. *J. Phys. Chem.* **97**, 6955 (1993).

35 Tsao, M-W. *Studies of Molecular Orientation of Langmuir Monolayers.* PhD thesis. U.C.L.A. (1994).

36 Rivière, S., Hénon, S., Meunier, J., Schwartz, D. K., Tsao, M.-W. and Knobler, C. M. *J. Chem. Phys.* **101**, 10045 (1994).

37 Schwartz, D. K. and Knobler, C. M. *J. Phys. Chem.* **97**, 8849 (1993).

38 Azzam, R. M. A. and Bashara, N. M. *Ellipsometry and Polarized Light.* North Holland, New York. (1977).

39 Irene, E. A. *Thin Solid Films* **233**, 96. (1993).

40 Erman, M. and Theeten, J. B. *J. Appl. Phys.* **60**, 959 (1986).

41 Meunier, J. *Light Reflectivity and Ellipsometry* in Light Scattering by Liquid Surface and Complementary Techniques. Marcel Dekker Inc. New York. (1992).

42 Motschmann, H., Reiter, R., Lawall, R., Duda, G., Stamm, M., Wegner, G. and Knoll, W. *Langmuir* **7**, 2743 (1991).

43 Beaglehole, D. *Rev. Sci. Instrumen.* **59**, 2557, (1988).

44 Rasing, Th., and Shen, Y. R. *Phys. Rev. A.*, **31**, 537. (1985).

45 Shen, Y. R. *Nature* **337**, 519 (1989).

46 Florsheimer, M, Looser, H., Küpfer, M. and Günter, P. *Thin Solid Films* **244**, 1001. (1994).

47 Weissbuch, I., Berkovic, G., Yam, R., Als-Neilsen, J., Kjaer, K., Lahav, M. and Leiserowitz, L. *J. Phys. Chem.* **99**, 6036 (1995).

48 Styrkas, D. A., Thomas, R. K., Adib, Z. A., Davis, F., Hodge, P. and Liu, X. H. *Macromolecules* **27**, 5504 (1994).

49 Lee, E. M., Thomas, R. K., Penfold, J., Ward, R. C. *J. Phys. Chem.* 93, 381, (1999).

50 Möhwald, H. *Rep. Prog. Phys.* **56**, 653 (1993).

51 Penfold, J., Richardson, R, M., Zarbakhsh, A., Webster, J. R. P., Bucknall, D. G., Rennie, A. R., Jones, R. A. L., Cosgrove, T., Thomas, R. K., Higgins, J. S., Fletcher, P. D. I., Dickinson, E., Roser, S. J., McLure, I. A., Hillman, A. R., Richards, R. W., Staples E. J., Burgess, A. N., Simister, E. and White, J. W. *J. Chem. Soc., Faraday Trans.* **93,** 1 (1997).

52 Lu, J. R., Li, Z. X., Smallwood, J., Thomas, R. K. and Penfold, J. *J. Phys. Chem.* **99**, 8233 (1995).

Chapter 2 THEORY OF BAM.

In 1991 Hönig and Möbius[1] and Hénon and Meunier[2] working simultaneously and independently studied the reflectivity of surfaces at the Brewster angle to image monolayers at the air/water interface and developed the technique of Brewster Angle Microscopy (BAM). The following chapter describes the design and development of the Brewster Angle Microscope used in this work. This chapter outlines the theory of the technique and describes some the work carried out by other groups using the technique.

2.1 Brewster's Angle

In 1815 the Scottish physicist Sir David Brewster first noted that there is an angle for *p*-polarised light at which there is no reflection from an interface. All optically transparent liquids and solids will have such an angle. When a *p*-polarised (the E-field is perpendicular to the surface) is incident, this angle is known as the Brewster angle for the material.

Figure 2.1 Reflection at the Brewster angle

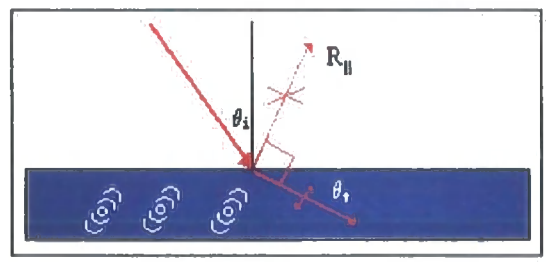

At the Brewster angle the incident angle (θ_i) and the refracted angle (θ_t) are at 90°, Brewster's angle can be derived from Snell's law:

$$n_1 \sin\theta_i = n_2 \sin\theta_r \quad \text{Snell's Law}$$
$$\theta_i + \theta_r = 90^\circ$$
$$n_1 \sin\theta_i = n_2 \sin(90^\circ - \theta_i) = n_2 \cos\theta_i$$
$$\tan\theta_B = \frac{n_2}{n_1}$$

Equation 2.1

Where:

θ_B = Brewster's angle,

n_1 = the refractive index of the incident medium,

n_2 = the refractive index of the transmitting medium.

Air has a refractive index of approximately 1 whilst water has a refractive index of 1.33, using equation 2.1 the Brewster angle for the air water interface is ~53°. The variation of angle versus intensity of reflection for the air/water interface is given in Figure 2.2 below.

Figure 2.2 Reflectivity curve for *p*-polarised light.

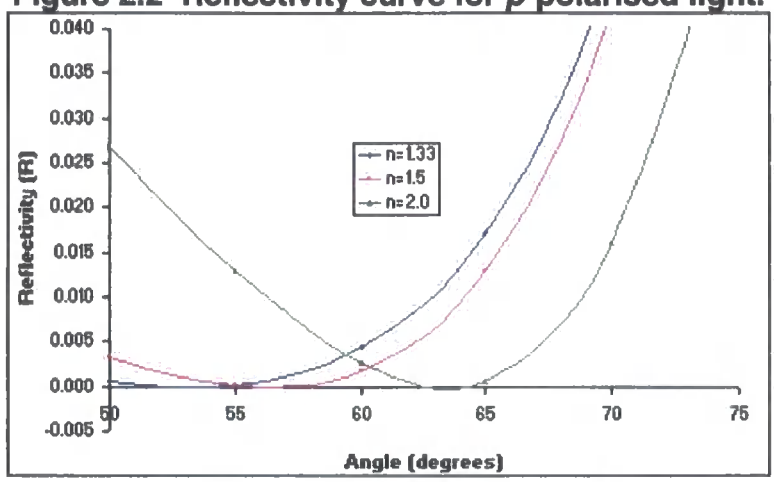

A small change in the refractive index of the surface therefore brings about a large change in the reflectivity of the interface. This can be shown mathematically using the Fresnel equations, the reflectivity of *p*-polarised light at the surface is described by:

$$E_r^p = \left[\frac{\tan(\theta_i - \theta_r)}{\tan(\theta_i + \theta_r)}\right] E_i^p \qquad \text{Equation 2.2}$$

Where:

θ_i = the incident angle,

θ_r = the refracted angle,

E_i^p = the incident wave's electric field amplitude for *p*-polarised light,

E_r^p = the reflected wave's electric field amplitude for *p*-polarised light.

When the incident angle (θ_i) and the refracted angle (θ_r) add up to 90° the reflectivity goes to zero as tan 90° = ∞. A physical picture of this behaviour is shown in Figure 2.1 above. When light is incident on a surface it induces electron oscillators near the surface to vibrate with refracted wave.[3] These oscillators re-radiate some of their energy in the form of the reflected wave as show in Figure 2.1. The intensity of the reflected wave depends on the angle between the transmitted wave and the plane of oscillation of the dipoles. The dipoles cannot have a component that radiates in the direction parallel to their direction of travel (the reflected wave) as this is forbidden for a electromagnetic (i.e. a transverse) wave. The reflected element will therefore vanish if the reflected and refracted wave are at 90°.

2.2 BREWSTER ANGLE MICROSCOPY

BAM has been used to study a wide range of materials at the air/water interface. Newly discovered compounds, such as fullerenes[4] have been studied using BAM as well as many fatty acids and alcohols.[5] This thesis reports results from the study of two novel compounds at the air/water interface, the first is a polymer that is used to produce vapour sensors (chapter 4) and the second describes the behaviour of phenylenevinylenes (PPV's) at the air/water interface Chapter 5. PPV's are currently under investigation for materials to produce ultra-thin television screens.[6]

Lipids form simple membranes and they are surface and so they have been widely studied at the air/water interface. Kaercher *et al.* used BAM to investigate the spreading velocities of Meibomian lipids which are found in the eye.[7] Lipp *et al.* have studied palmitic acid and protein SP-B at the air/water interface which are the major components of lung surfactants.[8] The understanding of the behaviour of biological compounds is required so that synthetic substitutes may be prepared.

Nikitento *et al.* have used BAM to study a monolayer of arachidic acid deposited onto glass substrate by the LB technique, although no images were published.[9,10,11] BAM may be used to study monolayers spread onto optically

transparent materials.

After the initial images were published other groups began to develop methods of quantifying the images and obtaining information about the molecular orientation in a film. The various methods used to determine the molecular tilt, tilt azimuth and film thickness using BAM are discussed below.

2.2.1 Reflectivity and film thickness.

At the turn of the century Drude derived corrections to Fresnel's equations to describe the reflection of light from an isotropic film.[12] These equations contain factors which depend upon the film thickness, refractive indices of the substrate, the film and the surrounding atmosphere (n_2, n_1 and n_0 respectively). Using the equations of Drude and Fresnel, de Mul and Mann performed experiments using BAM to determine the film thickness by reflectivity. The reflectivity (R) is proportional to ρ^2 (ρ is the ellipticity of the reflected light and is defined by equation 2.3.) [13]

$$\rho = \frac{\pi d}{\lambda} \frac{\sqrt{n_0^2 + n_2^2}}{n_0^2 - n_2^2} \frac{(n_0^2 - n_1^2)(n_2^2 - n_1^2)}{n_1^2} \qquad \text{Equation 2.3}$$

Therefore from equation 2.3 the reflectivity R is proportional the square of the thickness of the film.

At the Brewster angle the reflectivity for an isotropic film becomes:

$$R = \frac{r_{01} + r_{12}e^{-2i\beta}}{1 + r_{01}r_{02}e^{-2i\beta}} \quad , \quad \beta = \frac{2\pi d n_1}{\lambda}\cos\theta_1 \qquad \text{Equation 2.4}$$

Where:

R = reflectivity,

r_{01} = reflection from air/film interface,

r_{02} = reflection from air/water interface,

r_{12} = reflection from film/water interface

d = film thickness,

n_1 = the refractive index of the film,

θ_1 = the incident angle,

λ = the wavelength of the incident beam.

This equation is valid for isotropic films or anisotropic films with their optical axes perpendicular to the surface. To look at anisotropic films in general a 4 x 4 matrix method such as Bethune's[14] or Berreman's[15] is used to calculate R.

De Mul and Mann showed that the relationship between the reflectivity and the film thickness ($R \propto d^2$) was still valid for anisotropic films.13 They used the relationship between the reflectivity and film thickness to calculate the collapse of multilayers of liquid crystals (4'-n-alkyl[1,1'-biphenyl]-4-carbonitrile), specifically 8CB and 10CB at the air/water interface. The study of liquid crystalline materials at the air/water interface is useful in determining the behaviour at an interface, this in turn yields information on the bulk alignment in liquid crystal displays. They scaled the CCD signal intensity with respect to an incident beam, and used this to calculate the relative thickness of the film at different surface pressures. However they needed to know the various dielectric tensors and had to estimate the tilt angle of the molecules on the surface, these values for 8CB and 10CB are not accurately known at the air/water interface. They were able to determine that 8CB formed multilayer domains on a trilayer. De Mul and Mann were the only group to take into account the Gaussian intensity distribution of the laser beam. This distribution means that the intensity values vary across an image but this is due to the laser and not due to structural changes of the amphiphiles.

2.2.2 Molecular orientation in a film.

In the liquid phases (see 1.1.4) of a particular surfactant pressure/area isotherm the molecules spread at the air/water interface tend to aggregate and form small clusters with a definite structure and molecular orientation which are referred to as domains, the types of domains are described in more detail below.

Isotropic phases, such as the gas and liquid-expanded phases, can be distinguished by their changes in reflectivity and hence the change in thickness.

However the gas phases are often difficult to see in BAM as the surfactant molecules move independently across the surface and are too small to be visualised by microscopy, the domains need to be of the order of a few microns to be observed. Changes between liquid phases involve a change in tilt which results in a change in anisotropy i.e. a change in polarisation of the reflected light. Many complex structures have been reported for example; stars, stripes and spirals that have been imaged by BAM thus BAM may be used to image most of the possible phases of a monolayer. [16,17,18,19]

The intensity of the reflected light is proportional to the film's thickness, anisotropy and roughness (thermal fluctuations result in an approximately 3 Å ripple of the surface2). In an optically isotropic film changes in the film thickness and density will result in different reflected intensities. In optically anisotropic films the reflected light carries information about the molecular orientation of the film. For example the chains of palmitic acid are tilted in the liquid crystal phase, the polarisability along the chain is greater than perpendicular to the chain and so the refractive index parallel and perpendicular to the chain will be different. When the incident radiation strikes the molecule it is resolved, the different refractive indices means that an a *s*-polarised component is introduced into the reflected light. The addition of an analysing polariser between the surface and the microscope allows the amount of *s*-polarised light to be determined. The BAM images show regions with different intensities corresponding to different tilt angles of the molecules. A fixed polariser determines the tilt azimuth, this is defined in Figure 1.10.[19] The change in polar tilt is an excellent indicator of phase transition, some interesting BAM images of methyl arachidate have been published by Overbeck *et al.* Diagrams of typical domains are shown in Figure 2.3.

Figure 2.3 Sketch of a methyl arachidate domain

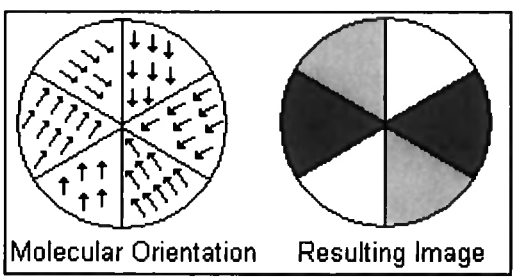

Although the material in each domain has the same molecular tilt there are discrete regions with different azimuthal tilt. Each region rotates some of the reflected light from the *p*-polarisation and by using the polariser the differences in the azimuthal tilt can be visualised.

A fixed polariser only shows molecules that lie along θ and $\theta + \pi$ (radians). If the second polariser is mounted on a small rotation stage, between the surface and the detector, so that it can be rotated (an analyser) it may be used to deduce the tilt of the domains. Fisher *et al.* claim that the spatial variation of the orientation of the molecular tilt azimuth within the monolayer cannot be unequivocally determined from techniques other than BAM.[16]

Tabe and Yokoyama[20] developed a Fresnel formula for Langmuir monolayers at the Brewster angle for optically uniaxial (one optic axis) monolayers. This used Berreman's[15] 4 x 4 matrix and equation 2.5 was derived which is dependent on the azimuthal angle (α), the tilt angle (β) and the dielectric constants (ε_1 and ε_3).

$$I(\alpha) = \left[\delta h \frac{\varepsilon_1(\varepsilon_3 - \varepsilon_1)}{\varepsilon_3 \cos^2\beta + \varepsilon_1 \sin^2\beta} \sin^2\beta \right]^2 \sin^2\alpha \left(\cos\alpha - \left(\frac{n^2 \tan\theta_t}{\varepsilon_1 \tan\beta} \right) \right)^2 \quad \text{Equation 2.5}$$

$$h = \frac{2\cos\theta_i \cos\theta_t}{(n\cos\theta_t + n\cos\theta_i)(n\cos\theta_t + n\cos\theta_i)}$$

This equation becomes significantly more complicated when a biaxial film (two optic axes) is considered and parameters such as the film thickness, the angle of rotation about the molecular axis and all dielectric constants are required. These values are difficult to determine.

The response of the CCD camera is not linear and the signal is therefore difficult to quantify, as the absolute intensities cannot be readily obtained but rather the relative intensities of one tilted region to another are recorded. Experimentally the background tends to change from image to image due to light scattering by the film. To simplify this problem the calculations have been

performed on individual images, thus the experimental conditions were the same.

Hosoi *et al.*[21] determined the tilt angle of a monolayer of stearic acid by normalising the differences between the brightest and darkest domains in one image and using this contrast as a scale they related this to the area/molecule. The experimental contrast was defined as:

$$C = \frac{I_{max} - I_{min}}{I_{max} + I_{min}} \qquad \text{Equation 2.6}$$

Where:

I_{max} = The intensity of the brightest domain,

I_{min} = the intensity of the darkest domain.

They took these values averaging over 3000 pixels and plotted a graph of contrast versus area/molecule. Using the Bethune's method to solve the Maxwell equations they were able to plot a theoretical graph of contrast versus tilt angle. Combining the theoretical and experimental plots they were able to plot a chart showing tilt angle as a function of area/molecule. They were unable to find stearic acid ($C_{17}H_{35}COOH$) X-ray data with which to compare their results, so they used the values of arachidic acid ($C_{19}H_{39}COOH$). This data followed the form of equation 2.7. (The value of 19.8 is an arbitary constant which was calculated by Hosoi *et al.* to fit the equation to the data.)

$$\cos\theta = \frac{19.8}{\text{area / molecule}} \qquad \text{Equation 2.7}$$

The measured values tended to be greater than those calculated by equation 2.7. Hosoi *et al.* attributed this discrepancy to the method of analysis, at a given area/molecule there is likely to be a distribution of intensity. Using the above contrast method the entire range is taken and this may bias the distribution to a higher contrast value and therefore increase the experimentally derived tilt angle.21

Tsao and co-workers studied a compound that formed well-known and relatively simple structures and then optimised their theoretical calculations.[16] The tilt and tilt azimuth cannot be taken as absolute values from the image so

they used theoretical values to predict the shape of the domains and then compared these to the greyscale values obtained from the image. The validity of the theoretical values were then tested by seeing if the theory could accurately predict the resulting change in signal with changing analyser orientation. Berreman's 4 x 4 matrix[15] and the transfer matrix of Bethune[14] were used to calculate the reflectivity, this required 9 parameters; the molecular tilt (θ), the tilt azimuth (φ), the thickness of the monolayer (d), the incidence angle of the laser (Θ), the polarisation of the incident beam from *p* orientation (δ_i, typically 0.1°), the analyser angle (δ_r), the dielectric constant of water (ε_w) and the dielectric constants of the film ε_{xx} and ε_{zz}. However these 9 required parameters are basically unknown and difficult to assess. The resulting theoretical values were then scaled by a factor S to relate them to the experimental values, a derivation of the equations is given by Tsao.[22] Methyl esters form star defects at high temperatures, when these are cooled slowly through the low temperature phase transition six new regions suddenly appear at the centre of each domain. The regions grow with the same tilt but each domain was divided into "6 pie-shaped" regions with the tilt azimuth varying by 60° from region to region. The change in the molecular orientation through the phase transition is called blooming.

The well defined structure of the domains simplified the calculations as the number of different tilt orientations was limited to 12. They showed that in practice the tilt azimuth may be determined from BAM images but difficulties arose with the lack of precise values for the 9 parameters.

Therefore it is difficult to quantify the values of the tilt and tilt azimuth of the molecules in a monolayer by analysing BAM images. The intensity of the reflected light needs to be recorded by a detector that gives absolute values.

2.2.3 Brewster Angle Autocorrelation Spectroscopy

As discussed above the absolute intensity cannot be extracted from the BAM images and it is also difficult to compare BAM images due to the variations in the background signal. Therefore it is difficult to extract quantitative information about molecular orientation. Lautz and Fischer have developed the technique of Brewster Angle Autocorelation Spectroscopy (BAAS) which allows molecular

tilt and BAM images to be extracted simultaneously.[23,24] The experimental set-up is very similar to that of BAM, the only exception is that on reflection from the surface the signal passes through a beamsplitter, part of the light is passes through to the CCD camera as usual but the remainder is diverted via a monomode fibre to a photon counter and an autocorrelation unit.

Figure 2.4 BAAS set-up

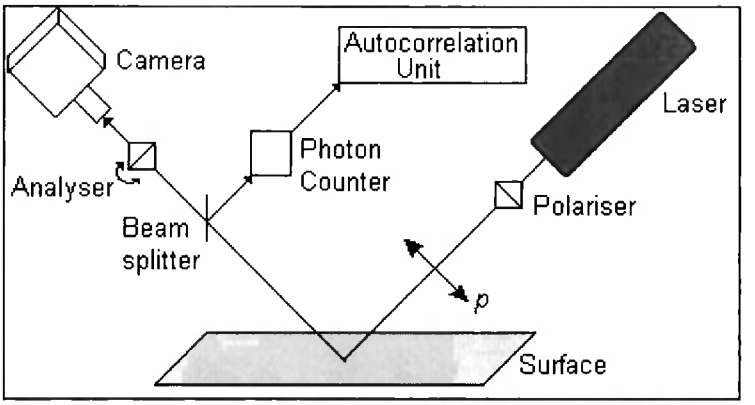

It takes approximately 2 minutes to record an autocorrelation spectrum. The tilt angle of the molecules within a domain is fixed but the tilt azimuth may vary from 0° to 360° see figure 1.10. The different tilt azimuths result in different optical anisotropy and hence the reflected signal will fluctuate. Each tilt azimuth has the same free energy and therefore each have the same probability of passing under the correlation region. The autocorrelation function decays as a function of time and is proportional to the intensity contrast (azimuthal tilt) between the domains. It does not depend on the film thickness nor any fit parameter just the dielectric constant and the analyser angle which are known and the tilt angle which is to be determined. Lautz and Fischer have used BAAS to determine the tilt angle of stearic and arachidic acids and octadeconal and compared these results to similar experiments performed by X-ray spectroscopy.[23,24] They found excellent agreement and determined that BAAS can determine tilt as a function of surface pressure of molecules oriented at the air/water interface to an accuracy of ± 2.5°.

2.2.4 Monolayer Flow By BAM.

Schwartz *et al.* have used BAM[25] and fluorescence microscopy[26] to study the flow of Langmuir (insoluble) films of NBD-stearic and eicosanoic acid. They were able to look at fatty acids rod and disk-like molecules. Most applications

of surfactant films are dynamic (see Chapter 6) but flow dynamics are extremely complex and are poorly understood. The flow of a monolayer is 2 dimensional therefore the theory is simplified and allows the study of model systems. Schwartz and co-workers used two methods to create flow in the monolayer. The first was a shear flow which consists of 2 Teflon bands rotating in opposite directions as illustrated in figure 2.5a. The second utilised channel flow, figure 2.5b, created by adding two fixed barriers, 3 mm apart, between co-rotating bands. These systems were used for fluorescence measurements.

Figure 2.5 Study of monolayer flow by Fluorescence.

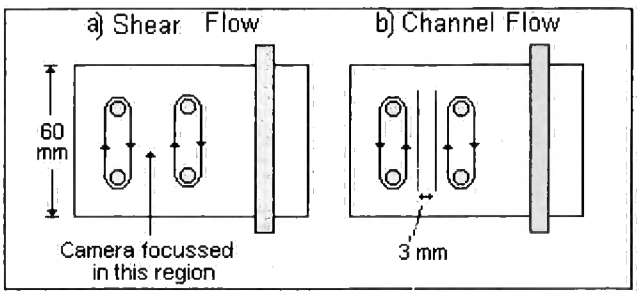

Schwartz found that a meniscus occurred at the edge of the barrier, this caused problems with the BAM images and so a slightly different set-up was used for BAM.[25] An uneven surface means that the incident radiation is not striking the surface at the Brewster Angle and is being scattered in all directions. The resulting BAM images have poor contrast due to the large amount of radiation scattered into the camera. The group suggest that by using a different band type the meniscus could be reduced and the images improved.

Thus BAM is a simple yet effective tool for imaging insoluble films at the air/liquid interface. A large amount of qualitative information concerning the film thickness and molecular orientation can be extracted from the images by comparing the image intensities. Recent advances indicate that the use of the technique may be expanded to yield quantitative results and to study flowing films.

---

1 Hönig, D. and Möbius, D. *J. Phys. Chem.*, **95**, 4590 (1991).

2 Hénon, S. and Meunier, *J. Rev. Sci. Instrumen.*, **62**, 936 (1991).

3 Hecht, E. *Optics.* Addison-Wesley (1987).

4 Castillo, R., Ramos, S., Ruiz Garcia, J. *Physica A.*, **236**, 105 (1997).

5 Castillo, R., Ramos, S., Cruz, R., Martinez, M., Lara, F. and Ruiz-Garcia, J. *J. Phys. Chem.* **100**, 709 (1996).

6 May, P. *Physics World.* **8**, 52. (1995).

7 Kaercher, T., Hönig, D. and Möbius, D. *Int. Opthalmol.* **17**, 341 (1993).

8 Lipp, M. M., Lee, K. Y. C., Zasadzinski, J. A. and Waring A. J. *Biophys. J.*, **72**, 2783 (1997).

9 Overbeck, G. A., Hönig, D., Wolthaus, L., Gnade, M. and Möbius, D. *Thin Solid Films,* **242**, 26 (1994).

10 Nikitenko, A. A. and Savranskii, V. V. *Opt. Spectrosc.* **72**, 200 (1993).

11 Nikitenko, A. A. and Savranskii, V. V. *Opt. Spectrosc.* **76**, 899 (1994).

12 Drude, P. *The Theory of Optics.* Longman, Green and Co. New York. (1929).

13 De Mul, M. N. G. and Mann, Jr., J. A. *Langmuir,* **14**, 2455 (1998).

14 Bethune, D. S. *J. Opt. Soc. Am.* B., **8**, 367 (1991).

15 Berreman, D. W. *J. Opt. Soc. Am.*, **62**, 502 (1991).

16 Tsao, M-W., Fischer, Th. and Knobler, C. M. *Langmuir,* **11**, 3184 (1995).

17 Hénon, S. and Meunier, J. *J. Chem. Phys.* **98**, 9148 (1993).

18 Ruiz-Garcia, J., Qui, X., Tsao, M.-W., Marshall, G. and Knobler, C. M. *J. Phys Chem.* 97, 6955 (1993).

19 Overbeck, G. A., Hönig, D. and Möbius, D. *Thin Solid Films,* **242**, 213. (1994).

20 Tabe, Y. and Yokoyama, H. *Langmuir,* **11,** 699 (1995).

21 Hosoi, K., Ishikawa, T., Tomioka, A. and Miyano, K. *Jpn. J. Appl. Phys.*, **32**, L135 (1993).

22 Tsao, M-W. PhD thesis. UCLA. (1995)

23 Lautz, C. and Fischer, Th. M. *Mater. Sci. and Eng. C.* **5**, 271 (1998).

24 Lautz, C., Fischer, Th. M. and Kildea, J. *J. Chem. Phys.* **106**, 7448 (1997).

25 Kurnaz, M. L. and Schwartz, D. K. *J. Rheol.* **41**, 1173 (1997).

26 Kurnaz, M. L. and Schwartz, D. K. *Phys. Rev. E.* **56**, 3378. (1997).

Chapter 3 EXPERIMENTAL

At the start of this project (1995) the BAM equipment had just been launched onto the market by Nanofilm Technology (NFT), this company was formed by the Möbius group. The project at Durham was to develop a BAM system to visualise thin films and to develop more versatile experiments in order to study other aspects of thin films such as film aging (see chapter 6). The background to the technique and current research is described in chapter 2.

Over the past four years a range of BAM systems have been introduced and commercial BAM kits are now widely used as a standard tool for the study of surfaces. BAM provides useful information yet the experimental procedure is relatively short and simple.

3.1 LIGHT SOURCE

The experimental set-up used in this work is shown below in Figure 3.1.

Figure 3.1 The Brewster Angle Microscope.

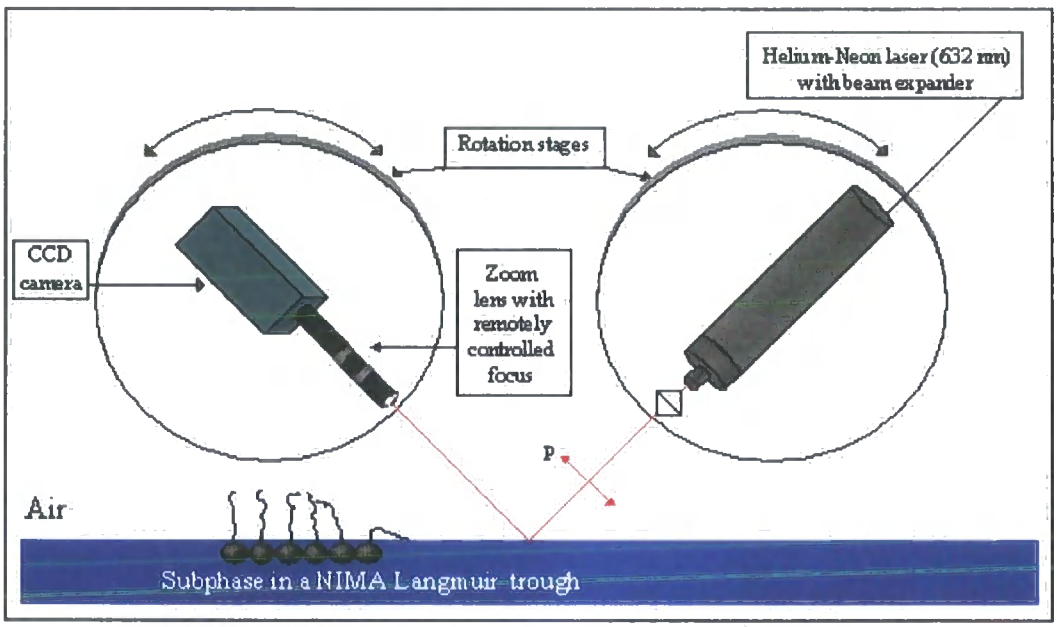

A relatively intense monochromatic polarised light source such that is provided by a low power laser (of the order of 15 mW) is required as at the Brewster angle >99% of the radiation is transmitted into the subphase.[1] However the

laser power has to be balanced by the photochemical damage and heating problems (convection currents) that a high power laser could cause to the film and the detector. Hénon and Meunier[2] used an argon ion laser (2 W), although the power was reduced to 500 mW at the surface by passing the beam through various optical components. However Fischer *et al.*[3] found that a laser with greater than 1W nominal power caused convection in the film. They used an argon ion laser with 500 mW nominal power that was reduced to 280 mW at the surface after passing through the focusing and polarisation optics. Hönig and Möbius[1] noted that when studying films using a 5 mW laser they had to attenuate the beam as the high intensity of the reflected light saturated the CCD chip. They were able to detect a difference of one CH_2 group in a series of fatty acids with a 5 mW laser. The advantage of using a high power light source is that a smaller numerical aperture in the microscope can be used and this gives a better depth of field, (see section 3.2.2.2). The argon ion laser was physically much larger than a He-Ne and so a monomode fibre was required to take the beam from the laser to the surface.[2] However the resulting beam was divergent and so a microscope objective and a polariser were used to produce a *p*-polarised beam. In the system constructed at Durham a helium-neon (He-Ne) laser operating at 632 nm (Melles-Griot) was used, this had a power output of 8 mW (Melles-Griot). The He-Ne laser also has the advantage of being lightweight and so is easily mounted eliminating the need for an optical fibre delivery system. The laser was held in two lightweight aluminium collars with 3-point plastic screws, these allowed small adjustments of the laser in all directions.

3.1.1 Polariser

To obtain minimum reflectivity at the Brewster angle a *p*-polarised incident beam (parallel to the plane of incidence) is required. The laser used here had a plane polarisation ratio of > 500:1, specified by the manufacturer, but even at the Brewster angle the initial images showed a substantial amount of reflected light from the water subphase. This was attributed to the residual amount of *s*-polarised light striking the surface. To overcome this difficulty a Glan-Thompson polariser (Melles-Griot) was added to the front of the laser. This

was mounted in an aluminium collar, built in-house, and this in turn was bolted onto a manual rotary stage (Ealing). Small adjustments around the Brewster angle could be made, see Figure 3.3. A Glan-Thompson polariser was selected rather than a sheet polariser, as it has a much higher extinction ratio,[4] 10^{-5} compared to 10^{-4} where the extinction ratio is defined as:[5]

$$\rho = \frac{T_1}{T_2} \qquad \textbf{Equation 3.1}$$

Where:

ρ = the extinction ratio,
T_1 = the maximum transmittance,
T_2 = the minimum transmittance.

Glan-Thompson polarisers are made from two pieces of calcite (transparent from ~5000 nm to 230 nm) that are usually cemented together by glycerine or mineral oil.[9] See Figure 3.2.

Figure 3.2 Glan-Thompson Polariser.

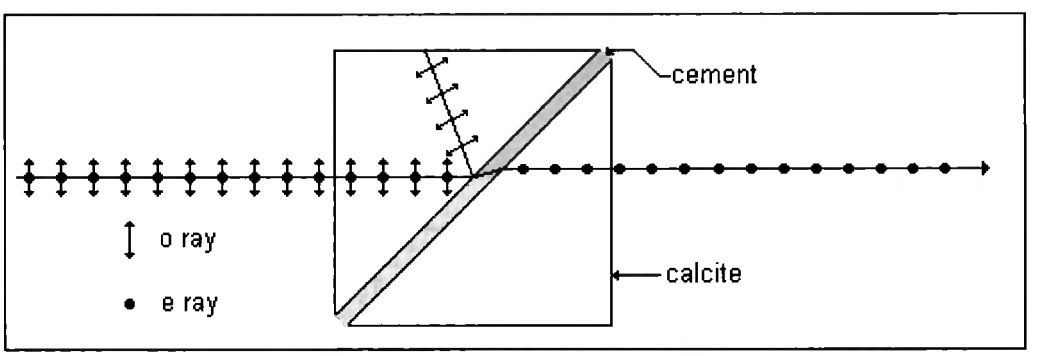

The incident beam is split into the extraordinary (e) ray and the ordinary (o) ray, which both travel through the calcite to the cemented region. The calcite is cut in such a way that the o-ray is totally internally reflected but the e-ray travels through.

Fischer *et al.* [6,3] performed many of their experiments with the polariser ~0.1°. and even 5° away from the Brewster angle as they found that this gave the greatest contrast in the images.

Figure 3.3. The laser head and attachments.

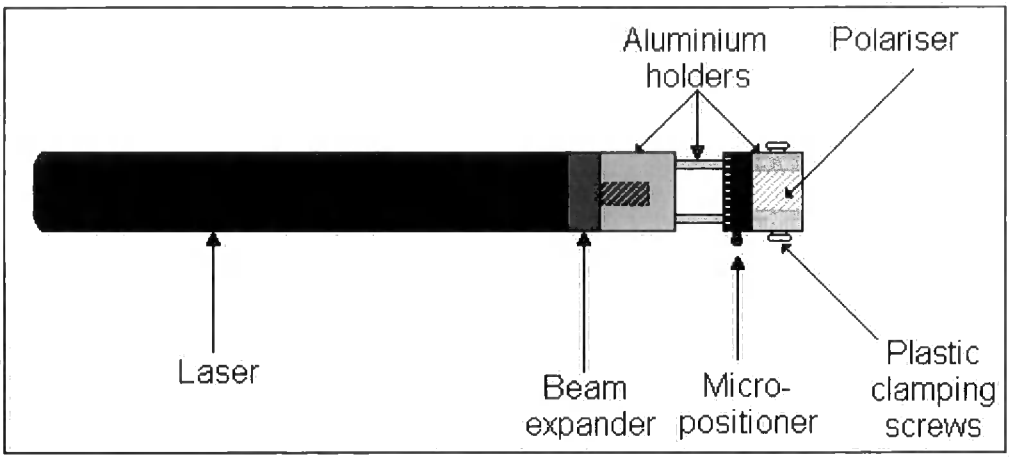

The first polariser (Melles-Griot, 03 PTH 401) was of standard quality but the aberrations in the calcite were so great that the image was streaked with interference patterns due to the coherent nature of the incident radiation. The signal of the camera is not linear with the intensity of the reflected light and so a background image could not easily be subtracted from the recorded film images. A laser quality polariser (Melles-Griot, 03 PTH 101) was then used, although there were still slight aberrations observed on the BAM images, higher quality polarisers are not available. The laser quality polariser was used in the *p*-polarised position as this gave good contrast and reduced the intensity of the aberrations.

3.1.2 Beam Expander.

The absolute intensity of the reflected light is proportional to the thickness and the anisotropy of the film and the intensity of the incident beam. It was important that the area under investigation was illuminated as uniformly as possible. At maximum zoom the microscope system imaged an area of 1.1 x 0.8 mm onto the camera's CCD chip. The small beam diameter of the He-Ne (0.8 mm) and the Gaussian profile of the beam meant that the area imaged

onto the CCD chip was not evenly illuminated. A 4x beam expander (Melles-Griot) was attached to the front of the laser, before the polariser, increasing the area under illumination to 5 mm^2. Although the beam profile was still Gaussian the CCD chip was more evenly illuminated see Figure 3.4.

Figure 3.4. The Gaussian profile of the beam.

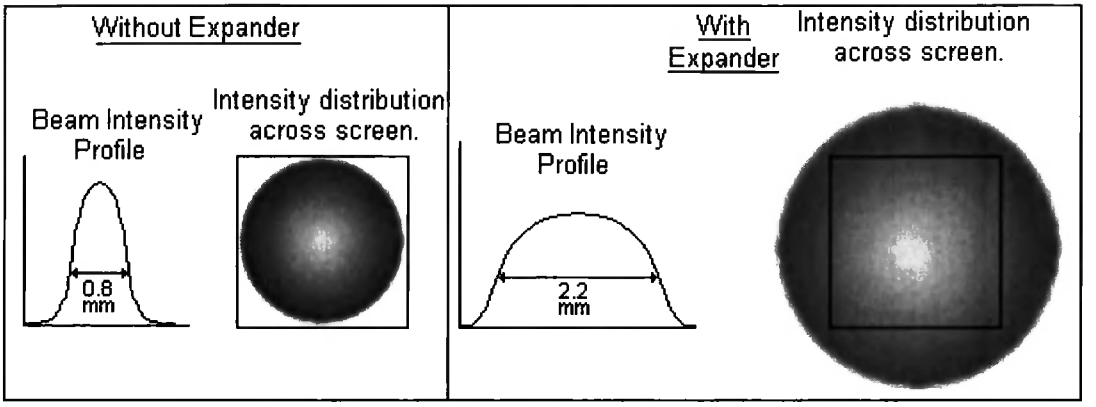

3.2 DETECTOR

3.2.1 Camera

A monochrome CCD camera (COHU, CCIR 4910 series) was used to image the surface. This was equipped with a ½" chip producing an image with resolution of 752 (H) x 582 (V) lines, and was connected to a monitor and to the frame grabber installed on a PC (Opus, Pentium). The COHU 4910 camera is capable of on-chip integration permitting images with very low intensity to be acquired. Control of the on-chip integrator requires the use of a specific frame grabber or control unit capable of providing the appropriate control signal. Initially the frame grabber (Neotech Ltd) was used in conjunction with an integration unit (Stealth 768, Vista Vision). This allowed multiple frames to be accumulated for one image enhancing the signal to noise. After an electrical failure in the integration unit the frame grabber was replaced by a different board (MuTech Corporation, MV 1500) equipped with 4 Mb of on board memory that was capable of directly controlling the CCD camera for long exposures.

Other groups[1,6] have observed circular artefacts on their images. These are known as Newton's rings which are due to the interference patterns that occur when the light reflects between the optical elements within the microscope and also between the CCD chip and its glass cover. It is possible to reduce this problem by removing the glass cover from the CCD chip but this is a difficult operation and the chip can be easily damaged.[13] Tsao[13] described two other methods of reducing the effect. The first was to use Fourier analysis to remove the interference but if the object of interest had the same length scale, then the rings and the object would both be eliminated. The second method was to use a fibre optic bundle as an image intensifier, at one end the bundle was cut at an angle to the signal being received and the other end was glued directly onto the input window. The intensity of the image was amplified by an image intensifier, the resulting intensified radiation was incoherent and so no rings were generated in the optical system.

3.2.2 Lens System

The optical concepts that are used to describe the lens system are briefly described below. *The field of view* of the camera is the visible area of the object imaged and is defined in millimetres. *The working distance* is the distance from the object to the lowest part of the optical system.

3.2.2.1 Resolution.

The magnification of an object may be increased by using a more powerful lens (a lens with an increased diameter and/or a shorter focal length) but eventually increasing the magnification does not increase the amount of detail that can be obtained from the image. At this stage the useful magnification is said to be exceeded. The ability to separate two points in an image is measured by the resolving power, which is an instrumental property, and the resolution, which depends on the detail available in the image. The Rayleigh criterion states that the images are resolvable when the central maximum of one coincides with the first minimum of the other, see Figure 3.5.[7]

Figure 3.5. Resolution.

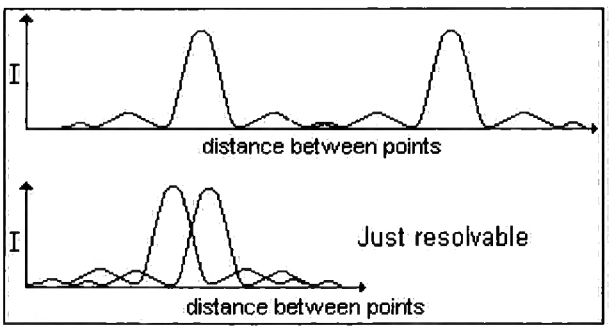

Using this criterion the minimal resolvable separation of incoherently illuminated points can be obtained:

$$d_{min} = \frac{0.61\lambda}{n \sin \alpha}$$ **Equation 3.2**

Where:

d_{min} = the minimal resolvable separation,

λ = the wavelength of the incident light,

n = the refractive index of the material,

α = aperture angle.

The aperture of a lens is defined as the amount of the lens that is illuminated and the aperture angle (α) is half the angle between the extreme rays reaching the lens from an object point. See Figure 3.6.

Figure 3.6. Aperture angle.

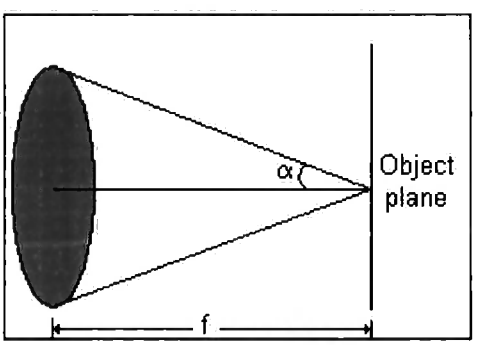

f = the focal distance, α = aperture angle.

The numerical aperture (NA) of an optical system is defined as $n\sin\alpha$, the maximum value this can be is 1 in air, (when $\alpha = 90°$), for example the NA of the human eye is 0.002. The square of the NA is proportional to the system's ability to gather light.

The resulting intensity from a coherently illuminated sample will depend on the change in phase of the light in the sample. The resolving power of a coherently illuminated sample is given by:

$$d_{min} = \frac{\lambda}{n\sin\alpha} \qquad \textbf{Equation 3.3}$$

Thus the resolving power of a coherently illuminated sample is slightly less that an incoherently illuminated sample due to the resulting interference.

It is clear from equation 3.3 that the magnification depends on the wavelength and so from this the maximum possible magnification using an optical microscope is 0.1-0.2 μm. An electron microscope with a beam of electrons (de Broglie wavelength of 0.0037 nm) has a magnification of the order of 0.005 nm.

3.2.2.2 Depth of Field and Focus.

The depth of focus is the axial distance above and below the geometric image plane, within which the image appears at an acceptable level of focus, see Figure 3.7 below.[8] The depth of field is the axial distance or depth, the specimen can be moved and it still appears in focus. Depth of field refers to object space and so is objective, whereas depth of focus refers to image space and is subjective according to the person viewing the image. For an imaging system, such as the CCD chip, the depth of focus is defined as the distance the chip can be moved whilst remaining at an acceptable level of focus. The depth of field and focus are often confused and are as such used interchangeably.

Figure 3.7. Depth of field and focus.

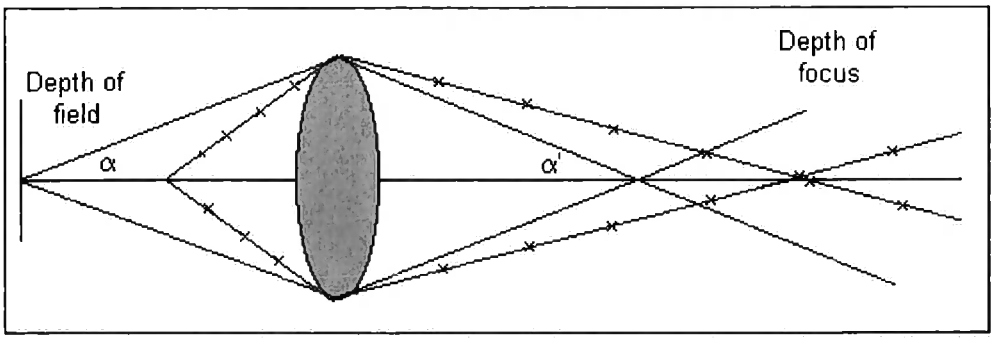

$$D_{Field} = \frac{\lambda}{NA \tan\alpha} \quad , \quad D_{Focus} = \frac{\lambda M}{NA \tan\alpha'} \qquad \textbf{Equation 3.4}$$

3.2.2.3 Magnification.

A point in an image will appear in focus if its diameter is less than Md_{min} where M is the magnification. Thus depth of field and focus are greatest in systems of restricted angular aperture. The magnification in the image is defined in the vertical and horizontal direction. The lateral (or transverse) magnification of an image is related to the focal length of the lens used:

Figure 3.8. Magnification.

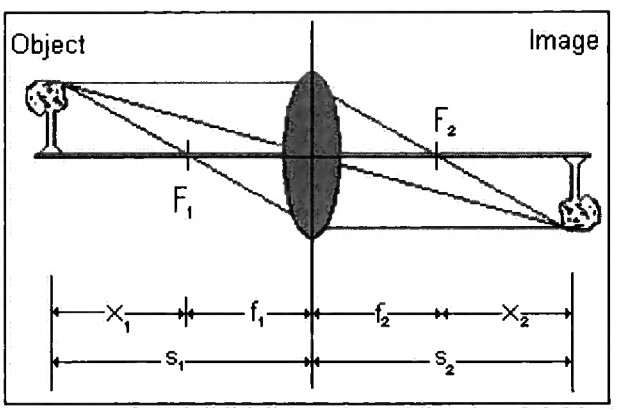

$$M_T = \frac{f_1}{f_2} \qquad \textbf{Equation 3.5.}$$

F_1 = the focal point of the lens,

F_2 = the second focal point of the lens,

f_1 = the distance from the first focal point to the image,

f_2 = the distance from the second focal point to the object,

s_1 = the distance from the object to the lens,

s_1 = the distance from the lens to the image,

x_1 = the distance from the object to the first focal point,

x_2 = the distance from the second focal point to the image.

A negative value of the magnification indicates that the image is inverted with respect to the object.

The vertical or longitudinal magnification is defined as the ratio of an infinitesimal axial length in the region of the image to the corresponding region of the object:[9]

$$M_L = \frac{dx_1}{dx_2} \qquad \textbf{Equation 3.6.}$$

This effect is normally too small in monolayer films to cause substantial errors but if the image plane is inclined the magnification changes across the image. Different points in the image will be magnified to different extents and this introduces a perspective error. A reticule may be used to measure this error across an image. Recent developments in the construction of telephoto lenses has lead to the production of telecentric gauging lenses which effectively eliminate the effects of perspective. These lenses have found applications in machine-vision systems. So far no equivalent microscope lens have been marketed with good optical performance and adequate magnification.

The image size goes as the square of the magnification, therefore if an image is magnified 4 times the image size is 16 times smaller, with correspondingly less light striking the detector.[9] Hence to maintain the same magnification the light source must be increased by an equivalent factor. An intense source is

therefore required to maintain the image quality but an intense source may damage the material being investigated or swamp the detector.

3.2.2.4 Optical Performance.

From equation 3.2 it is clear that the resolving power of a microscope depends on the NA. The NA is normally controlled by an iris that is positioned near to the lens. At high NA the depth of field is minimal i.e. only a thin section of the image is in focus, therefore continual adjustments of the focal plane are required. However reducing the NA by means of closing the iris (a pinhole that can be manually opened or closed) reduces the amount of light that passes through the lens and strikes the CCD chip, this in turn reduces the contrast of the images.

The depth of field becomes particularly important when the incident beam strikes the surface at an angle other than at normal incidence. Figure 3.9 below shows a beam striking the surface at a sharp angle of incidence. At point A the image plane will be focused above the surface, point B will produce a focused image of the surface but at point C the image is focused below the surface. The resulting image will thus have a narrow strip in focus in the centre, to overcome this there are 3 methods: (i) to scan the focus across the image recording focused strips and then recombining the strips to make a focused image but this takes time, (ii) use mathematical formulae to reconstitute the image and (iii) to use telecentric gauging lens.

Figure 3.9. Inclined incident angle.

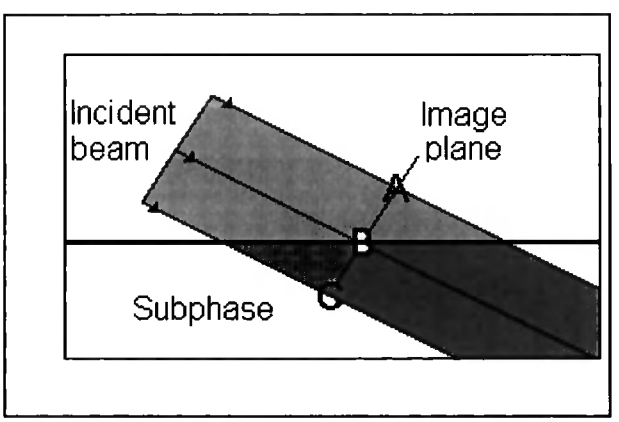

For optimum performance at the Brewster angle large depths of field and focus are required but this is achieved at the expensive of the resolution.

3.2.2.5 Our Magnification System.

Other BAM systems reported in the literature use microscope objectives to magnify the BAM image.[3,1] The short working distance of a microscope objective means that alignment of the lens system is difficult as it has to be positioned very close to the water surface. To change the focus the entire microscope objective has to be moved up and down the optic axis. Hönig[1] used an achroic lens to give a greater focal length (f = 25 mm), which improved the depth of field but reduced the resolution (see section 3.3). However the mounted lens system was only 4 mm away from the water surface. They had to place their lens system onto a linear positioner so that it could be moved above the trough to allow cleaning of the surface as the barrier could not pass underneath the lens. The magnification of a microscope objective is also fixed, to overcome this problem Hénon and Meunier[2] used two lenses positioned after the microscope objective which could be moved to change the magnification of the image.

In the system developed at Durham a telephoto macro lens (Optem Zoom 70 lens, model 29-96-91) was used rather than a microscope objective. The zoom lens had a variable focal distance (79-89 mm) which is considerably longer than the focal distance of an average high power microscope objective (< 10 mm). This allowed easy positioning of the lens system and also the trough barrier to pass freely under the lens. The elements in the Zoom 70 lens were encased in a tube and the magnification, iris and focusing were each adjusted by simply rotating 3 thumb-wheels. This meant that the lens could be rigidly mounted onto the rotary stage bearing the camera eliminating the need to use methods such as rack-and-pinion to focus or magnify the image. The large working distance also gives a relatively large depth of field and focus see equation 3.4 which is essential when viewing at the Brewster angle.

A 1x TV tube (Optem, 29-90-73) was used to mount the lens to the camera, a low power TV tube provides maximum field of view whilst a high power tube offers optimum resolution. A TV Tube is a hollowspacer that magnifies the image by increasing the distance between the lens and the CCD chip, see equation 3.5.

Adding a 2.0x auxiliary lens (Optem, cat. no. 29-20-14) between the TV tube and camera further increased the magnification as it increases the value of s_2 in equation 3.5. Due to the large incidence angle (~ 53°) only a small strip of the image was in focus (see section 3.2.2.2) and so to increase the area of the image that was recorded the focus of the lens was scanned across the image and several images were taken. At full magnification the average size of the strip was 0.2 x 0.8 mm wide, these focused strips were recombined using an image processing package (Paintshop Pro version 4.14). This gave a sharp image of dimensions 1.1 x 0.8 mm at maximum magnification and 6.6 x 5 mm at minimum magnification. As the focusing on the zoom lens was manually controlled this process took many minutes and any contact with the optical table disturbed the liquid surface, moving the region of focus out of the camera view. To overcome this problem the control of the focus was motorised so that is could be controlled remotely. A rubber edged disc was attached to a motorised micropositioner (Ealing), this was then clamped against the thumb-wheel of the focus, see Figure 3.10. The micropositioner had a hand-held control (Ealing) that meant that the focus could be scanned across the image and strips could be recorded quickly without causing disturbance to the surface.

Figure 3.10. The Optem Zoom Lens

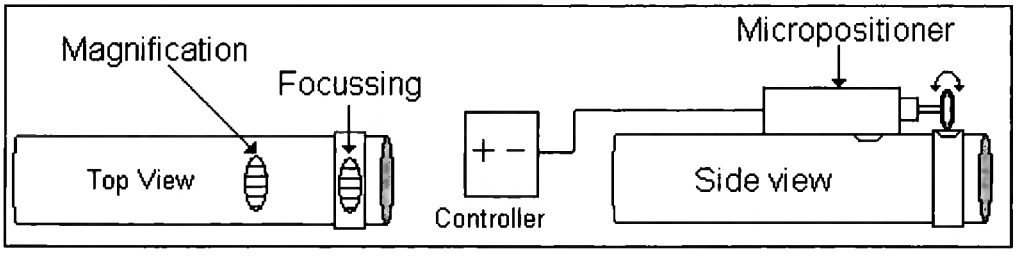

A method of automating the above process was considered for our system using a software package such as LabView. This would control the focus from a PC, take strips and then automatically combine the images to give a fully

focused image in a matter of seconds. Unfortunately the software was expensive and priced out of the constraints of our research budget. Commercial systems such as the NFT BAM2 now incorporate such systems.

Hénon and Meunier[2] used a similar method but recorded the greyscale (numerical) value of each pixel in the strips into a table and then used the table values to plot the final image. Hönig and Möbius[1] chose simply to use a lens with a large focal length and hence had a large depth of field (see section 3.2.2.2), this allowed the observation of rapid phenomena but reduced the spatial resolution (4 μm per pixel compared to Hénon and Meunier's 1-2 μm, see 3.2.2.1).

The camera was mounted on a plate in an aluminium U-shaped channel, which was designed and built in-house. The plate could be slid along the channel and the optic axis allowing easy adjustment of the working distance of the lens system, see Figure 3.11.

Figure 3.11. The Camera Mount.

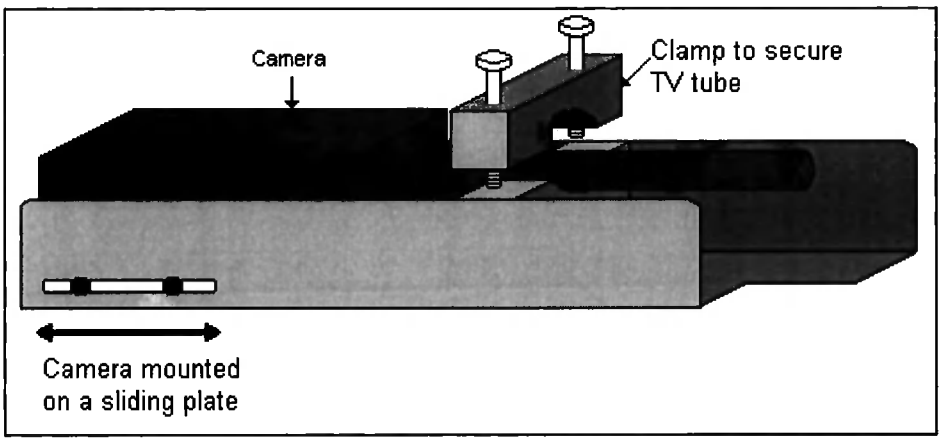

3.3 THE LANGMUIR TROUGH.

The first trough was introduced by Agnes Pockels in 1891 who simply used a rectangular tin trough, which was filled to the brim with water with the material of interest spread across the surface. The film was compressed using another strip of tin and a button attached to a small balance was used to measure the

surface pressure. Irving Langmuir proceeded to develop the trough which now bear his name and although the materials have changed the basic principle is still very much the same. Round and even diamond shape troughs have been produced. The round trough allows the use of a high ratio barrier for greater control over dipping speeds and the diamond shape trough means that the film is compressed symmetrically with low shear forces. Most troughs are fabricated from poly-tetra-fluoro-ethene (PTFE) which must be of high quality (i.e. no contaminants that may affect the isotherm). PTFE is resistant to most chemicals and has a very low surface tension. PTFE is a very difficult material to work with as it has a high expansion coefficient (95 x 10^{-6} /°C) and undergoes a solid-solid phase change at 20 °C.[10] The trough is usually milled from a single block of PTFE as the glue used to join pieces together may cause contamination or may dissolve when cleaned (chloroform is used). The low surface tension of the PTFE means that the trough can be overfilled by a couple of millimetres, the barrier is usually a strip of PTFE, wider than the milled out width of the trough. This is placed at the end of the trough, furthest from the pressure sensor, and the film is compressed by moving the barrier along the trough. The surface layer is contained between the edge of the trough and the barrier and so no leaks are possible for a Langmuir (insoluble) film. Langmuir-Blodgett troughs are designed in the same way except that they have a dipping well under the pressure sensor. Figure 3.12 shows some common trough designs.

Figure 3.12 a, b. Various trough designs.

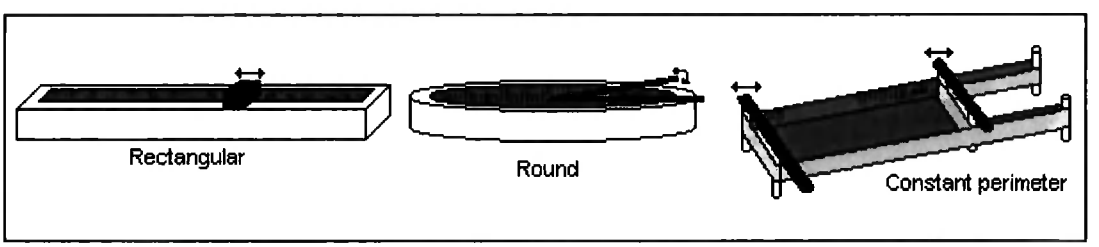

Another method of compressing the monolayer is to contain the monolayer film in a flexible plastic belt that is partially submerged into the subphase, this is known as a constant perimeter trough. This type of trough can be used to study a liquid/liquid interface as they are deeper and the liquid level is not critical (the trough is not overfilled). A constant perimeter trough can be

partitioned allowing alternate layer LB films to be deposited. A sketch of a constant perimeter trough is shown in Figure 3.12b above. The disadvantages of this design are due to the difficulty in cleaning the trough, a clean trough is essential and the belt is difficult to remove, compared to the PTFE block barrier which is simply held down by a spring-loaded arm. The constant perimeter trough requires a large amount of subphase solution, approximately 5L whereas a standard Langmuir trough requires typically 500 ml or less, cleaning and refilling the trough is therefore significantly more time consuming and expensive.

Virtually all of the light is transmitted into the subphase at the Brewster angle. The water depth in Langmuir troughs is usually only a few millimetres, thus the scattered and reflected light from the PTFE overlaps with the surface reflected light on the image. PTFE scatters light well and the reflected light from the bottom of the trough was of sufficient intensity to obliterate the BAM image. Using image processing software a spatial filter may be used to remove the scattering from the subphase.[13] The frequencies must be different to those of the surface reflected light, otherwise the reflected and scattered light will both be removed from the final image. Therefore removing the scattered light at its source is the preferred option, the deeper the subphase the great the distance between the surface reflected light and the PTFE scattered light.

Trough design was studied at the beginning of this project and two prototypes were built; a small trough (20 x 3.5 cm, 5 mm deep) and a larger trough (8 x 30 cm, 15 mm deep). The troughs and barrier were made from PTFE for the above reasons, the PTFE having been etched and glued onto an aluminium base.

The larger trough was 15 mm deep, this was of a sufficient depth that the scattered and reflected light did not overlap and a pinhole was used to allow the reflected light to pass through to the camera but block out the scattered light, see Figure 3.13.

Figure 3.13 Trough depth.

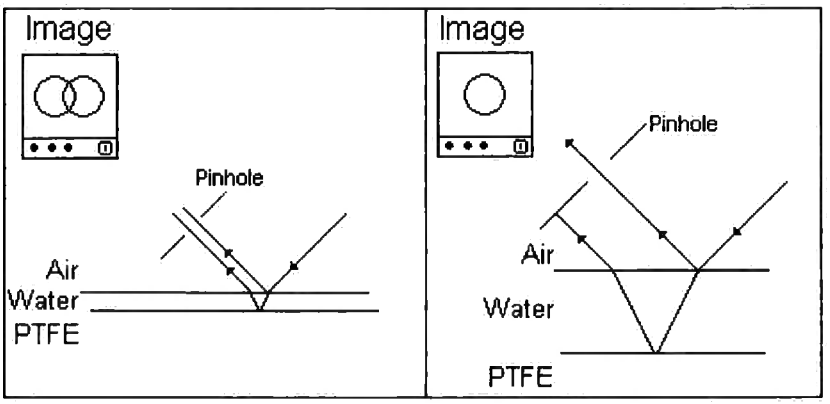

However the depth of the trough meant that it was very susceptible to movement of the table; any contact with the table resulted in waves travelling up and down the trough for some time, rendering this design unsuitable and thus another method had to be found to remove the excess light.

Nima Technology produce a PTFE trough (601BAM) with a scattering-reducing hole. This had a hole (2 cm in diameter) drilled through the base at the pressure sensor end with a quartz disc held in place with a threaded metal ring. This was so that light would be transmitted under the trough and away from the camera. The trough was long and narrow with a working area of 426 x 26 cm. This gave a high compression ratio and allowed easy positioning of the optics on either side of the trough but only required a low volume (~300 cm^3) of the subphase. However some reflected light from the disc was still recorded by the camera and several designs were looked at to overcome this problem. The light had to be taken out of the system but the material used had to be such that it could be cleaned easily but it was not likely to react with the subphase. Materials such as matt black plastic would be an ideal choice in terms of absorbing the light but they may introduce impurities and also desorb ions from the subphase that cannot be easily removed. Any impurities in the subphase could have a great effect on the resulting isotherms. Hönig *et al.*[11] used a piece of black glass dropped into the subphase to absorb the transmitted light, they also used a mirror to reflect light from the trough. We tested various designs fabricated from glass. Glass was chosen as it could be cleaned in acidic conditions to remove bound metal ions and organic materials and is also resistant to most chemicals. A Wood's horn was made from glass, this was

curved in such a way that the light is reflected down and out of the tip, see Figure 3.14. Such devices are used as beam dumps in high intensity laser experiments.

Figure 3.14 Wood's horn.

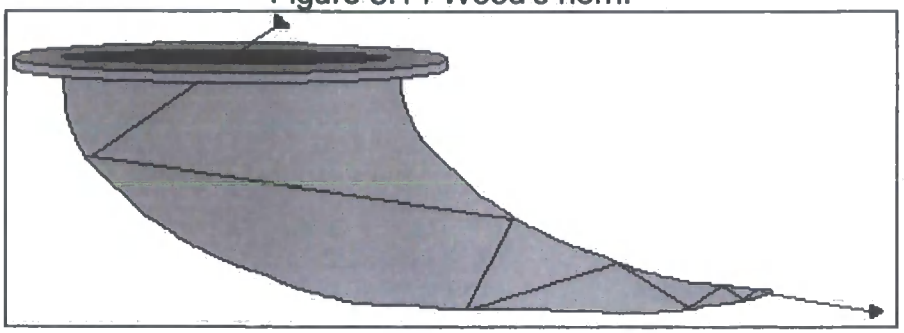

Although precise shape and curvature was not required it proved too difficult to produce a horn with uniform sides due to the small size required and some light was still scattered back into the camera. A simple "top-hat" shape was then used, this was made from a glass cylinder so that the sides were smooth reducing back scattering. The rim of the hat was ground flat and a good water-tight seal with the trough was ensured by wrapping this with PTFE tape. See Figure 3.15.

Figure 3.15. Top-hat

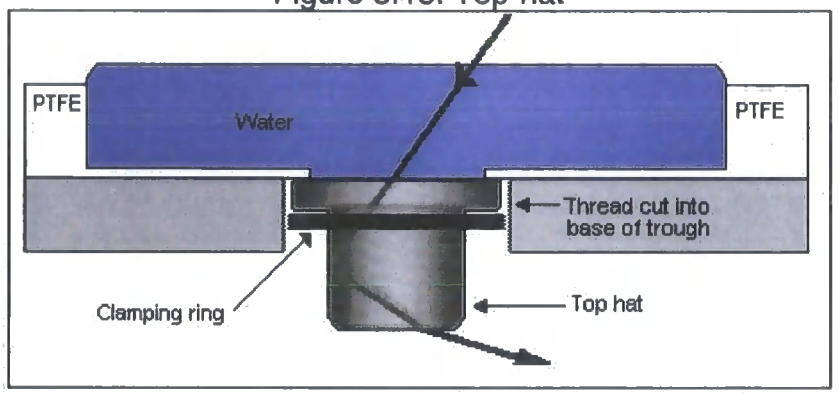

The surface pressure was recorded using a Wilhelmy plate (see section 1.1.2), the films were compressed using a mechanically operated PTFE barrier and the isotherms were recorded onto a PC using the supplied software (Nima). The Wilhelmy plate was a 10 mm strip of grade 1 chromatography paper (supplied by Nima) and had to be carefully positioned so that the plate was parallel to the barrier otherwise the meniscus produced by the plate interfered with the

images. As the images were recorded over the trough hole the camera could not be moved any further away from the Wilhelmy plate. The sensor was calibrated using the supplied weighing pan and weight and has an accuracy of ± 0.1 mN/m.

3.3.1 Cleaning

Any contamination of the trough would result in a change in shape of the isotherm and the resulting images. The trough and barrier were wiped with chloroform (Sigma, chloroform - methanol stabilised) soaked tissues (Kimberly-Clark Kimwipes). The trough was then filled with ultrapure water (Fisons Purite Still Plus, 18 mΩ) and the surface compressed to the minimum area. Any particles were then aspirated from the surface after which the barrier was opened. This was repeated until the surface pressure remained constant when the water surface was fully compressed, the barrier was then opened and ready for use. Chloroform was used as the spreading solvent for all experiments, see section 1.1.3.

3.4 ROTATION STAGES.

The camera and laser were each mounted on large rotation stages (Ealing 226 mm in diameter), which were vertically mounted on stands (Ealing). The stands had a series of holes drilled in to them so that the stages could be moved up and down allowing the camera and laser to be positioned at a variety of heights. Clamping the stands to the optical table (i.e. not directly bolted), allowed them to be placed anywhere across the table. The rotation stages were controlled by a Digital Positioning System (Ealing) which could in turn be operated by a PC or a hand-held controller (Ealing). The angle of the rotation stages could be adjusted to ± 0.00025°. The Brewster angle was determined by setting the laser to approximately 46.7° from the horizontal (as judged by a spirit level) and then small adjustments of the angle and polariser were made until the reflected light intensity reached a minimum. The camera was then set to the same angle and was moved across the table until an image was viewed on the attached

monitor. The zoom lens had an built-in diaphragm iris and this aided the alignment process, the angle and position of the camera were adjusted until the iris could be reduced in size to a minimum and the reflected light still travelled through to the camera i.e. the light was travelling along the optical axis. The rotation stages were then clamped into position and left at this angle for the experiment. This design was preferred over those published by other groups as it offered a greater amount of flexibility for adjustments within the system.

Many different approaches to mount the equipment have been investigated. For example Hönig and Möbius have reported two methods of mounting the laser and microscope system.[11,12] The first method involved mounting the laser and microscope system onto one mount which was referred to as the optical mount. The incident radiation was directed onto the surface at the Brewster angle using a mirror and the reflected radiation was magnified by a lens and detected by the CCD camera, see Figure 3.16.

Figure 3.16. Hönig and Möbius' set-up.

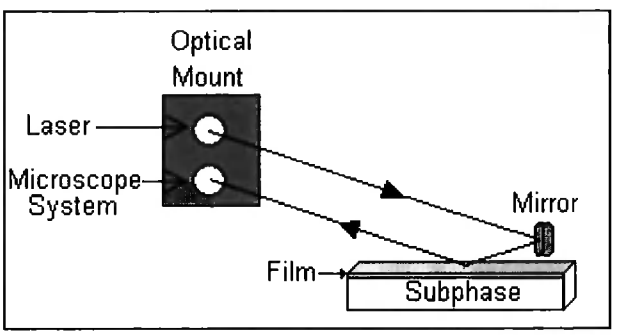

The second experimental method consisted of a laser that was fixed horizontally, a mirror was used to direct the beam onto the surface. The microscope system was mounted onto a linear stage which was in turn mounted onto a tripod. The microscope head was positioned by adjusting micrometer screws, which tilted the tripod, but such adjustments moved the reflected signal away from the optic axis and so the water height had to be increased accordingly.[1,12]

Using the present BAM systems it is not possible to observe one domain as the monolayer is compressed due to the camera and laser being fixed in position for the experiment. It would be advantageous to mount the laser and

microscope system onto horizontal linear stages so that the apparatus could be moved in all directions over the trough, this would allow a domain to be followed across the surface during compression. This would also increase the area of the trough to be studied as with the present system only a tiny area (0.88 mm^2 at full magnification) is under observation during the experiment. Practically this would be difficult to achieve as the rotation stages are heavy and would require substantial linear stages meaning that the trough may have to be mounted onto a separate anti-vibration table as the stages may cause vibrations and disrupt the film surface.

3.5 OPTICAL TABLE

To obtain sharp images a level surface is required, any vibrations may damage the film and may cause the liquid to flow out of the trough. The laser and camera are carefully aligned and any small vibration causes deviation of the reflected light from the optical axis and the resulting image may be lost from the screen or blurred due to the area of interest passing back and forth under the focus of the camera. The basic BAM kit had been designed but room for further expansion was required to allow for any changes during the building process. An optical table met both of these criteria, it reduced vibrations from the surroundings and the top was drilled with an array of threaded holes that allowed equipment to be positioned anywhere across the surface of the table.

An anti-vibration optical bench (Melles-Griot, 1.25 x 2.0 m) was initially used, this was mounted on 3 self levelling legs (Melles-Griot), the fourth leg acting as a pivot. The three self levelling legs each contained a piston that was joined to the table via a magnetic lever arm; if the table was disturbed air from an attached air cylinder was pumped into or released from the pistons adjusting the table level. Melles-Griot specified that the table levelled to ± 0.5 mm. However after extensive trials it was found that the table did not meet specifications and the water could not be contained in the trough (only a few mm in depth) due to the slope of the table after being disturbed. The table legs were exchanged for passively damped, free-standing legs (Melles-Griot). By changing the pressure in the 4 legs the table could be levelled, this was

monitored using an engineers spirit level. This arrangement was found to be stable and damped all vibrations sufficiently. The top of the table was stainless steel with M6 mounting holes with their centres on a 25 mm grid.

3.6 CASING

To prevent dust contamination and to retain a constant temperature Fischer *et al.* [3] covered their trough with a glass cover which was heated to prevent condensation. However they reported problems positioning the cover due to the limited space between the microscope objective and the surface of the subphase. Tsao[13] also reported that reflections from their glass cover interfered with the BAM image. Hönig *et al.*[1] encased their experiment in a box which reduced the air currents and dust contamination but did not interfere with the images. Although the zoom lens used in this work had a much greater working distance that might have allowed the use of a glass cover a Perspex box was used as it provided a simple and effective method of reducing dust contamination. The box was equipped with sliding doors on the front and removable side panels to allow easy access.

3.7 CALIBRATION

The calibration of the trough area was carried out by measuring the trough area with a vernier gauge and comparing this value to the value of the area displayed on the PC. The trough barrier was clamped onto a belt that pulled it along the trough, by simply unscrewing the clamp the barrier could be moved to the required position. An isotherm of stearic acid was recorded and this was compared to a literature value confirming the correct calibration of the trough area.[14]

A graticule (Comar) ruled at 10 μm was used to calibrate the scale of the images, this gave a horizontal resolution of 1.2 μm per pixel and a vertical resolution of 0.8 μm per pixel at maximum resolution. The reticule was also used to test for variations in the magnification across the image due to

perspective and depth of field effects. It was determined that such effects were negligible.

The equipment was tested against images of compounds from published BAM papers. The phospholipids (dimyristoylphosphatidylethanolamine) DMPE and DPPC were tested but no images could be obtained, it was discovered later that the chloroform used for film spreading was not of sufficient purity and this prohibited structure formation.[15] De Mul and Mann have studied 4'-octyl[1,1'biphenyl]-4-carbonitrile (8CB) and published BAM images and the corresponding isotherms. They found that this material formed large stable domains of approximately 10 μm in diameter on a uniform trilayer.[16] The pressure-area isotherm and the corresponding BAM images recorded by our system are shown in Figure 3.17:

Figure 3.17 Isotherm of 8CB.

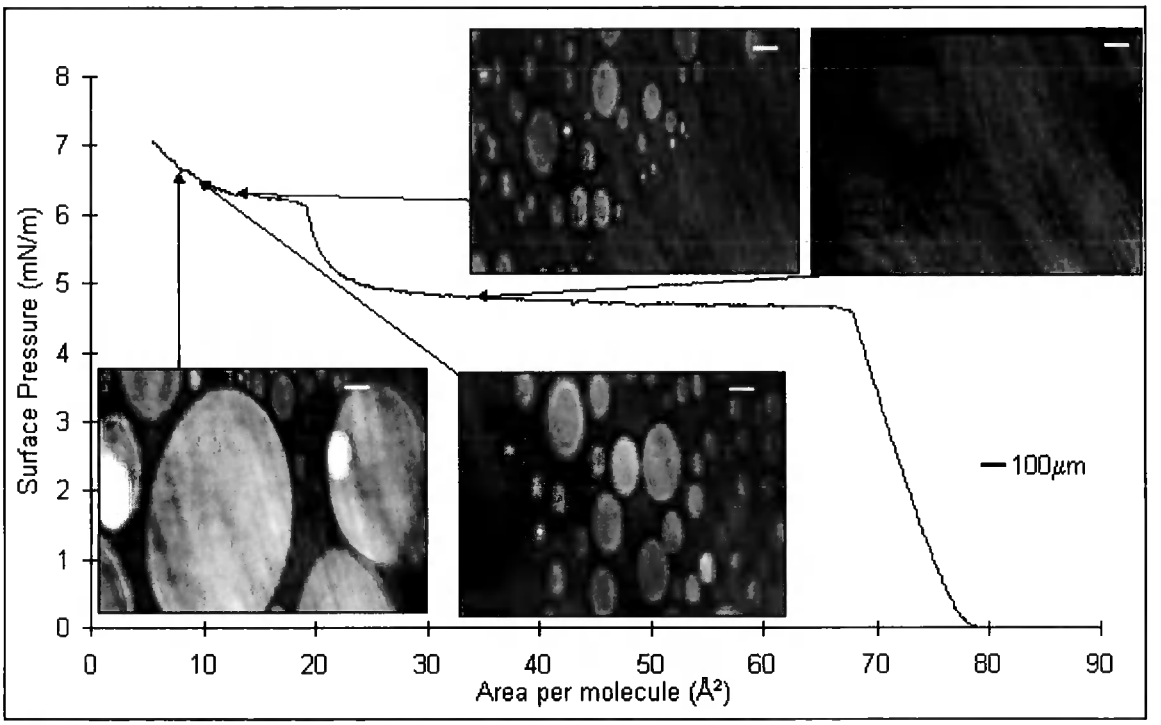

These images were recorded without the 2.0x auxiliary lens and with the standard polariser; the streaking of the images is due to the striae of the polariser. The image quality and magnification compared well with the published values, the only defect with our images being the streaking due to the standard polariser which was solved by using the laser quality polariser.

The ability of the camera to detect intensity changes was also tested. A film of 8CB was spread, compressed and multilayers were formed. The figure below shows the coalescence of a domain (indicated by the arrow). The brighter regions are of greater thickness and over a period of a couple of minutes the three thicker regions spread out and eventually join together. Thus the sensitivity of the equipment was satisfactory.

Figure 3.18 Coalescence of 8CB domains.

3.8 SOFTWARE

The images were recorded using the 8-bit CCD camera, giving 256 different shades of grey, however the human eye can only discern approximately 16 shades of grey.[17] As previously mentioned the intensity of the reflected light is proportional to the thickness of the film, therefore subtle differences in the film intensity and hence thickness cannot be easily detected by eye. Image processing techniques such as contrast stretching or false colouring are used to enhance the images and make the intensity differences more easily discernible to the eye. The eye can detect around one million different colours[18] and so a program that would false colour the images was needed. Although such programs were available they only came as part of large image processing software which were extremely expensive. The greyscale images were converted to binary files (ppm) and a program was written (Turbo Pascal 3, see Appendix A) to give a false colour composite image which was plotted onto the

screen. The screen grab option in image processing software captured the coloured image which could then be then saved to a disk.

---

1 Hönig, D., Overbeck, G. A. and Möbius, D. *Adv. Mater.* **4** (6). (1991).

2 Hénon, S., and Meunier, J. *Rev. Sci. Instrumen.* **62**, 936. (1991).

3 Fisher, B., Tsao, M.-W., Ruiz-Garcia, J., Fisher, Th. M., Schwartz, D. K. and Knobler, C. M. *J. Phys Chem.* **98**, 7430. (1994).

4 Melles-Griot Catalogue. (1997-8).

5 Driscoll, W. G. Ed. *Handbook of Optics*, Optical Society of America. McGraw-Hill 1978 USA.

6 Tsao, M.-W., Fisher, Th. M. and Knobler, C. M. *Langmuir.* **11**, 3184. (1995).

7 Slayter, E. M. and Slayter, E. M. *Light and Electron Microscopy.* Cambridge University Press, USA. (1992).

8 Rochow, G. T. and Tucker, P. A. *Introduction to Microscopy by Means of Light, Electrons, X-Rays or Acoustics.* 2nd Edition. Plenum NY.

9 Hecht, E. *Optics.* Addison-Wesley, USA. (1987).

10 Grunfeld, F. *Rev. Sci. Instrum.* **64**, 548 (1993).

11 Kaercher, T., Hönig D. and Möbius D. *Int. Ophthamology.* **17**, 341 (1993).

12 Hönig, D. and Möbius, D. *Thin Solid Films.* **210/211**, 64. (1992).

13 Tsao, M.-W. *Studies of Molecular Orientation of Langmuir Monolayers.* PhD Thesis. UCLA. (1994).

14 Mingotaud, A-F., Mingotaud, C. and Patterson, L. K. *Handbook of Monolayers.* Vol 1. Academic Press. (1993).

15 Weidemann, G. Private Communication.

16 De Mul, M. N. G. and Mann, Jr., J. A. *Langmuir*, **10**, 2311. (1994).

17 http://www.rspac.ivv.nasa.gov/nasa/education/reference/false/fascol.html

18 Hunt, R. W. D. *Measuring Colour*, 2nd edit. Ellis Horwood Ltd. (1991).

Chapter 4 A BAM STUDY OF 5,5'–METHYLENEBIS (N-HEXADECYL-SALICYLIDENEAMINE (MBSH).

The emission of solvent vapours is strictly controlled in most countries but at present there are few cheap, portable and reliable devices for sensing vapours.[1] The ideal detecting material needs to be non-volatile and allow the vapour to rapidly diffuse throughout its structure resulting in a short response time. This also allows evaporation of the vapour to give a short recovery time. Inorganic materials such as the tin or zinc oxides have been used for vapour sensing but often these have to be used at elevated temperatures and so are not practical as every day devices.[2] The semi-conducting nature of some LB films allows them to be used for electronic devices such as vapour sensors at room temperature.[3,4,5] Materials such as phthalocyanines[6,7] and porphyrins[8,9,10] have been used in devices that consist of 20 to 40 layers. Two methods of detecting the vapours are used; the first method uses the change in resistance of the film when exposed to an oxidising or reducing vapour. The second method detects the change in the optical properties of the film when exposed to vapours.[5,11] Changing the central metal ion in the macrocycle and substitutions to the ring changes the sensitivity and selectivity of the film. Vapours such as NO_2, Cl_2, Br_2, I_2, NO_2 H_2S, toluene and benzene vapour may be detected with such devices.[11]

The advantage of LB production over other methods, such as evaporation, is that the sensors are easy to manufacture and as a vacuum is not needed production is inexpensive. Although spin coating is a simple process it does not allow any control over the structural ordering or exact thickness of the deposited film, however this is possible with LB film production which offers significant benefits, see section 1.2. Sensors based on change in film resistance are produce by initially evaporating an interdigitated metal electrode such as gold,[12] silver[2] or platinum[5] onto the clean substrate and then depositing the LB film onto this substrate using the normal LB methods. A typical resistance sensor structure is shown in Figure 4.1 below:[11]

Figure 4.1 A Resistance Vapour Sensor.

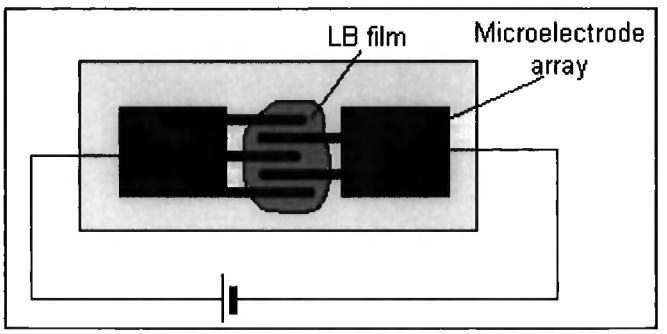

The device is then exposed to the vapour and the resistance monitored. Vapours can be detected by measuring the change in the optical response of an LB film. This type of sensor consists of a metal coated substrate, the metal is often silver approximately 50 nm thick.[13] The LB films are deposited onto this substrate in the normal manner. The technique of surface plasmon resonance (SPR) is used to measure the change in the properties. SPR measures the oscillations of free electrons at the boundary between a metal and a dielectric material, in this case the organic compound. The substrate is coupled to a glass prism and a photodiode is used with a laser (He-Ne) is used to detect a change in the reflectivity when the vapour of interest is passed over the LB layers. Reflectivity is recorded as a function of angle .[11]

A major drawback with LB devices is the degradation of the film material over time, commercial applications ideally require the devices to have a lifetime of at least 5 years. Research is moving towards the fabrication of polymer LB films which are thermally and mechanically more stable than low molecular weight materials.[14,15] The highly ordered structure of polymers facilitates the adsorption/desorption of the vapour from the active sensing sites.[10] Generally polymers are not truly amphiphilic, rather they are insoluble and tend to float on the surface resulting in less stringent structural requirements. They can therefore be manipulated more easily than low molecular weight materials to obtain the desired conducting or optical properties and yet they can still be transferred using the LB method. The two current methods of fabricating polymer LB films are by polymerising the film after deposition, using for example UV light,[16,17] and by directly depositing the polymer onto the substrate.[14,18,19] The second method has been applied Petty *et al.* (University of

Durham engineering department) who have successfully deposited polymeric Schiff base coordination complexes producing sensors that can measure benzene, ethanol, water and toluene vapour.[1]

Coordination polymers, in which the linked monomers linked by coordination bonds, are temperature resistant and potential applications include high temperature lubricants and surface coatings.[20] Metal complexes such as Schiff base metal complexes have fascinating chemical, optical, electrical and thermal properties[20,21,22] and have been successfully transferred onto solid substrates using the LB technique.[23] These polymers form coordination bonds with metal (II) cations to give stable films with conducting properties.

Petty *et al.* studied the behaviour of the polymer Cu(II) 5,5'–methylenebis(N-hexadecyl-salicylideneamine (poly (CuMBSH)) but found that it did not dissolve easily in common spreading solvents. However the monomer 5,5'–methylenebis(N-hexadecyl-salicylideneamine (MBSH) was soluble in chloroform. Hence they developed a procedure in which MBSH was spread at the air/water interface and polymerised by the addition of Cu (II) ions into the subphase. Using this method Y-type poly(CuMBSH) were successfully deposited onto quartz substrates. The structure of MBSH and poly(CuMBSH) are shown in Figure 4.2.

Figure 4.2 MBSH and Poly(CuMBSH) structure.

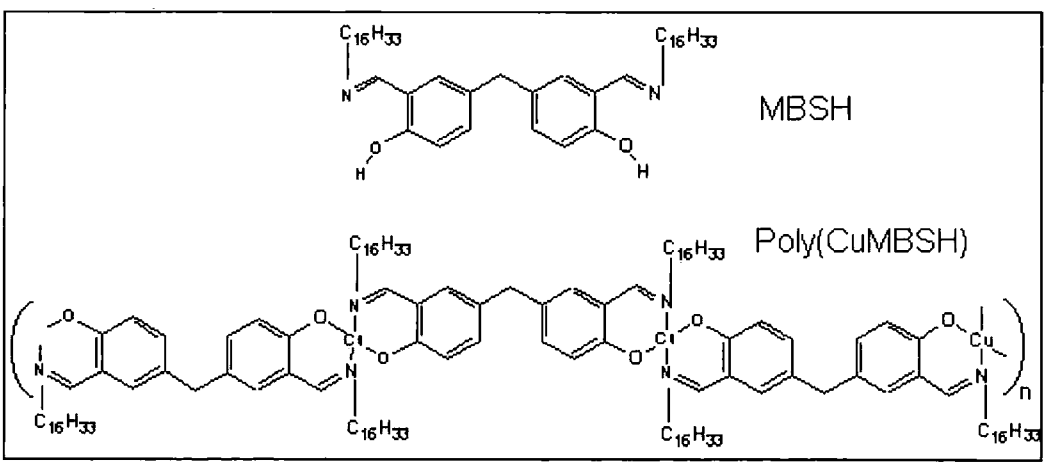

The UK Health and Safety executive recommends that the level of short-term exposure to benzene to be no greater than 160 vapour parts per million (vpm)

over a 15 minute period.[24] The poly(CuMBSH) vapour sensors were able to detect 100 vpm of benzene (in a nitrogen atmosphere) the response time was less than one minute and had a recovery time of 60 minutes with little background drift (a major problem with other devices[13]). The hydrocarbon chains form an open structure allowing vapour to react with the metal giving a fast response and also a fast recovery due to the ease of re-evaporation. After repeated exposure to benzene for 20 days there was little change in the response characteristics of poly(CuMBSH) thus making it a viable material for vapour sensing uses.[1] The device is also sensitive to water vapour (the minimum detectable limit was 1300 vpm) however such devices could be used as a disposable item due to the low manufacturing cost.

This chapter describes a BAM investigation into the morphology of MBSH and poly(CuMBSH) at the air/water interface to assist future developments in LB film production. BAM was used to monitor the polymerisation process at the air/water interface and clearly demonstrates the difference in structure between the monomer and polymer of MBSH.

4.1 CHARACTERISATION OF LB MBSH AND POLY(CuMBSH) FILMS.

The previous work carried out by Petty *et al.* is briefly described below. Work was carried out on films of poly(ZnMBSH) and poly(CuMBSH) but the focus of this chapter will be on poly(CuMBSH) and so only the results for poly(CuMBSH) are described. MBSH was synthesised using the method of Dey[25] by Dr. Jurgen Nagel at the Institut für Polymerforschung, Dresden. Petty *et al.* spread MBSH films over a pure water subphase (pH 5.8, 20°C), a headgroup area of 45 $Å^2$ was reported.[26]

The stability of the MBSH films was tested by spreading material at the air/water interface and leaving films for a varying amount of time. The films were then compressed but in each case there was no change in the resulting isotherm. This indicates that MBSH films are stable at the air/water interface.

The LB films were transferred to the substrate at a surface pressure of 20 mN/m, the pressure/area isotherm indicated that at this pressure a condensed film was formed and so film deposition was expected to be uniform (see section 1.2). They were unable to deposit a film of MBSH onto a substrate (glass, single crystal silicon or silvered glass slides) using the LB method but a monolayer was deposited by the Langmuir-Schaefer method (horizontal lifting method as described in section 1.2). This monolayer film of the monomer was used for comparisons with polymer films.

Subsequent work by Wilde *et al.*[26] has shown that MBSH LB films may be transferred when a fatty acid (tricosanoic acid (TA, $C_{23}H_{46}O$)) is included in the film at the air/water interface. Fatty acids are often used in alternate layer deposition as they act as "lubricants" for film production.[11] For example when transferring layers of long-chain amines the fatty acid donates a proton to the amine reducing the repulsion between layers. This produces a more stable and ordered film, the optimum molar ratio was found to be 1:1.7 MBSH to TA.[27] The fatty acid acts as a spacer improving the packing of the MBSH onto substrates (hydrophobic glass, single crystal slides and silvered glass slides). The first layer had a deposition ratio of 0.6 ± 0.1, which is poor see equation 1.9. Subsequent layers showed an excellent deposition ratio of 1.0 ± 0.1. The thickness of each layer was measured using low angle X-ray diffraction, alpha step measurements (surface profiling), surface plasmon resonance (SPR) and ellipsometry, the data from these experiments is given in the table below:

Table 4.1 Thickness of deposited MBSH/TA layers. [26]

Technique	Average layer thickness (nm)
X-ray	5.0 ± 0.1
Alpha-step	5.9 ± 0.5
SPR	4.98 ± 0.06
Ellipsometry	5.4 ± 0.2

Molecular modelling (Hyperchem) performed by Petty *et al.* estimate the length of the MBSH alkyl chain to be 2.8 nm, which should represent the thickness of a layer if a monolayer is deposited. Referring to Table 4.1 above it clear to

see that this theoretical value is approximately half that of the experimental values. The d-spacing from the X-ray measurements (see section 1.3.4) gave a value of 4.98 nm, this should reflect the repeat distance of each layer of the material and should be a symmetrical for Y-type deposition as shown in Figure 1.8. Two possible structures were suggested; the first is a bilayer with the second layer of MBSH inverted with respect to the first layer, the chains are interleaved; the second is with the MBSH stretched out and standing on one of its chains, these structures are shown in Figure 4.3.

Figure 4.3 MBSH/TA on solid substrates.

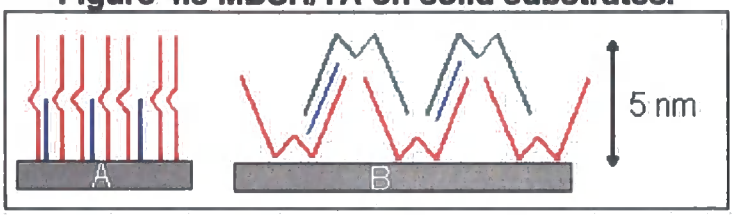

Both of these structures would account for the thickness of a layer (the interleaving of the chains cannot be resolved by the characterisation techniques). There has been no previous discussion of the structures that may be formed at the air/water interface by MBSH and poly(CuMBSH) but the structures for solid substrates shown above in Figure 4. are unlikely to be found at the air/water interface. The possible orientation of the molecules at the air/water interface will be discussed in further detail below.

Fourier transform infra-red (FTIR) experiments performed by Dr. J. Nagel determined that the polymerisation occurred between the azomethine nitrogen and the phenolic oxygen linking 2 MBSH units together.[28] Polymerisation of the MBSH was carried out at the air/water interface, MBSH was spread over a subphase containing copper (II) acetate at various subphase concentrations, this greatly altered the isotherm shape, an isotherm is shown with the BAM results in Figure 4.6 below.

Poly(CuMBSH) could be transferred onto a variety of substrates with a deposition ratio of 1.0 ± 0.1. A shift in the UV absorption spectrum was observed between the monolayer of MBSH and 10 layers of poly(CuMBSH) indicating that the film had reacted with the metal ion and that this metal ion

was transferred in the film to the substrate. Films of poly(CuMBSH) were found to be thermally stable.[26]

The LB films were then characterised by Surface Plasmon Resonance (SPR), low angle X-ray diffraction and ellipsometry.[26] The findings indicate that there is good order from layer to layer, the table shown below shows these results.

Table 4.2 Thickness of deposited Poly(CuMBSH) layers.

Technique	Average layer thickness (nm)
X-ray	2.26 ± 0.06
Ellipsometry	1.71 ± 0.25
SPR	1.97 ± 0.05

Molecular modelling performed by Petty *et al.* predicted the thickness of one layer of poly(MBSH) to be 2.8 nm, they account for the experimental value to be low due to the chains being oriented at 45° to the surface normal giving a height of 2 nm, consistent with the above results.[26]

Electron spin resonance (ESR) studies of poly(CuMBSH) suggest that the copper ion is oriented at 30° to the surface normal and the polymer is thought to have a zigzag type structure as shown in Figure 4.4. However these studies also indicate that there is poor order within each layer.

Figure 4.4 Poly(CuMBSH) structure.

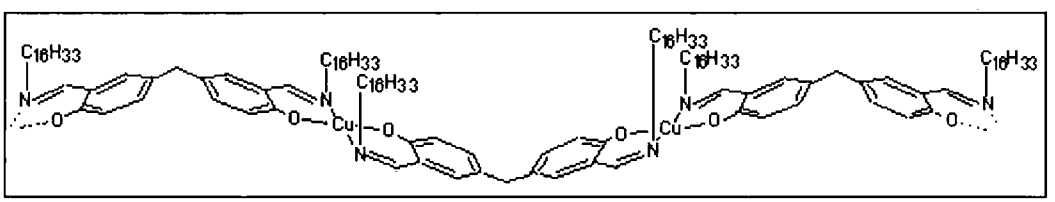

4.2 BREWSTER ANGLE MICROSCOPY STUDIES

The BAM experimental set-up described in chapter 3 was used to study the MBSH and poly(CuMBSH) film under similar conditions to those used by Petty

et al. for film production. No studies were carried out on the TA/MBSH films as at the time of the BAM measurements this technique had not been demonstrated by Petty *et al.* MBSH films on pure water were initially studied followed by an in situ investigation into the polymerisation of MBSH to poly(CuMBSH).

The trough was prepared for each experiment in the manner described in section 3.3.1, it was then filled with deionised water (conductivity < 0.02 μS/cm). MBSH was dissolved into ethanol stabilised chloroform to a concentration of 1 mg/ml. A small volume of the MBSH solution (typically 30 μL) was deposited dropwise onto the surface using a microlitre syringe. The surface pressure remained at zero at the maximum trough area of 125 $Å^2$/molecule, i.e. the film was in an expanded phase. The film was left for approximately 20 minutes to allow full evaporation of the spreading solvent. It was then compressed at 20 $Å^2$repeat $unit^{-1}s^{-1}$ until a domain of interest passed under the field of view of the microscope. During the compression process at large surface areas (> 60 $Å^2$/molecule) the domains could be seen on the monitor but passed under the microscope too quickly for a sharp image to be recorded. The compression had to be halted for the image to be recorded. At smaller surface areas the film moved very slowly or was stationary and images could be recorded without stopping the compression of the film. An image-isotherm is shown in Figure 4.5 below, the bar represents 50 μm.

Figure 4.5 MBSH image isotherm on a pure water subphase.

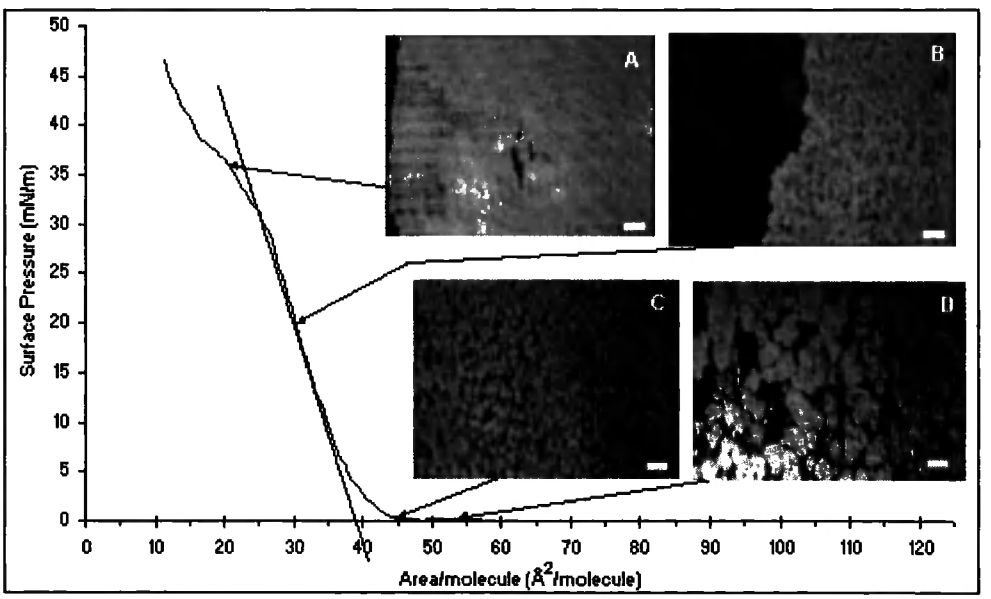

At high surface area (> 50Å^2/molecule) the domains were roughly circular and were approximately 40 μm in diameter as shown in Figure 4.5D. These domains moved rapidly across the surface as it was compressed. If the barrier was stopped they continued to move over the surface. As compression continued the domains were pushed close together but as they were solid they did not coalesce rapidly but crumpled at the edges. At approximately 60 Å^2/molecule a ripple was observed on the screen and the domains locked into a solid-like phase, then the domains moved very slowly across the surface of the water under compression. This change was not observed in the isotherm as the surface pressure was too low (Π = 0 mN/m). As the compression continued the domains merged together and they appeared to decrease in size, see Figure 4.5B and C. The water subphase was still visible as dark areas around the domains but the images lost their sharp structure.

BAM images show that at the surface pressure used for deposition (20 mN/m) the domains have formed large uniform rafts but the surface coverage is not uniform as shown by the dark edge (water subphase) in image A of Figure 4.5. BAM clearly shows that transferred MBSH films would not be homogeneous and therefore unsuitable for use as vapour sensors.

Petty *et al.* have shown that the polymerised form of MBSH (poly(CuMBSH)) could be deposited as uniformly deposited LB layers. The polymerisation was carried out at the air/water interface by spreading a film of MBSH over a subphase containing copper (II) ions. The next step was to repeat this experiment and use BAM to see if any structural changes could be observed. The minimum ratio of MBSH to copper (II) ions was 2:1 as 2 MBSH units were linked together with one copper (II) ion.

A solution of copper acetate was prepared (3.7 mg/L) in pure water, the trough was filled with this solution and the surface cleaned in the usual manner. MBSH (30 μL, 1 mg/ml) was spread and 20 minutes were allowed for solvent evaporation. The film was then compressed at 20 Å^{2}repeat unit^{-1}s^{-1}, but no structures were observed by BAM. However the overall intensity of the reflected light was greater than that observed for a plain water or a copper acetate subphase with no film, indicating that a film was present at the

interface. The pressure/area isotherm of poly(MBSH) is given below along with the isotherm of pure MBSH for comparison of the relative headgroup areas.

Figure 4.6 Poly(CuMBSH) and MBSH isotherms.

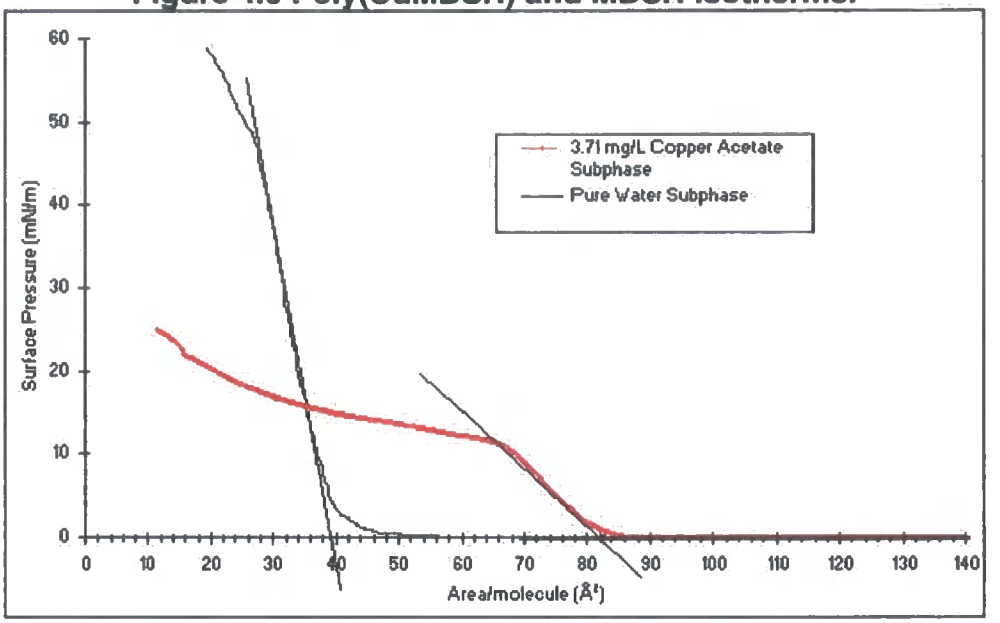

We calculated the headgroup area of poly(CuMBSH) to be 82 $Å^2$/molecule using a molecular modelling package (CAChe) which is consistent with the pressure/area isotherm value shown above. This strongly suggests that a homogeneous monolayer of the poly(MBSH) is formed.

The next stage was to see if BAM could be used to image the polymerisation process by injecting copper (II) acetate solution into the subphase of a MBSH film and observing the surface. The effect of injecting the copper solution into the subphase was initially investigated The trough was cleaned and refilled with pure water, a small volume of pure water (approximately 6 ml) was injected into the subphase increasing the surface pressure to 0.1 mN/m, this acted as a control. Copper (II) acetate (6 ml) was then injected into a pure water subphase to give a subphase concentration of 12 mg/L, i.e. a value significantly greater than the concentration used in the experiment. An increase of 0.2 mN/m was recorded but on compression of the barrier no further increase in the surface pressure was recorded. Thus, any change in surface pressure during the polymerisation process could be attributed to changes in the structures of the surface bound material and not artefacts due to surface active impurities in the copper (II) acetate or due to the addition process.

The surface was prepared for the BAM experiments by spreading a MBSH film over a pure water subphase (15 μL, 1mg/ml), 20 minutes were left for solvent evaporation. The film was compressed until a domain of interest passed under the microscope (at surface areas of 60-90 $Å^2$/molecule), the surface pressure remained at zero. Previous BAM experiments have shown that in this region the film is stable and is not greatly affected by convection currents, thus one domain may be studied for some time, an image was recorded and this was termed as time zero. The copper acetate was then injected into the subphase, behind the barrier to reduce surface noise, to give a subphase concentration of approximately 4 mg/L. Images were then taken during the polymerisation process which took approximately 40 minutes to complete. The integration unit was used to enhance the contrast of the images but the image acquisition conditions were kept constant throughout the experiments. Hence any changes in the reflectivity could be used to provide information regarding the structural ordering of the surface, in particular the film thickness. When the area per molecule was less that 80 $Å^2$/molecule prior to injection of the Cu (II) ions the surface pressure of the film increased during the polymerisation process. This is due to the rise of the poly(CuMBSH) isotherm see Figure 4.6. The polymerisation process as observed by BAM is shown in Figure 4.7 below, these images were recorded at 90 $Å^2$/molecule. During the course of the measurement the surface pressure increased from 0.0 ± 0.1mN/m to 0.2 ± 0.1 mN/m on addition of the copper (II) acetate:

Figure 4.7 Polymerisation of MBSH.

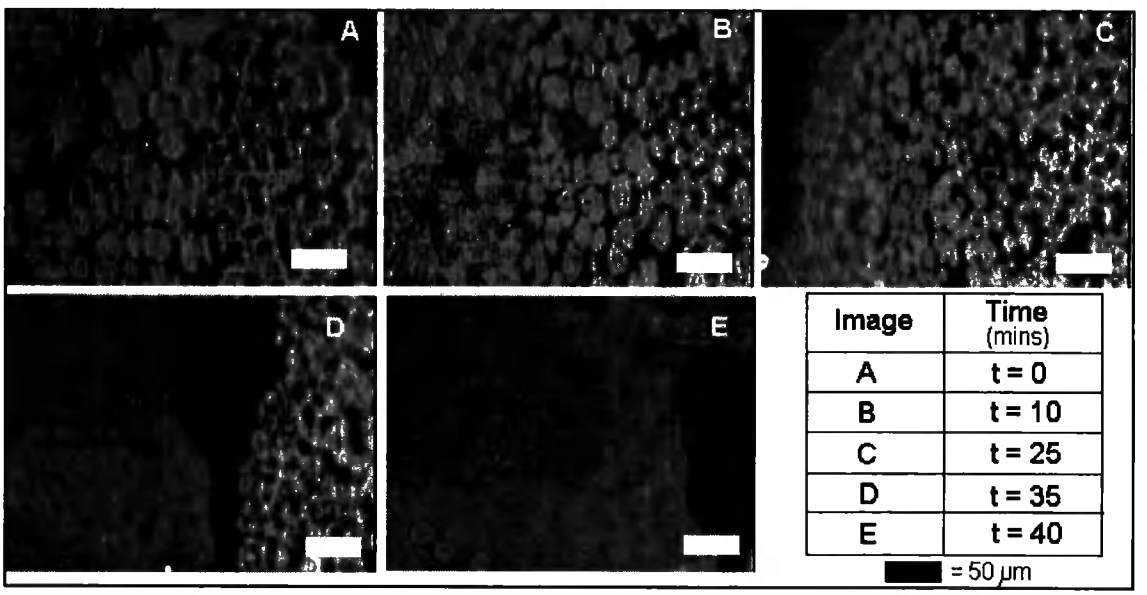

Image A was taken at time = 0, image D was taken after 35 minutes and image E was taken 40 minutes after injection of copper (II) acetate into the subphase. Image D shows two rafts of material; a partially polymerised region on the right and a fully polymerised region on the left. The degree of polymerisation is determined the homogeneity and the thickness (intensity) of the imaged film. An increase in the homogeneity and a decrease in the image intensity denotes greater polymerisation. The film was then compressed and the resulting isotherm was identical to that of the poly(CuMBSH) isotherm shown in Figure 4.6 and so the film is fully polymerised. To aid the interpretation of the images, images A, D and E were false coloured using the software described in Appendix A.

Figure 4.8 Coloured images of the polymerisation process.

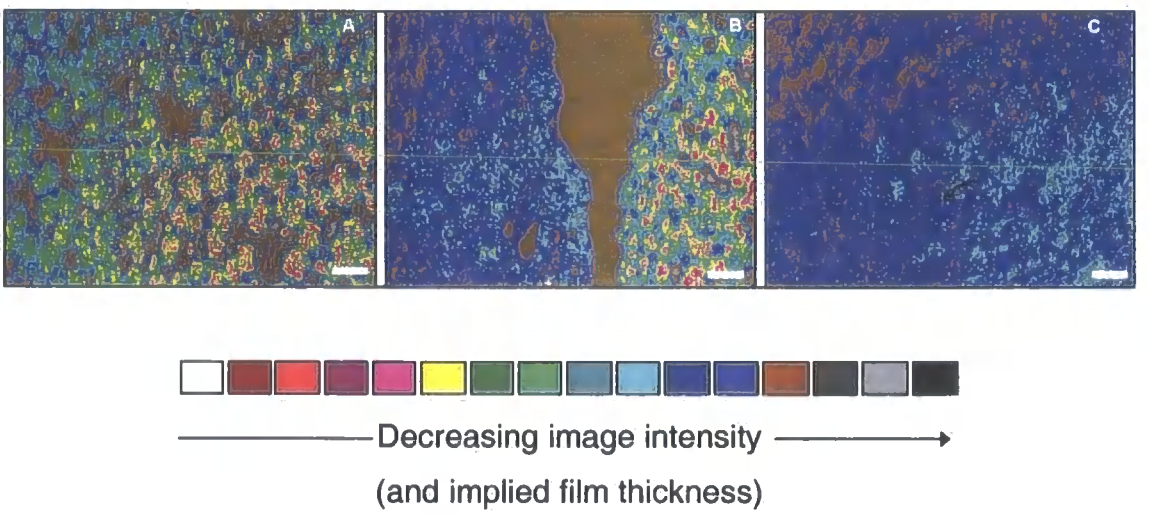

Image A of the pure MBSH shows MBSH domains on a water subphase. Image B (Figure 4.7D) shows a film of similar thickness on the right hand region of the image but the left hand region is clearly reduced in thickness. The final image C is of lower intensity than the film in image A and B, no further change in reflectivity was noted in subsequent images indicating that the polymerisation process was complete.

Ellipsometry measurements performed by the engineering department gave a refractive index of 1.52 for MBSH and 1.56 for poly(CuMBSH). The intensity of the images should therefore increase slightly as the film polymerises. The

decrease in film reflectivity can be attributed due to a decrease in film thickness only.[26]

The headgroup area of poly(CuMBSH) is calculated to be 80 ± 5 $Å^2$/molecule (CAChe). The film collapses above this point but the collapse is smooth as the layers slide over each other, no changes in the surface structure are observed.

The above results raise a number of questions concerning the structure of MBSH at the air/water interface, this is discussed in further detail below.

4.3 DISCUSSION

The exact orientation of the MBSH molecules on the pure water subphase is not known, however the BAM experiments clearly show that the area taken up by the film increases during polymerisation and the film thickness decreases. Two possible explanations have been derived.

The first is that MBSH forms bilayers on pure water and upon addition of copper (II) ions these bilayer domains polymerise, and thus expand, to form a monolayer. The limiting area/molecule obtained from the isotherm (See Figure 4.5) indicates a surface area of 39 ± 2 $Å^2$/molecule for the MBSH. Clearly this value is markedly different from the 75 $Å^2$/molecule calculated by Petty *et al.* using Hyperchem molecular modelling programme and an assumed internal angle of 114°. Our computer modelling gave a value of 70 - 80 $Å^2$/molecule, a more exact value could not be calculated without the constraints of the water subphase being included. The simplest explanation for this observation is that on a pure water surface MBSH forms bilayers. This is supported by the BAM results which show the high reflectivity of the MBSH domains which are characteristic of a multilayer structure. Addition of copper (II) ions into the subphase polymerises the film and increases the area to just over more than double that for pure MBSH. It is perceived that two overlaid MBSH molecules expand to form one planar molecule with the addition of one copper (II) ion. This also accounts for the decrease in film thickness and is substantiated by the decreasing intensity of the BAM images.

The question that arises from this theory is the possible structure of the bilayer. If the molecules are aligned as proposed in Figure 4.b, what would be the driving force to flip the upper layer and bring it to the surface? It is likely that the OH groups are directed into the water but the chains are perpendicular to the water surface and the nitrogens are lifted from the water surface. Using molecular modelling (CAChe) the area of the MBSH was estimated to be 46 $Å^2$ in this configuration, a value that is consistent with the observed pressure area isotherm. As the film undergoes polymerisation the MBSH flattens out, the nitrogen is dragged down onto the water surface increasing the area decreasing the overall thickness of the film.

The layer sitting on the water surface would be able to interact readily with aqueous Cu (II) ions forming the polymer but the upper layer would not be completely polymerised. This means that the film would vary in thickness, however the images of the poly(CuMBSH) film appear uniform. The limiting headgroup area indicates that a complete monolayer is formed.

A more feasible structure of the bilayers is where the upper layer is not inverted but simply sits at an angle (approximately 90°) to the lower layer as show in Figure 4.9A below:

Figure 4.9 MBSH structure on water.

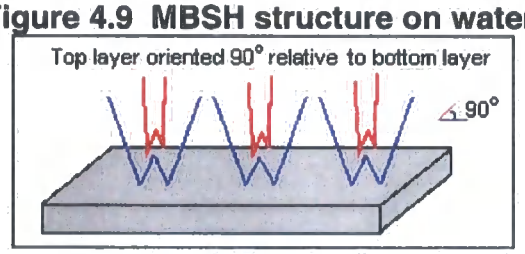

As the polymerisation process begins the lower layer becomes planar bringing the upper layer closer to the surface so that it too may be polymerised.

The second theory is that the molecule sits as a monolayer, the molecules are stretched out with one chain oriented towards the water surface as shown in Figure 4.3A. Ashwell *et al.* have used SHG to demonstrate that certain long chain dyes do sit on the water surface in this manner.[29, 30] This arrangement is

consistent with the experimental observations, the rings would be pulled down to the water surface during polymerisation, increasing the limiting area and decreasing the film thickness. However this means that the long hydrophobic chains are sitting on the surface which is energetically unfavourable especially at low surface coverage.

The pressure/area isotherm of poly(CuMBSH) indicates a collapse at 80 ± 5 $Å^2$/molecule but no changes in the images are observed. Similar isotherms are recorded with the 8CB multilayers, the isotherm showed a smooth transition from a trilayer structure to a five layer system, see figure 3.17. Poly(CuMBSH) has very little affinity for the water surface, and so when compressed the film will collapse easily, the only hindrance being caused by the alkyl chains.

4.2.2 CONCLUSIONS

MBSH forms inhomogeneous layers at the air/water interface with rough circular domains approximately 40 μm in diameter. These domains are postulated to be bilayers. With the information provided by BAM it is clear that MBSH itself forms an inhomogeneous layer and hence explains the findings that it cannot be readily transferred to a substrate as an LB film.

Upon addition of copper (II) ions the film rearranges on the water surface to give the ribbon-like poly(CuMBSH) with an area/molecule of approximately double that of MBSH, this film is homogeneous. During this process the BAM image intensity decreases indicating that there is a decrease in the thickness of the polymerised film. The film appears flexible and at pressure above 20 mN/m a collapse occurs to form a multilayer. On a copper (II) acetate subphase MBSH spreads forming a uniform monolayer, this provides an excellent film for deposition as it appeared to be free from defects.

This work has demonstrated that BAM can be used as an informative and diagnostic probe for Langmuir monolayers prior to deposition and that it may be used in situ to directly observe the progress of polymerisation processes. Although the technique is not quantitative at present further information may obtained from the images by comparing the intensity of the images.

1 Wilde, J. N., Nagel, J. and Petty, M. C. *Thin Solid Films* **327-329**, 726 (1998).

2 Zhu, D.-G., Cui, D.-F., Petty, M. C. and Harris, M. *Sens. Actuators B.* **12**, 111 (1993).

3 Shin, H-K., Choi, Y-S., Lee, B-J. and Kwon, Y-S. *Synth. Met.* **86**, 2253 (1997).

4 Milella, E., Musio, F. and Alba, M. B. *Thin Solid Films* **284-5**, 908 (1996).

5 Mukhopadhyay, S., Hogarth, C. A., Thorpe, S. C. and Cook, M. J. *J. Mater. Sci.: Mater. Electron.* **5**(6), 321 (1994).

6 Baker, S., Roberts, G. G. and Petty, M. C. *Proc. IEEE, Part 1.* **1p12130**, 260 (1983).

7 Woltjen, H., Barger, W. R., Snow, A. W. and Jarvis, N. L. *IEEE Trans. Electron. Devices* **32**, 1170 (1985).

8 Tredgold, R. H., Young, M. C. J., Hodge, P. and Hoorfar, A. *Proc. IEEE, Part 1.* **132**, 151 (1985).

9 Loschek, R. and Möbius, D. *Chem. Phys. Lett.* **151**, 176 (1988).

10 Smith, V. C., Batty, S. V. Richardson, T., Foster, K. A., Johnstone, R. A. W., Sobral, A. J. F. N. and Rocha Gonsalves, A. M. d'A. *Thin Solid Films*, **284/5**, 911 (1996).

11 Petty, M. C. *Langmuir-Blodgett Films, An Introduction.* Cambridge University Press (1996).

12 Hann, R. A., Gupta, S. K., Fryer, J. R. and Eyres, B. L. *Thin Solid Films*, **134**, 35 (1985).

13 Granito, C., Wilde, J. N., Petty, M. C., Houghton, S. and Iredale, P. J. *Thin Solid Films* **284-5**, 98 (1996).

14 Nagel, J. and Oertel, U. *Polymer* **36**(2), 381 (1995).

15 Adams, J., Rettif, W., Duran, R. S., Naciri, J. and Shashidhar, R. *J. Phys. Chem.* **97**, 2021 (1993).

16 Hodge, P., Davis, F. and Tredgold, R. H. *Phil. Trans. R. Soc. Lond. A.* **330**, 153 (1990).

17 Christie, P., Petty, M. C., Roberts, G.G., Richards, D. H., Service, D. and Stewart M. J. *Thin Solid Films.* **134**, 75 (1985).

18 Oertel, U. and Nagel, J. *Thin Solid Films.* **284/5**, 313 (1996).

19 Rikukawa, M. and Rubner, M. F. *Langmuir*, **10**, 519 (1994).

20 Bajpai, U. D. N., Rai, S. and Bajpai, A. *Synth. React. Inorg. Met.-Org. Chem.* **24(10)**, 1719 (1994).

21 Patel, M. N., Sutaria, D. H. and Patel, J. R. *Synth. React. Inorg. Met.-Org. Chem.* **24(3)**, 401 (1994).

22 Woodman, P., Hitchcock, P. B. and Scott, P. *Chem. Commun.* **24,** 2735 (1996).

23 Nagel, J. Oertel, U., Friedel, P., Komber, H. and Möbius, D. *Langmuir*, **13**, 4693 (1997).

24 Health and Safety Executive EH40/97, Occupational Exposure Limits, HSE Books, Suffolk, 1997.

25 Dey, A. K. *J. Indian Chem. Soc.* **63**, 357 (1986).

26 Wilde, J. N. *Optical Sensing of Organic Vapours Using Langmuir-Blodgett Films.* PhD Thesis, Durham, UK. (1997).

27 Wilde, J.N., Wigman, A. J., Nagel, J., Öertel, U., Beeby, A., Tanner. B. and Petty, M. C. *Acta Polymer.* **49**, 294 (1998).

28 Nagel, J. and Oertel, U. *Thin Solid Films* **327-329**, 495 (1998).

29 Ashwell, G. J., Jeffries, G., George, C. D., Ranjan, R., Charters, R. B. and Tatam, R. P. *J. Mater. Chem.* **6**, 131 (1996).

30 Ashwell, G. J., Jackson, P. D., Jeffries, G., Gentle, I. R., Kennard, C. H. L. *J. Mater. Chem.* **6**, 137 (1996).

Chapter 5 PROPERTIES OF POLYPHENYLENEVINYLENE'S AT THE AIR/WATER INTERFACE.

As technology grows so does the demand for high quality thin screen devices with low power consumption and good resolution. For the next generation of displays there are two thin film types of interest at present; polymer dispersed liquid crystal displays (PDLC) and light emitting polymer devices.[1] PDLC's consist of a polymer matrix with droplets of a birefringent liquid crystal embedded and one of the refractive indices of the liquid crystal is the same as that of the matrix.[1] In the absence of an applied field the display scatters light as the molecules area randomly oriented. When an electric field is applied the liquid crystal molecules become aligned with the forward direction of the matrix and a reduction in the scattering intensity is observed. However this contrast may not be sufficient to observe the display under direct illumination . Light emitting polymers (LEPs) such as conjugated polymers are self emitting and so have better contrast allowing a viewing angle of 180° and can be used in low light conditions. These polymers combine the physical properties of polymers such as being light and flexible with excellent electrical properties (semi-conducting). Thus displays can be produced that are flexible, large in size, innovative in design and inexpensive. The polarisers, colour filters and backlights that are used in conventional displays are not required. PDLCs use a low voltage dc source with a low power consumption making the polymer displays lightweight with many potential applications in portable devices. The luminescent intensity is such that LEPs are under investigation as lasing medium.[2]

Conjugated polymers have double or triple bonds between carbons enabling the formation of a delocalised π electron cloud over several atomic sites along the polymer backbone. This produces delocalised π valence (bonding) and π^* conduction (anti-bonding) bonds with a definite bandgap which is the requirement for semi-conducting behaviour. Conjugated materials are often strongly fluorescent and may have π-π^* energy gaps in the range 1 - 4 eV (1240 – 310 nm) spanning the Near IR to the UV making them extremely useful for optical devices.[3]

Devices based upon these polymers are produced by methods such as spin coating or by the Langmuir-Blodgett technique. Unlike traditional semi-conductors LB films can be produced in atmospheric conditions greatly reducing the cost and complexity of production. Although light-emitting polymers are not as stable as inorganic semi-conductors and their response times (approximately 2μs) are slower due to the non-crystalline structure of the polymer, their response times are sufficient for most devices. Films produced by spin coating are amorphous, whilst the advantage of the Langmuir Blodgett technique is that it enables control over the position and orientation of the molecules in the film producing more ordered films (see section 1.2). During the LB dipping process the molecules may exhibit a preferential orientation allowing the preparation of devices with polarised light emission.[4] Also spin coating requires a relatively large amount of the expensive polymer compared to the LB technique. This chapter will focus of the materials used for producing polymer LEDs by the LB technique. The typical structure of a working LED device is shown in Figure 5.1 below:

Figure 5.1 LED structures.

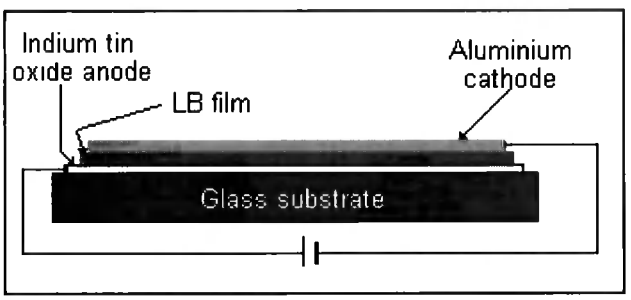

The first polymer LEDs were produced by the Cambridge Display Technology (CDT) in 1990 using Poly(para-phenylenevinylene) (PPV) and they have produced a light emitting diodes on flexible substrates,[5] as well as complex devices. For example working with Seiko-Epson they have produced a black and white TV display that is 50 mm^2 and 2 mm thick.[6,7] Many PPV's derivatives are currently under investigation for LB fabricated LED applications.[1,3,8,12] PPV itself is difficult to process as it not soluble in the common spreading solvents (see section 1.1.3) so substituents such as alkoxy groups are added to aid solubility. These substituents are also used to fine tune the luminescent spectrum as they subtly

alter the bandgap. LEDs of different colour may be fabricated i.e. red, green and blue LEPs which are essential in making colour displays. Because of the low solubility of the final polymer PPV precursors (usually a salt such as *p*-xylene-bis-tetrahydro-thiopenium[9]) are often deposited onto the substrate as they are much more soluble in chloroform. After deposition on to the substrate e.g. quartz the film is then thermally treated to convert the salt to PPV.[10,11]

The Physics and Engineering departments at the University of Durham are studying two derivatives of PPV for use as polymer light emitting diodes; poly(2-methoxy, 5-(2' ethylhexyloxy)-*p*-phenylenevinylene) (MEH-PPV)[12] emitting at 587 nm and Poly(2, 5 – dihexyloxy)-*p*-phenylenevinylene (DHPPV)[13] emitting at 590 nm, their structures are shown below in Figure 5.2.

Figure 5.2 MEH-PPV and DHPPV.

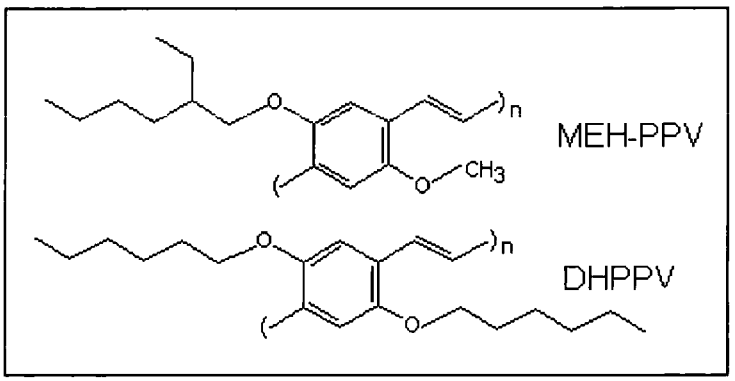

Brewster Angle Microscopy has been used to study these polymers at the air/water interface prior to deposition to try and optimise the monolayer. A brief outline of the work performed on MEH-PPV by the engineering and physics departments is initially described below followed by the BAM work, the DHPPV studies are then similarly discussed.

5.1 CHARACTERISATION OF MEH-PPV ON SOLID SUBSTRATES.

Petty *et al* produced MEH-PPV films by spreading a film (200 μL, 1.8 mg/ml dissolved in chloroform) over a water subphase in a constant perimeter trough (working area = 600 cm^2). The film was compressed (10^{-2} $Å^2$ repeat $units^{-1}$ s^{-1})

and the isotherm was recorded. The MEH-PPV film was found to withstand surface pressures of 40 mN/m and was stable at 20 mN/m for at least 12 hours. The limiting headgroup area was 2.7 $Å^2$, this is far too small for the molecular dimensions, suggesting that the MEH-PPV is forming multilayers, although this was not discussed in the original paper.[12] The normal dipping pressure was 20 mN/m giving Y-type deposition with a deposition ratio of 0.9 ± 0.1, inferring that the transferred layers are not uniform because the dipping ratio is defined as being from a monolayer, see equation 1.9 so this value is not an accurate reflection of film transfer. MEH-PPV was deposited onto quartz and glass slides patterned with indium tin oxide (ITO) strips (1.5 mm wide). To complete the device aluminium strips (1mm wide) were evaporated on top of the LB films to make the second electrode, see figure 5.1. The working area of the LED was typically 1.5 mm^2, using films with 46, 64 and 150 MEH-PPV layers were studied.

Alpha-step measurements were performed on the deposited layers and gave an average layer thickness of 10 Å.[12] Sluch *et al*[12] argue that this value is too small for the molecular dimensions suggesting that not all of the polymer is transferred and that some simply "falls back" to the spread film, again indicating that a multilayer is formed under these conditions. Literature reports indicate PPV layers to be 3.4 Å thick,[10] Kim *et al* determined layers of the PPV precursor salt (*p*-xylene-bis-tetrahydro-thiopenium) to be 15 Å.[9] In light of these range of values a thickness of 10 Å for a MEH-PPV layer is a reasonable value.

A straightforward test of reproducibility of film transfer from the water surface to the substrate is to record the optical absorption (UV/visible) spectrum. The Beer-Lambert law means that the absorbance should be proportional to the concentration of the absorbing species. This was found to be the case for MEH-PPV showing that although transfer of the film to the substrate is poor on a macroscopic scale the same amount appears to be deposited each time. The photoluminescence spectrum was independent of the number of layers and increasing the number of layers simply increased the photoluminescent intensity proportionaly. When operated as an LED the MEH-PPV films had an intensity of

100 Cd/cm^2 under an applied voltage of 5 – 10 V, a similar value to that observed by a cathode ray tube.[14]

The optimum thickness of an MEH-PPV film for LED devices was determined to be 64 layers. These films had a fluorescence decay lifetime of 1.4 ± 0.3 ns, much greater than that observed for spin coated films (0.58 ns[15]). The difference in results can be interpreted in two ways; firstly that the extent of delocalisation is reduced in spin coated films which in turn reduces the oscillator strength and radiative rate constant; secondly that the morphology in the LB films means that there is a greater degree of inter-molecular interaction.[12]

Informal discussion with Dr. Sluch indicated that deposition was found to improve when the water subphase had been left to "age" for 3-4 days. Although no reasons were given for this ageing process it may be due to changes in the pH of the subphase, brought about by the absorption of atmospheric CO_2. It has been shown that small changes in pH (or ion concentration) can affect monolayer formation and hence the shape of the pressure area isotherm.[16] This effect is discussed in more detail below.

5.2 RESULTS OF BAM STUDIES OF MEH-PPV.

MEH-PPV was obtained from the Physics Department (a gift from Dr. I. Samuel, synthesised by Hoescht) and spread using chloroform (99 +% pure, Aldrich). A solution of 1mg/ml was made up and a spreading volume of 20 µL added to the subphase to give a trough area of 120 Å^2/molecule. The isotherm shown in Figure 5.3 was generated by compression and indicates a limiting headgroup area of 20 ± 2 Å^2. As the domains were relatively large the images were not recorded at full magnification to allow several domains to be visualised in one image.

Figure 5.3 MEH-PPV image isotherm on pure water.

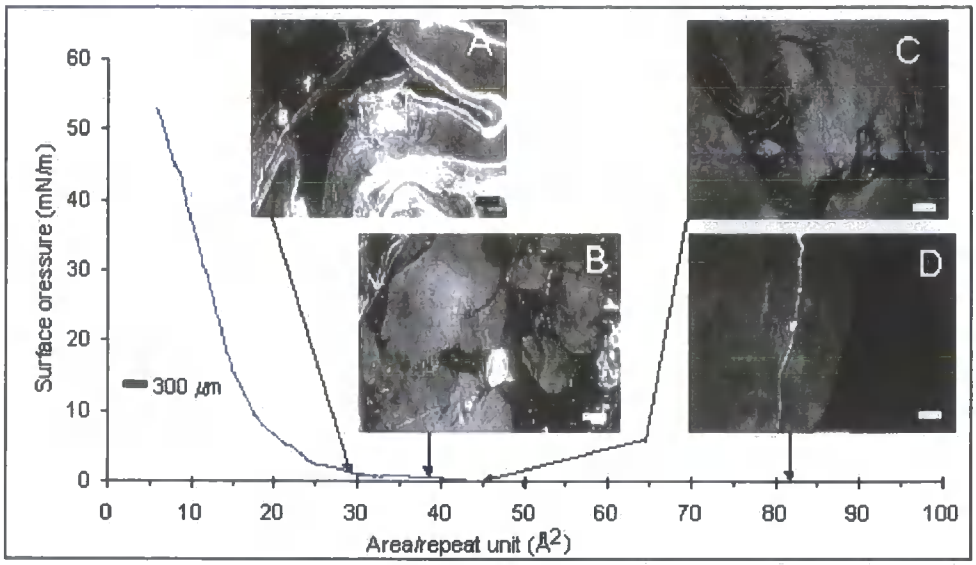

PPV derivatives are reported to form condensed layers at the air/water interface.[8;17] This is confirmed by large rafts of material observed in the BAM images obtained in this work, the domains are not uniform at large area/molecule. Even at low surface pressures Figure 5.3A shows regions of increased brightness due to multilayering. When compressed the domains tended to crumple rather than coalesce, a phenomenon indicated by the brighter lines on the images, implying that these rafts of polymer are extremely rigid. Figure 5.4 shows an image of MEH-PPV on a pure water subphase which has been false coloured to show more clearly that the film consists of multilayers of MEH-PPV.

Figure 5.4 False coloured image showing various MEH-PPV layers.

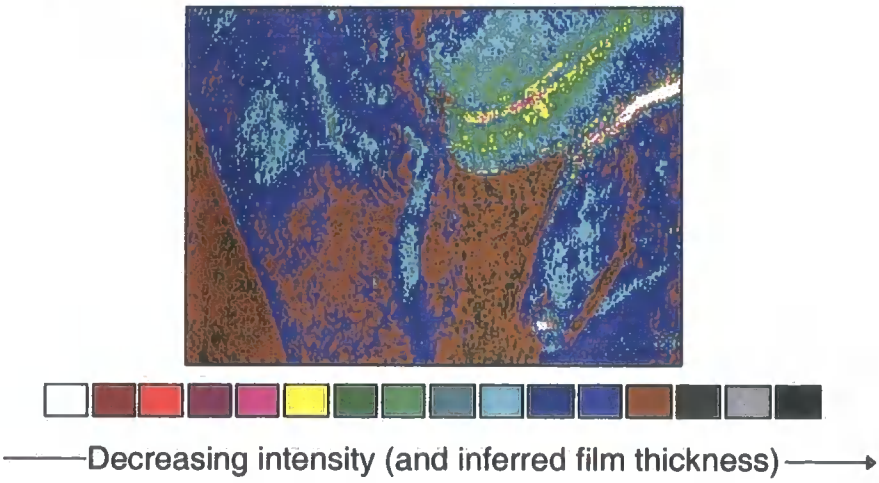

This image shown in Figure 5.4 was recorded at 47 $Å^2$/molecule (Π = 0 mN/m) i.e. before the increase of the surface pressure and the onset of the condensed phase. It is clear from the range of intensities across the image that even at surface pressures well below the dipping pressure multilayers are formed. This is because the initial spreading of the film is inhomogenous due to the rigidity of the material.

Sluch had found that film production was better on old water i.e. water that has been left standing for a few days in the trough in a dedicated clean room. The reasons for this practise were not explained nor did he carry out any experiments to determine the cause of this change and shortly after the discussion returned to Moscow. It was not clear whether the water had been left to age with or without the polymer film spread across the surface, thus both conditions were investigated. To discover the reason for improved film deposition with the aging of the subphase a systematic study of MEH-PPV films at the air water/interface was performed in our laboratory utilising a variety of conditions.

A film of MEH-PPV was spread over a pure water subphase and the isotherm with the corresponding images was recorded, see Figure 5.3. The experiment was repeated 24 hours and 48 hours after deposition, the results are shown below.

Figure 5.5 24 hour old MEH-PPV film.

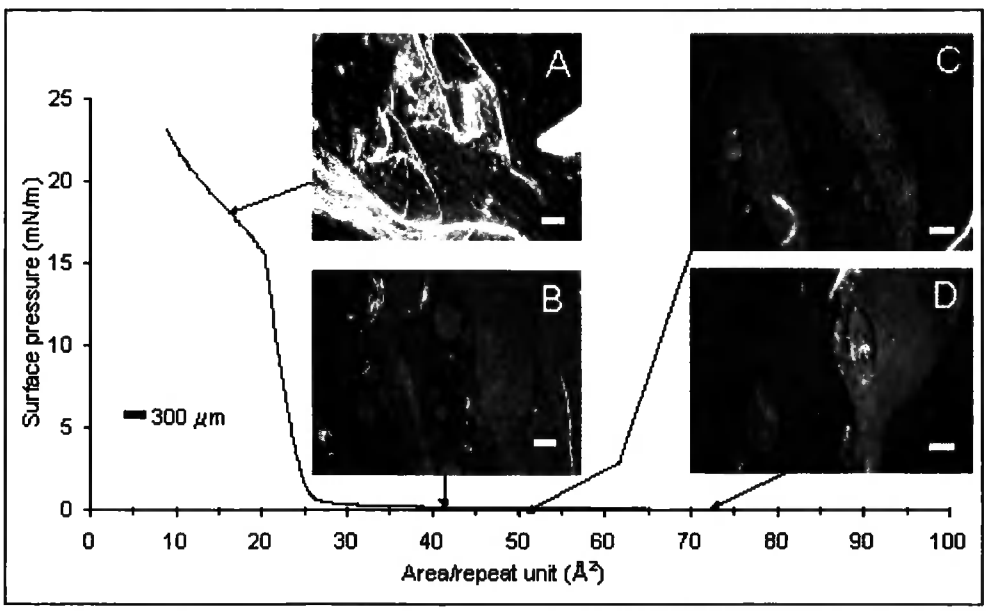

Figure 5.6 48 hour old MEH-PPV film.

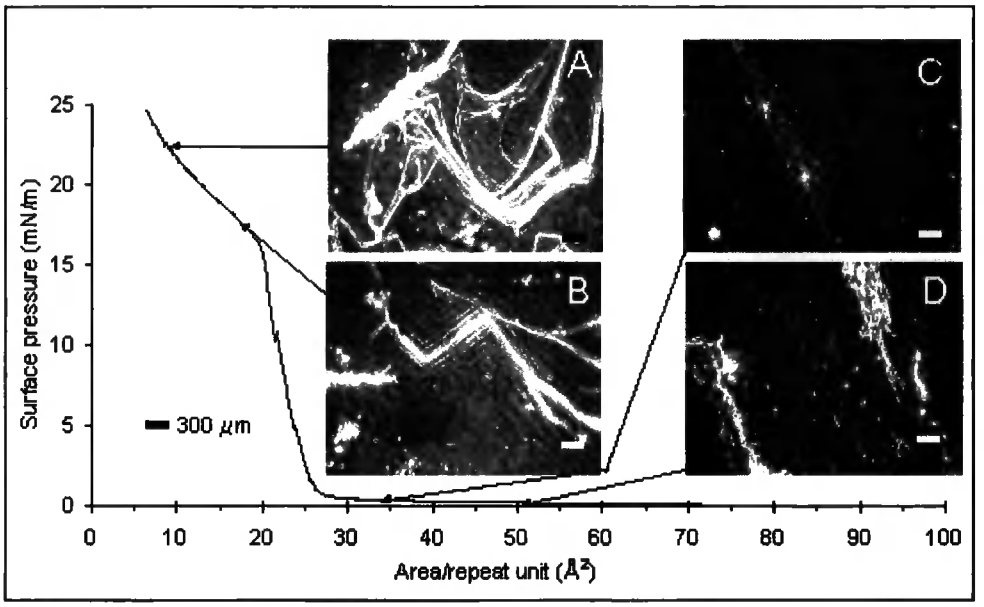

The shapes of the isotherms of the 24 and 48 hour old films were markedly different to that of the pure water subphase. A shoulder appears in the isotherm (approximately 17 mN/m, 20 $Å^2$/molecule) as the film begins to age indicating that there is some rearrangement process occurring. The area/molecule also increases to 25 ± 2 $Å^2$. Large domains are observed in the 24 hour old film but the images of the 48 hour films shows poor film quality and that the film is extremely rigid and does not relax after compression. Annealing of the MEH-PPV films is discussed in section 5.2.1 below.

To determine the cause of this change a number of experiments were carried out to eliminate various factors. The change in the isotherm could have simply been due to the recompression (annealing) of the film, some polymer films are inelastic and so on recompression a different isotherm is recorded. The MEH-PPV films are known to be photosensitive, it was therefore possible that the film was simply decaying on the surface. Sluch used a glass trough for a variety of previous experiments, leaving water in the trough for several days could cause materials (e.g. metal ions) to leach out of the glass into the water subphase in turn changing the isotherm shape. However in this work a PTFE trough was used a material chosen for its chemical resistance but the possibility of contamination had to be

investigated further. The experiments were carried out at different times of the day and so temperature could cause a change in the observed isotherm. A series of experiments were then performed to try and ascertain the cause of the changing isotherm shape.

5.2.1 Annealing

The film was recompressed several times, initially it was compressed to an area of 10 $Å^2$ and then on the second compression the surface pressure of the film did not increase until 10 $Å^2$/molecule where the increase was near vertical, see figure 5.7. The third compression also showed this sharp behaviour but no shoulder was observed. This again indicates that the film is extremely rigid and is not relaxing when the barrier is opened after compression, the rigidity of the film means that the deposition will not be even as there will not be an even flow of material over the substrate and this is reflected in the low deposition ratio reported by Sluch *et al.*[12]

Figure 5.7 Annealing of MEH-PPV film of fresh water.

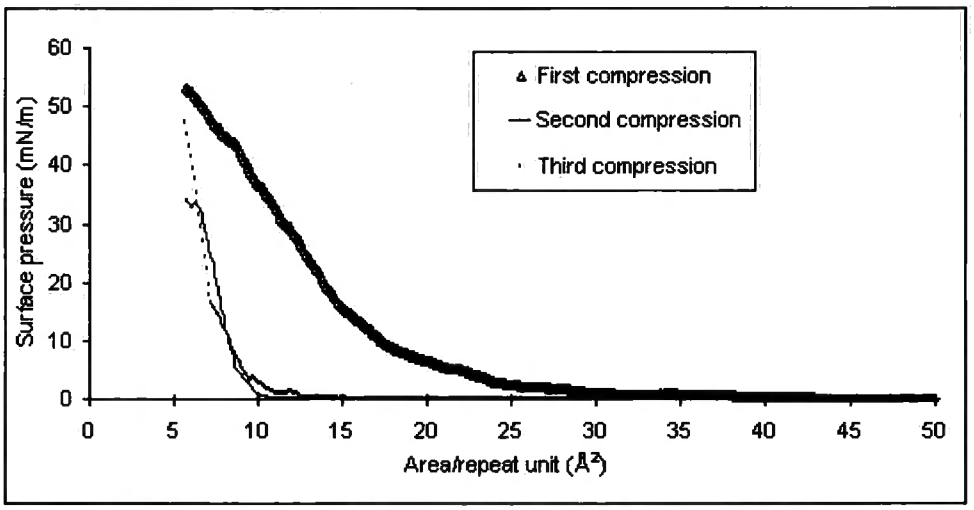

Annealing of the MEH-PPV on old water gave a repeatable isotherm indicating that this film is more flexible which is the most likely reason for the improved transfer of the film to the substrate.

Samuel *et al*[18] suggested that the CNPPV was arranged on the water with the molecule lying flat on the substrate and the alkoxy chains interdigitated. A similar ordering of MEH-PPV on the water surface would explain the change in isotherm shape with the annealing. After initial spreading the polymer would be well dispersed on the water surface but when compressed the alkoxy chains would mesh together. As the barrier is reopened the chains would be tangled and the film would not expand out to its original area.

5.2.2 Decomposition and Ion Contamination.

To establish whether the shoulder was due to decomposition of the MEH-PPV on the water surface fresh water was left in the trough for 2 days, a fresh sample of MEH-PPV was spread and the isotherm recorded. The shoulder was still observed so this eliminated the possibility that the film was decomposing on the surface leading to the assumption that subphase changes were responsible for the change in isotherm shape.

It was conceivable that ions were leaching from the glass trough used by Sluch into the subphase, however this effect cannot be readily simulated with our trough. To imitate the aging (CO_2 absorption) of the water without the possibility of contamination solid carbon dioxide (cardice) was added to the subphase, this is referred to later as freshly aged water. A shoulder in the isotherm would lead to the conclusion that the change in isotherm shape was due to CO_2 absorption and not ion contamination. A fresh sample of MEH-PPV was deposited on freshly aged water and the isotherm recorded, see Figure 5.8 below. The isotherm with the water/cardice subphase shows a shoulder but after 24 hours on the surface this becomes much sharper. The old water isotherm (fresh film) shows a sharp shoulder suggesting that the effect is like to be due to the changing acidity of the subphase.

Figure 5.8 Isotherms of old water and CO_2 acidified subphases.

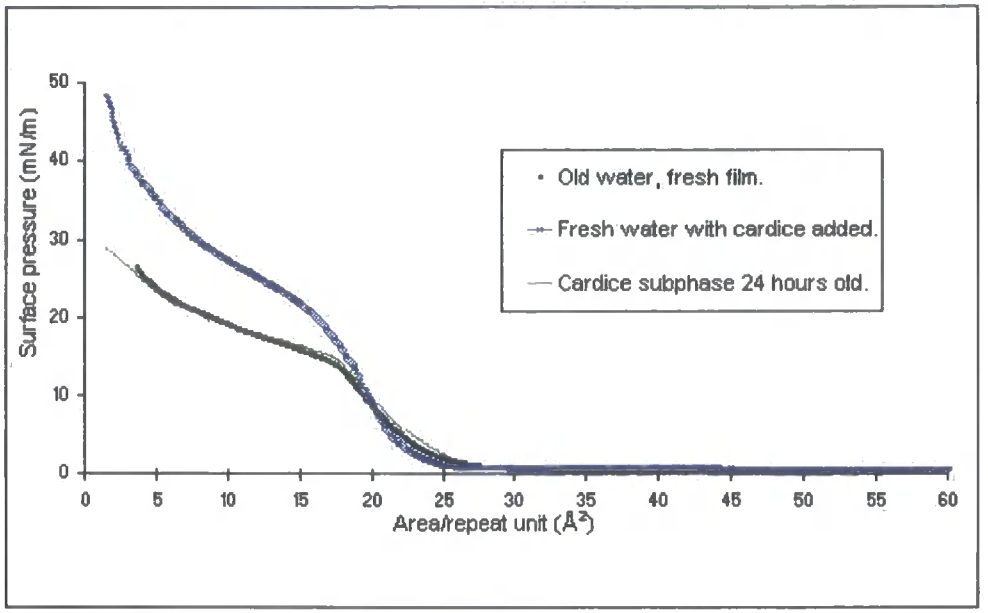

5.2.3 pH of the Subphase.

The following experiments were carried out using a new batch of MEH-PPV, the samples were obtained from Dr. Samuel (synthesised by Hoescht) for light emitting polymer studies. No formal data were given with the sample, however the Physics Department found the new batch to have a higher molecular weight than the first batch. The resulting isotherm was different to the original isotherm and a kink at approximately 17 mN/m (20 $Å^2$/molecule) was observed.

Isotherms of MEH-PPV with varying subphase pH were recorded to confirm that the sharp shoulder was due to the acidity of the subphase. A film with sodium hydrogen carbonate (pH ~ 7.9) subphase was measured as a comparison to the acidified subphase.

Figure 5.9 Image isotherm of MEH-PPV with an $NaHCO_3$ subphase

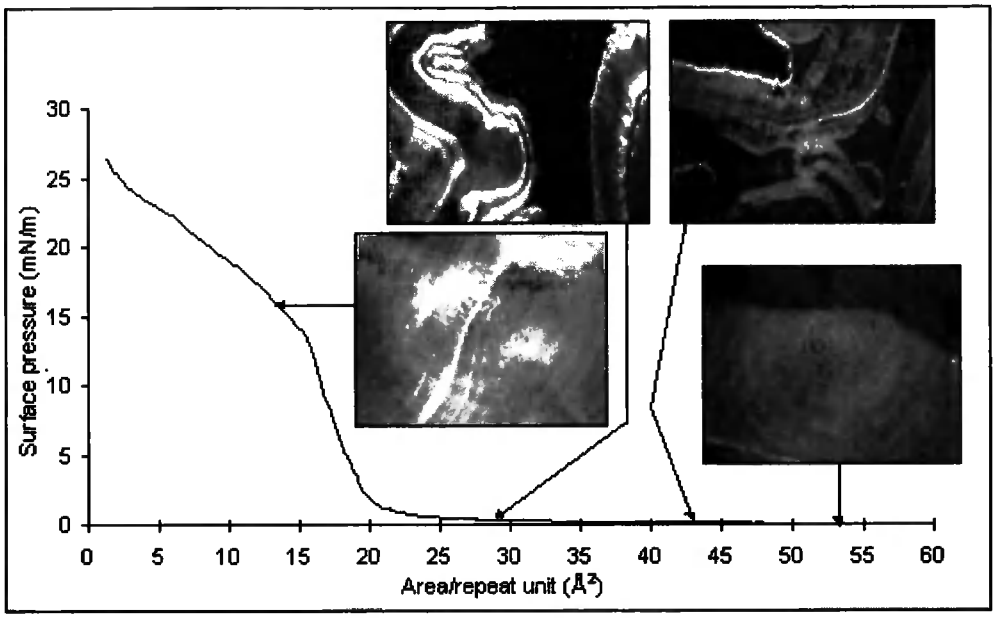

An experiment was performed with an ammonium chloride subphase (pH 5.4), a shoulder was observed in the isotherm.

Figure 5.10 Image isotherm of MEH-PPV with an NH_4Cl subphase.

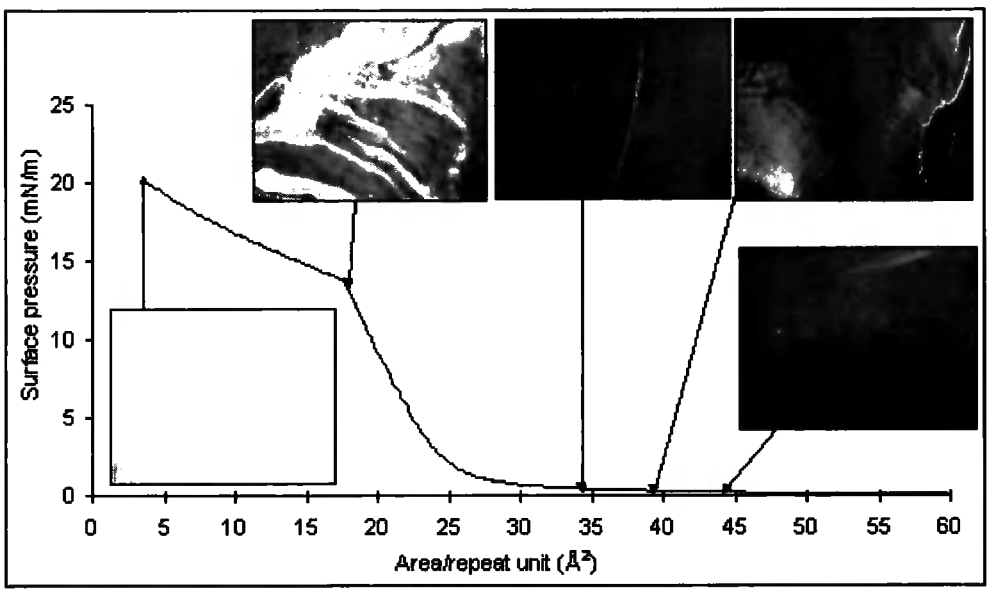

The image in Figure 5.10 recorded at 5 $Å^2$/molecule shows a highly reflective and therefore thick film. Comparing this image to the image recorded at 43

$Å^2$/molecule it is clear that a monolayer is not present. To investigate this phenomena hydrochloric acid was added to lower the pH, figure 5.11 shows the resulting isotherms of MBSH with a subphase at pH 2.8 and at pH 2.3. This should have confirmed that the change on isotherm shape was due to increased acidity of the subphase and the first 2 runs showed a sharp shoulder but when the experiments were repeated under the same conditions no shoulder was observed.

Figure 5.11 MEH-PPV isotherms with varying pH subphases.

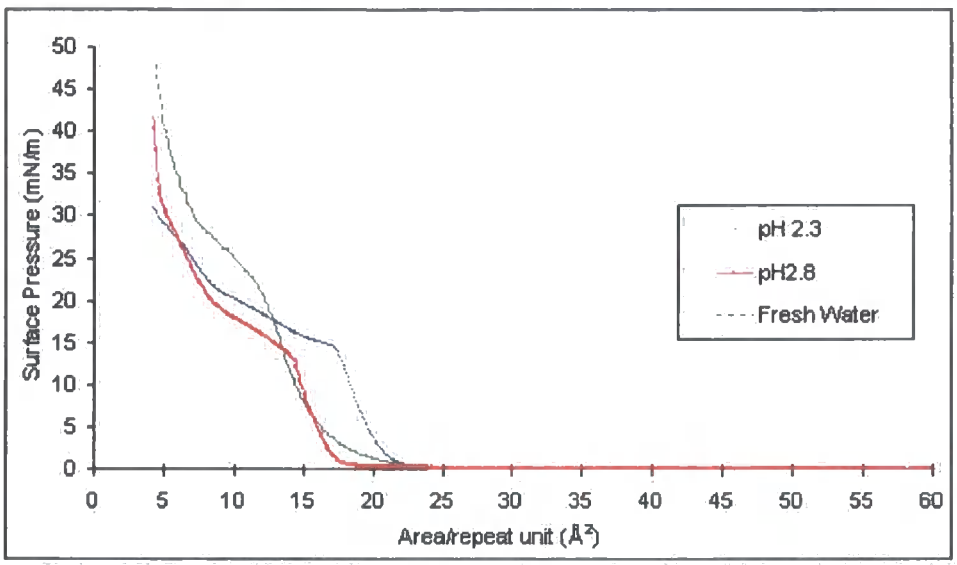

5.2.4 Temperature Dependence of MEH-PPV Films at the Air/water Interface.

A water bath was attached to the trough to control the temperature of the subphase. Isotherms of MEH-PPV on fresh water were recorded at 18 °C, 22 °C, 26 °C and 35 °C, the same volume of material was spread each time (30 µL) and compressed at the same rate (30 cm^2/min), i.e. all other conditions were kept constant. A variation in the limiting headgroup area was observed but no sharp shoulder was seen. The increase in the surface pressure indicates the onset of a condensed phase, normally the phase should occur at the same area/molecule each time if the experimental conditions are the same, see section 1.1.4. However multilayers are formed when the MEH-PPV is deposited and the extent of multilayer formation will differ each time a film is spread so that for each isotherm the condensed phase will be shifted slightly.

Figure 5.12 MEH-PPV Temperature Dependence.

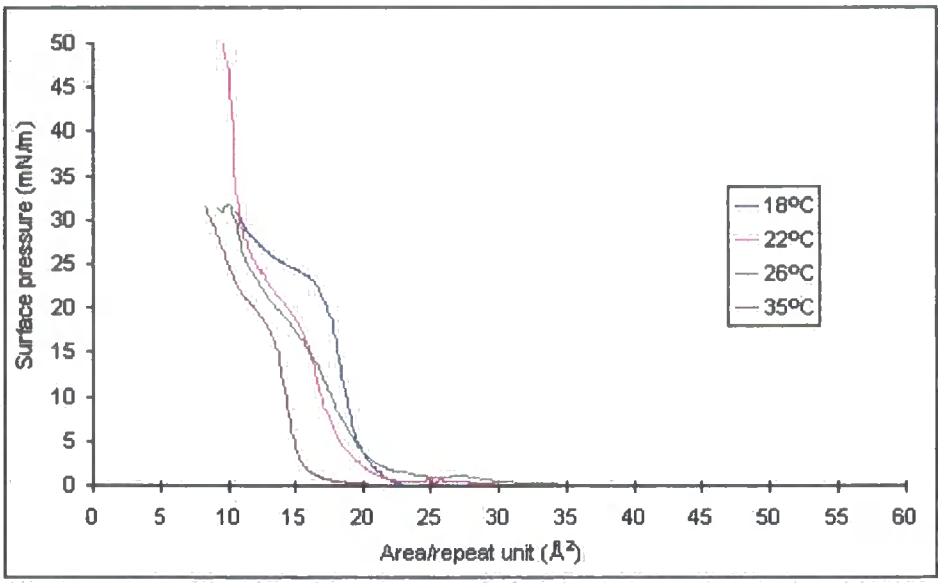

5.2.5 Compression Speed

Compression speed may effect the shape of the isotherm, high weight polymers take some time to come to equilibrium and so require slow compression.[19] MEH-PPV forms extremely rigid layers and compressing the film at different speeds may cause the film to move across the surface and collapse in different ways. A film was compressed at 30 cm^2/min and another 15 cm^2/min, the same volume of solution was spread each time (30 μL) i.e. all other conditions were kept constant, similar isotherms were observed at both compression speeds with no sharp shoulder.

5.2.6 Film Deposition

The BAM trough is relatively narrow and when the MEH-PPV film was deposited the spreading solvent caused it spread out and hit the edge of the trough. On hitting the edge of the trough the film collapsed to form multilayers. These multilayers were visible to the eye as orange lines on the water surface, therefore inhomogeneous films were being spread. To establish whether the shoulder effect

was due to rearrangement on the surface smaller amounts of material were spread and compressed but no shoulder was observed. Each film was deposited using a microlitre syringe (50 μL) which deposited approximately 5 μL per drop (30 μL in total). To reduce the amount spread per drop the plunger of the syringe was closed slightly to form a drop of the material on the needle tip, the tip was then gently touched onto the water surface depositing approximately 2 μL per drop. There was no sharp shoulder observed in the resulting isotherms.

Sluch reported spreading MEH-PPV solutions with a concentration of 2.0 mg/ml. During the course of this work solutions of 1.0 mg/ml were used as we were unable to prepare more concentrated solutions. It was conceivable that at higher concentrations the MEH-PPV was not being solvated to the same extent as the lower concentration solution that we used which may have effected the spreading properties. To clarify this point solutions of 0.1, 0.5 and 1.0 mg/ml of MEH-PPV in chloroform were each spread over clean water surfaces and compressed. The volume of the solution deposited was kept constant for each run. The results of these tests are shown in Figure 5.13 below, the concentration appeared to have no effect on isotherm shape.

Figure 5.13 Same volumes different concentration of MEH-PPV.

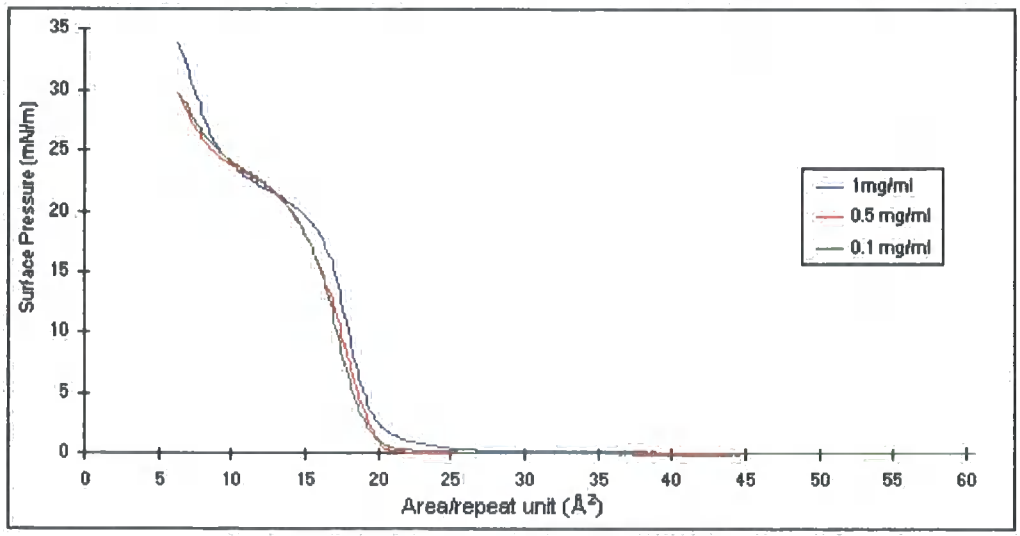

5.3 MEH-PPV DISCUSSION AND CONCLUSIONS

On average 4.5 x 10^{16} repeat units were spread on our trough, even when accounting for the differences in trough size we spread much less material than the Engineering/Physics departments (typically 3.8 x 10^{17} repeat units). They reported that they were unable to observe an increase in surface pressure under compression with any less material. Attempts to deposit a similar amount of material on to the surface as used for device preparation with the barrier fully open gave a large increase in surface pressure if we deposited the same amount indicating that condensed multilayers was forming. Thus, it is unlikely that a uniform layer was spread and this would produce defective films.

Our experimentally determined headgroup area of 20 ± Å^2/molecule is a more realistic value than the value determined by Sluch *et al*[12] (2.7 Å^2/molecule) but still not close to the theoretical area of 32 Å^2 derived by our molecular modelling (CAChe). The images in Figure 5.3 clearly display regions of different thickness showing that a true monolayer was not formed, thus explaining the lower experimental value of the molecular area. The closest published isotherm of PPV derivatives was Liu *et al*[8] for C_{16}NPPV, the structure of which is shown below.

Figure 5.14 The structure of C_{16}NPPV

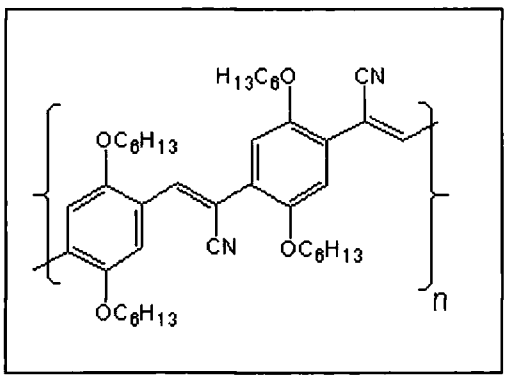

This repeat unit of C_{16}NPPV is approximately twice that of MEH-PPV with a theoretical area of 68 $Å^2$. An experimental value of 61 $Å^2$ was calculated from the pressure/area isotherm indicating that the MEH-PPV should have a limiting headgroup area in the region of 30 $Å^2$.

The dipping pressure used by Sluch *et al* was 20 mN/m. The BAM study reported here shows that at this pressure and below the film forms multilayers. In the films spread for LB film deposition much higher surface concentrations were spread than have been studied here. Deposited layers often retain the structure of the monolayer and so good film production relies on the production of a uniform monolayer of material at the air/water interface.[17] Clearly this is not the case for the PPV studied here and this is reflected in the relatively low deposition ratio.

Using a subphase of old water a shoulder was observed in the isotherm, this was thought to be due to the changing acidity of the subphase but experiments were inconclusive. The pKa of methoxy benzene is –6 therefore it is unlikely to be protonated by a weak acid.[20] Further experiments need to be performed to determine the cause of this effect. At surface pressures above the shoulder (~ 15 mN/m) on the old water subphase the film collapses relatively smoothly. At the transferring pressure of 20 mN/m practically the entire water surface is covered by at least one layer of MEH-PPV. It is conceivable that this is the reason why more uniform layers are transferred to the substrate from the old water, the isotherm with the shoulder, than from the fresh pure water subphase where there will be regions uncovered by the MEH-PPV film due to the rigidity of the domains.

5.4 DHPPV STUDIES BY THE ENGINEERING AND PHYSICS DEPARTMENTS.

Similar studies were carried out on DHPPV (see figure 5.1) by Petty *et al* and in our lab with the BAM equipment. Although as this is a new material for LED work and so has not been so well characterised as the MEH-PPV. DHPPV was dissolved into chloroform (2 mg/mL) and spread over pure water, the usual

spreading volume was 200 μL. The films were compressed at 48 cm^2/min and were found to withstand pressures of 50 mN/m, they were stable at 25 mN/m for at least 12 hours.[21] The limiting headgroup area was determined to be 6 $Å^2$, this is much too small for a DHPPV repeat unit indicating that multilayers are being formed. The LB layers were deposited at a surface pressure of 25 mN/m onto quartz substrates giving a deposition ratio of 0.8 ± 0.1.

Alpha-step measurements of the deposited film gave an average layer thickness of 7.5 ± 2 Å which is less than the value measured for MEH-PPV (10 Å) but greater than PPV (3.4 Å). The branching of the MEH-PPV chain may prevent the chains from packing efficiently therefore increasing the average layer thickness. Therefore it would be expected that the thickness of a DHPPV layer would be between that of a PPV and MEH-PPV layer.

20, 40 and 80 layer films were built up on the substrate, the UV/vis absorption increased linearly with film thickness suggesting good reproducibility. LB DHPPV films are reported to have a fluorescence lifetime of 300 ps,[13] significantly shorter than MEH-PPV (580 ps)[15] this decrease in lifetime may be due to the more efficient packing of DHPPV increasing the non-radiative relaxation pathways for the excited electronic states.

5.5 BAM STUDIES OF DHPPV

Films of DHPPV (1 mg/ml, 20-30 μL) were spread over a pure water subphase and compressed at 30 cm^2/min. The limiting headgroup area was found to be 10 ± 2 $Å^2$ inferring that a multilayer is present as the area would be expected to be in the region of 30 $Å^2$.

Figure 5.15 Image isotherm of DHPPV.

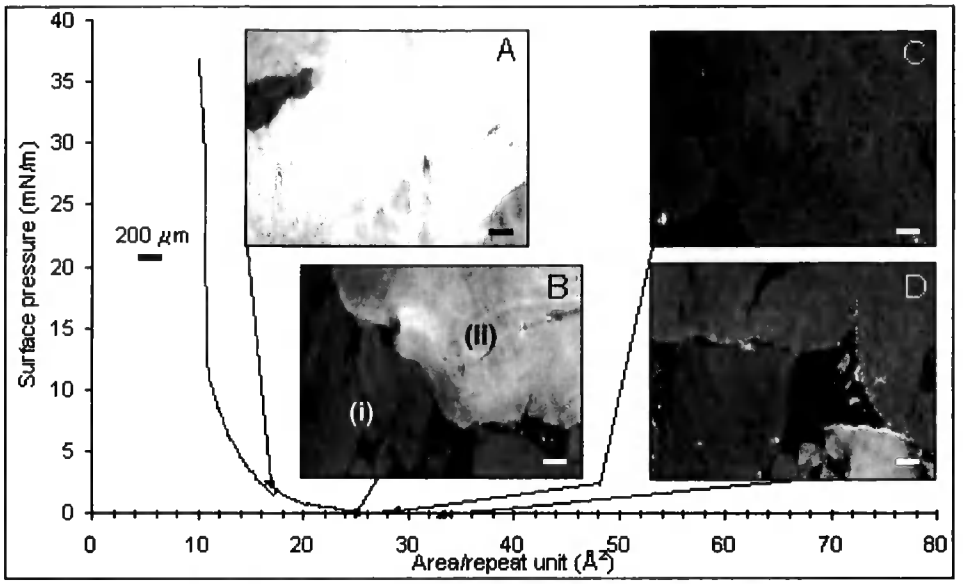

Like the MEH-PPV samples reported earlier, large, rigid rafts were seen which did not coalesce, Figure 5.15B shows two rafts of different intensity and hence thickness (i) and (ii) when the surface pressure is still low indicating that the initial spreading of the film was poor and a monolayer was not formed.

The same film was then recompressed, the limiting area/molecule decreases to approximately 8 ± 2 $Å^2$ but the large shift observed with the MEH-PPV recompression was not seen with DHPPV films. It is suggested that the DHPPV films are more fluid than MEH-PPV films due to lack of chain branching .

Figure 5.16 Image isotherm of recompressed DHPPV.

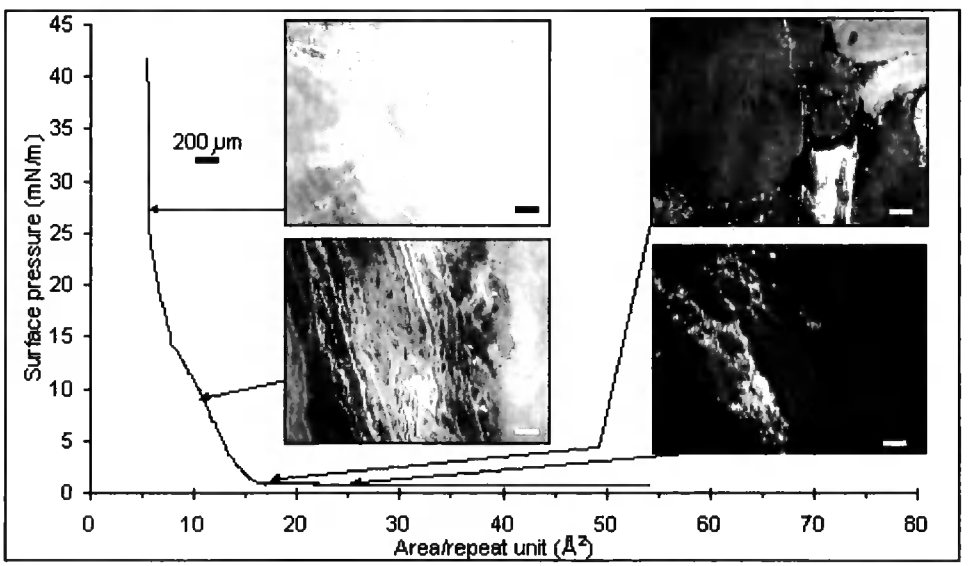

A film was similarly spread over the surface of a CO_2 acidified subphase and compressed but no change in shape of the isotherm was noted. The hexyloxy chain of the DHPPV will be much more hydrophobic than the methoxy group of the MEH-PPV, this may be quantified by calculating the partition coefficient which is defined below:

$$\log p = \log \frac{[\text{solution in oil}]}{[\text{solution in water}]} \qquad \textbf{Equation 5.1}$$

Using Rekker coefficients the partition coefficient, log p, for methoxy benzene was calculated to be 2.2. Hexyloxy benzene was significantly more hydrophobic with a value of 5.5.[22]

5.6 DHPPV CONCLUSIONS

DHPPV forms large rigid multilayer rafts at the air/water interface which appear to be unaffected by weak acids. Although both MEH-PPV and DHPPV have the same polymer backbone the substituents have very different properties which greatly affect the packing of the molecules and the resulting isotherms.

Although BAM cannot be used as a quantitative tool for determining the thickness of the observed films the technique clearly shows heterogeneity in film thicknesses at the air/water interface. In this case where the structure of the film was under discussion the BAM images show without question that homogeneous monolayers are not being spread at he air/water interface. More work needs to be carried out to determine the ideal conditions for monolayer films of MEH-PPV and DHPPV so that the transfer to the substrate may be optimised.

If the deposition of monolayers of substituted PPV's is required then BAM has demonstrated its utility as a diagnostic tool for monitoring the film on the subphase. However, the work presented here shows that these materials do not behave ideally and further work will be necessary to obtain ideal conditions for deposition.

1 May, P. *Physics World.* **8**, 52. (1995).

2 Tessler, N., Denton, G. J. and Friend, R. H. *Nature*, **382**, 695. (1996).

3 Holmes, A. B., Bradley, D. D. C., Brown, A. R., Burn, P.L., Burroughes, J. H., Friend, R. H., Greenham, N. C., Gymer, R. W., Halliday, D. A., Jackson, R. W., Kraft, A., Martens, J. H. F., Pilcher, K. and Samuel, I. D. W. *Synthetic Metals.* **57**, 4031. (1993).

4 Cimrova, V., Remmers, M. Neher, D. and Wegner, G. *Adv. Mater.* **8**, 146. (1996).

5 May, P. *Nature*, **347**, 539 (1990)

6 Friend, R. H., Gymer, R. W., Holmes, A. B., Burroughes, J. H., Marks, R. N., Taliani, C., Bradley, D. D. C., Dos Santos, D. A., Brédas, J. L., Lögdlung, M. and Salaneck, W. R. *Nature*, **397**, 121 (1999).

7 Friend, R. H., Burroughes, J. H. and Shimoda, T. Physics World, 12, (1999).

8 Liu, Y. Q., Li, Q. L., Xu, Y., Jiang, X. Z. and Zhu, D. B. *Synthetic Metals.* **85**, 1279. (1997).

9 Kim, Y. K., Kim, K. S., Kang, W. H., Yang, S. S. and Sohn, B. C. *Thin Solid Films*, **291-294**, 312 (1998).

10 Wu, A., Fujuwara, T., Jikei, M., Kakimoto, M., Imai, Y., Kubota, T. and Iwamoto, M. *Thin Solid Films*, **284-285**, 901. (1996).

11 Wu, A. and Kakimoto, M. *Adv. Mater.*, **284-285**, 901. (1996).

12 Sluch, M. I., Petty, M. C., Samuel, I. D. W., Madden, P. C. and Crayston, J. *Synthetic Metals.* **94**, 285. (1998).

13 Sluch, M. I., Petty, M. C., Samuel, I. D. W., Madden, P. C. and Crayston, J. *In press.*

14 Roitman, D. B., Antoniadis, H., Sheats, J. and Pourmirzaie, F. *Laser Focus World.* **34**, 163. (1998).

15 Samuel, I. D. W., Rumbles, G., Collison, C. J., Friend, R. H., Moratti, S. C. Holmes, A. B. *Synt. Metals* **84**, 497 (1997).

16 Furono, T., Sasabe, H., Nagata, R. and Akaike, T. *Thin Solid Films*, **133**, 141 (1985).

17 Petty, M. C. *Langmuir-Blodgett Films, An Introduction.* Cambridge University Press (1996).

18 Samuel, I. D. W., Rumbles, G. and Collison, C. *Phys. Rev. B.* **52**, 573. (1995).

19 Roberts, G. *Langmuir-Blodgett Films.* Plenum Press, New York. (1990).

20 March, J. *Advanced organic chemistry : reactions, mechanisms, and structure.* Wiley, NY. (1992).

21 Sluch, M. I., Petty, M. C., Samuel, I. D. W. and Crayston, J. A. To be submitted.

22 Albert, A. *Selective Toxicity* 7th edn, Chapman and Hall, (1985).

Chapter 6 BREWSTER ANGLE REFLECTIVITY - A NON-INVASIVE METHOD OF ANALYSING SOLUBLE SURFACTANTS.

Surfactants are used in wide range of fields such as foaming,[1] detergency,[2] enhanced oil recovery,[3] inkjet printing[4] and replacements for biological surfactants[5] to name but a few. Although equilibrium properties of surfactant systems, such as adsorption and micellisation are quite well understood this is not the case for dynamic properties. The majority of surfactant solutions are used in non-static processes which means that the surface properties such as the surface excess concentration or surface tension are constantly changing and are not equal throughout the system.[6] To improve and optimise these processes an understanding of the forces acting over a flowing surface is required.

Although there are many methods to characterise static surfactants, such as tensiometry[4] or neutron reflectivity,[7,8] until recently there were no non-invasive, non-perturbative methods of determining the non-equilibrium interfacial properties. In this work a new experimental method called Brewster Angle Reflectivity (BAR) has been developed. The technique uses the changing reflectivity of a solution with increasing surfactant concentration to study the ageing of soluble surfactants at the air/liquid interface.

Similar studies have been recently carried out by Bain and co-workers at the University of Oxford, the group have recently published their work measuring the dynamic surface excess concentration of a cationic surfactant Cetyltrimethylammonium bromide.[9,10] A general introduction to surfactants and the current methods of characterisation are discussed below.

6 .1 SOLUBLE SURFACTANTS: STRUCTURE AND FORMATION.

In 1913 McBain observed large changes in the properties of surfactants over a region of surfactant concentration that is now known as the critical micelle concentration (CMC),[11] see Figure 6.1.

Figure 6.1. Properties of Surfactants

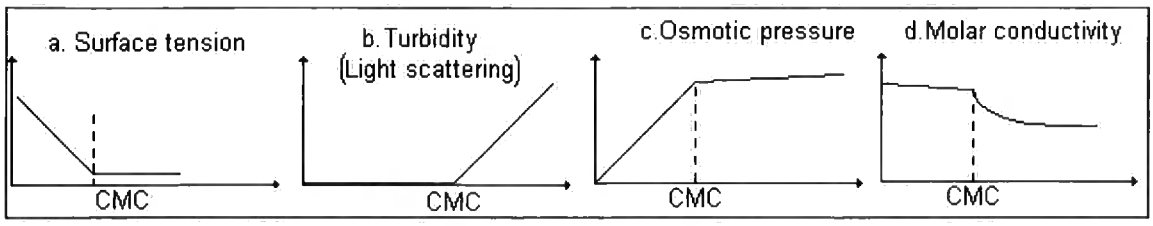

He suggested that such variations were due to a change in the structural ordering of the molecules in the solution which he attributed to the formation bilayer sheets of surfactants which were known as micelles.[12] The laminar sheet theory by McBain does not describe this narrow size range of micelles, thermodynamically it would expected that the sheets increase size to try and reduce the interfacial energy at the edges of the sheet.[13] Hartley in 1936 used conductivity to show that at lower concentrations micelles are spherical in shape.[14] In 1949 Debye used light scattering to determine the size of n-alkyl trimethyl ammonium bromide micelles.[15] Spherical micelles are narrowly dispersed in size usually (50 – 100 surfactant molecules per micelle particle), for example a sodium dodecylsulphate (SDS) micelle contains on average 60 monomer units.[12] Therefore current theories consider micelles to be spherical just above the CMC although it is known that at higher surfactant concentration the micelles become distorted and lamellar sheets are formed. Complex phase diagrams are observed in which regions of hexagonal packed cylinders, disklike and liquid crystal-like structures may be found, see Figure 6.2 below.

Figure 6.2. Micelle structures.

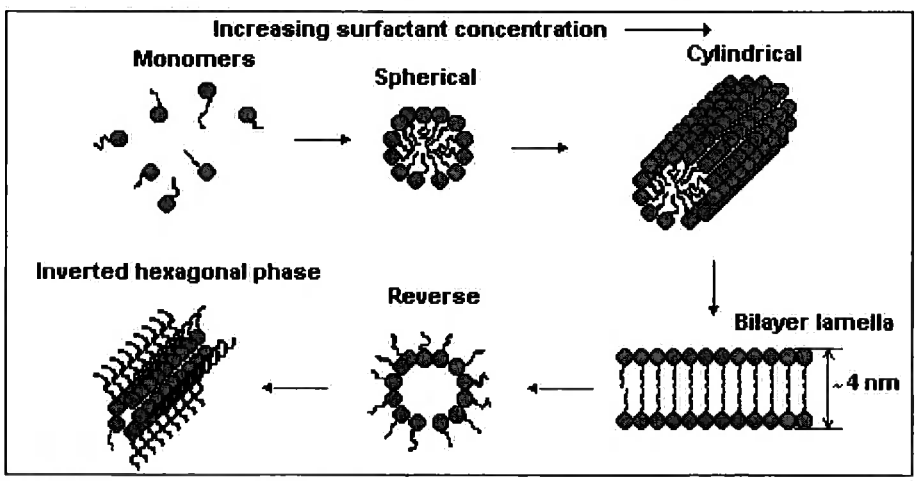

The structure of a spherical micelle in aqueous solutions is shown in Figure 6.2 above, the hydrocarbon chains are directed towards the centre of the micelle. Thus, the centre is hydrophobic and water is repelled from the core. Water is present in the outer shell of the micelles both as water of hydration and as free molecules, this region is known as the palisade layer.[16]

Not all surfactant molecules form micelles for example long chain alcohols for example have a polar headgroup and a hydrophobic tail but they do not form micelles. The balance of forces that dictate whether micelle particles form is delicate, if the hydrophilic effect is too strong the material will dissolve but if it is too weak the material is insoluble. For micelle formation it is therefore necessary for the surfactant molecule to contain a specific solubilising headgroup type. There are 3 common types of headgroups: A charged headgroup (cationic or anionic), a zwitterionic group and the third being a large oxygen containing hydrophilic group (nonionic), some common examples are shown in Figure 6.3 below.[17]

Figure 6.3 Classification of surfactants.

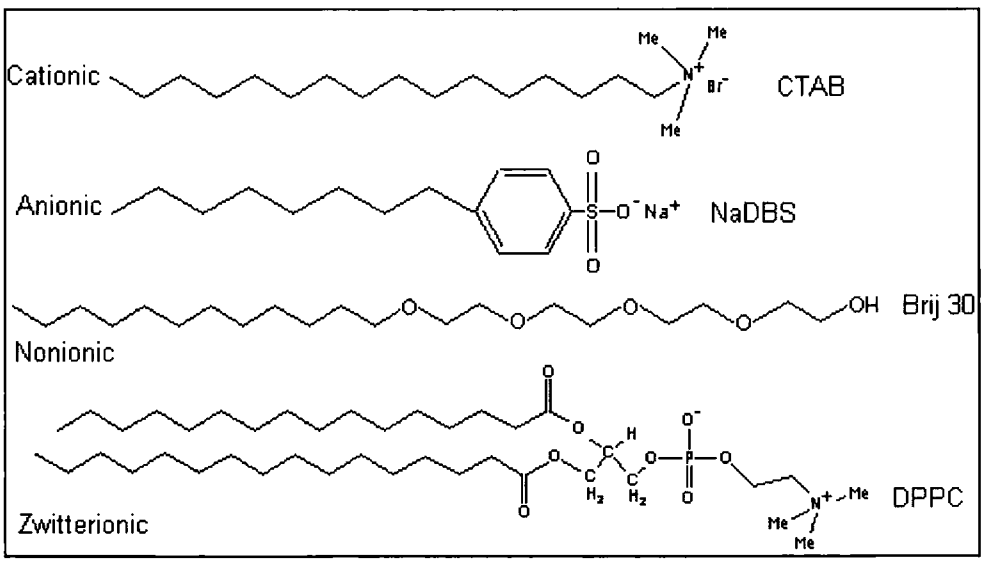

The hydrophilic group of anionic surfactants carries a negative charge, there are four main types: carboxylates, sulfonates, sulfates and phosphates.[18] Anionic surfactants are manufactured in greater volume than any other types of surfactants due to their good detergency properties (see below) and their low

production costs.[19,28]

Nonionic surfactants rely on weak, hydrophilic groups to provide the hydrophilic balance. These are most commonly based on polyether esters, alkyl-aryl polyether alcohols and amides.[4] Nonionic surfactants make excellent detergents and are often used in combination with anionics in commericial detergent formulations. They are also used as solubilisers or emulsifying agents in foods or cosmetics.

Cationic surfactants have positive hydrophilic groups, the headgroups are usually quaternary ammonium compounds. Many organic substrates e.g. wool, cotton, skin and hair are negatively charged at the surface,[20] therefore cationic surfactants with their positive charge bind well to these surfaces. However this means that the monomer species are binding over the entire surface with the headgroup end attached to the surface. It is the hydrophobic tail which is used to change the surface tension of the soil and help desorption (see below), consequently cationics generally make poor detergents. As cationic surfactants coat many surfaces well they have many applications in surface coatings for example as softeners, anticaking agents and corrosion inhibitors.[18] Cationic surfactants are highly toxic to micro-organisms but show low toxicity to man and so are used as topical antiseptics, germicides and deodorisers.[20] The positive charge of the cationic surfactant is attracted to the negative charge of the bacterial proteins. The surfactant denatures the protein and changes the cell permeability which causes membrane damage and kills the micro-organism.[20]

The formation of micelles initially appears as though it would be an energetically unfavourable process.[13] The molecules are going from a disordered system to the more ordered structure of a micelle which would lead to an increase in entropy. However it is thought that in aqueous solutions water molecules coat the hydrocarbon chain and this introduces a degree of structural ordering of these solvating water molecules. When the surfactant goes from the aqueous solution to a micelle, these molecules are lost to the bulk where they have greater freedom. This ordering effect known as the hydrophobic effect is lost.[21] This gives rise to an increase in entropy and so micelle formation is favourable.

The driving force for sharp onset of micellisation is not clearly defined, the process is usually described by two models; the law of mass action and as a phase change. The first model considers micellisation as an aggregation process, where K is the equilibrium constant:[17]

$$Z + Z \overset{K_2}{\rightleftarrows} Z_2 + Z \overset{K_3}{\rightleftarrows} Z_3 + Z \ldots\ldots \overset{K_n}{\rightleftarrows} Z_n + Z \rightleftarrows \ldots\ldots \qquad \text{Equation 6.1}$$

Using this theory there is one dominant value of K_n.

$$K = \frac{[\text{micelles}]}{[\text{monomers}]^n} = \frac{C_m}{C_s^n} \qquad \text{Equation 6.2}$$

At the CMC the total surfactant concentration is:

$$C_T = C_S + nC_m \qquad \text{Equation 6.3}$$

Combining Equation 6.2 and Equation 6.3 gives:

$$K = \frac{C_m}{(C_T - nC_m)^n} \qquad \text{Equation 6.4}$$

Differentiating the above equation and plotting dC_m/dC_T verus C_T gives a plot that increases slowly until a critical concentration, rises sharply and then levels off. As n increases the transition becomes sharper, see Figure 6.4, this accounts for the sharp onset of micelle formation.

Figure 6.4 Aggregation of monomers.

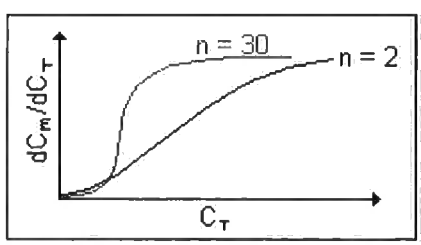

The phase change theory treats micellisation as a simple phase separation of surfactant in an associated form.[13] Referring to Figure 6.4 the behaviour can

be considered as a first order phase transition when n is large.

The exact value of n will depend on the delicate balances of forces within the micelle. The micelle has to have sufficient monomer such that the hydrocarbon chains are sufficiently shielded from the aqueous environment. This is balanced by trying to keep the headgroups as far away as possible and so the value of n is finite.

Below the CMC the majority of the surfactant added to an aqueous solution goes to the surface, however some monomers are still found in the bulk. A measure of the number of surfactant molecules found at the interface versus the bulk is known as the surface excess concentration, see section 6.3 below. Above the CMC any further addition of surfactant results in the formation of micelles only, see Figure 6.5, and the concentration of monomers species remains approximately constant.

Figure 6.5 Surfactant behaviour through the CMC.

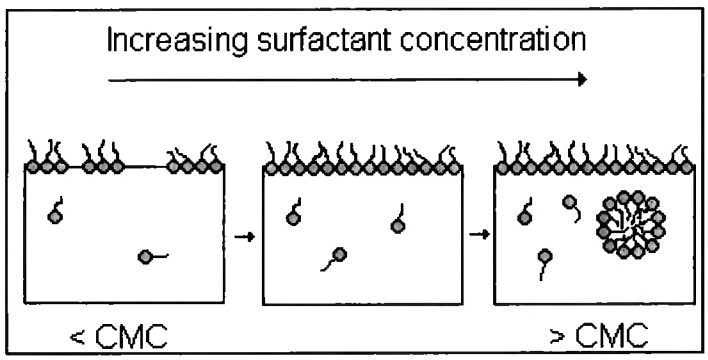

Generally a decrease in the CMC means that micelles are formed more easily and are therefore more stable. Nonionic surfactants generally have a lower CMC to that of ionic surfactants, typically 10^{-4} M compared to 10^{-2} M.[16] This is due to the repulsion of the headgroups in ionic micelles which means that ionic surfactants do not aggregate so readily. For example, the anionic surfactant ($C_{12}H_{25}SO_4Na$) has a CMC of 8.6 x 10^{-3} M whereas the nonionic surfactant with the same length hydrophobic chain ($C_{12}H_{25}O(CH_2CH_2O)_4H$) has a CMC of 4 x 10^{-5} M.[18] Addition of salt to an ionic surfactant solution greatly reduces the CMC as the salt partially screens the headgroups from each other, stabilising the micelle and decreasing the value of the CMC.[17,18] The value of the CMC is also dependent upon the properties of the surfactant such as chain length, the solvent and factors such as pH and the presence of impurities. An increase in

chain length results in a decrease of the CMC. Longer chains disrupt the bulk water to a greater extent and so the formation in micelles becomes more energetically favourable.[13] Intermolecular interactions between the chains in the micelles increase with increasing chain length and this again favours the formation in micelles and therefore results in a decrease in the CMC.[13] Surfactants such as C_{14}TAB often have impurities such as amides which are surface active, these impurities will greatly affect the CMC and the surface tension of the solution.[22]

Compounds that would normally be insoluble in water may be included into the centre of micelles such as organic solvents, dyes or proteins. This gives rise to numerous applications, for example in the areas of detergency, emulsion polymerisation, micellar catalysis of organic reactions and in pharmaceutical industry where mixed micelle solutions are widely used.[2,4] A full understanding of the behaviour of the surfactant systems is required so that these applications may be fully exploited.

Whilst Hartley was developing his theories on micelle formulation Davson and Danielli conducted a series of experiments and proposed that cell membranes consisted of a bimolecular layer of proteins and lipids with the hydrocarbon chains of the lipid oriented towards the centre of the bilayer.[23] The lungs are coated in lipid layers known as pulmonary surfactants which prevent the lungs from collapsing,[24] it is thought that under compression, when air is expelled, these lipids form spheres with a bilayer shell which are known as vesicles.[25] Therefore a great deal of research has centred on surfactants as simple artificial membranes[26] and as replacements for biological surfactants.[5,27] Vesicles also have potential uses as vehicles for controlled drug release within the body.[4]

As discussed above the most common use of anionic and nonionic surfactants is for detergency which is defined as the removal of dirt from a surface by chemical means.[12,13] Soap is the detergent that comes most readily to mind, soap is a generic term for the alkali metal salts of a carboxylic acid derived from animal fats or vegetable oils.[28] More recently soaps have been replaced by synthetic surfactants as these are more environmentally friendly. Builders are

now added to industrial laundry detergents to prevent the production of scum in hard water regions which is useful when cleaning your whites! The scum comes from the metal ions, such as Ca^{2+}, in hard water interacting with the negatively charged surfactant and forming precipitates.[12] An effective detergent must have good wetting characteristics, i.e. it must be able to wet both the fabric and the soil. It must have the ability to take the soil from the surface of the material into the bulk. A good detergent must also be able to solubilise the soil into the micelles for removal otherwise the dirt would be simply redispersed and not removed. The ability of the detergent to remove dirt levels off above the CMC, it is therefore accepted that the monomers act as the detergent by changing the surface tension of the dirt and aiding its removal from the surface.[12] The micelles solubilise the dirt preventing redeposition, detergency is therefore a competing process to micelle formation.[4] This process of removing dirt from the surface occurs by one of two methods, emulsification and roll-up shown in Figure 6.6 below.[19]

Figure 6.6 Removal of dirt from a surface.

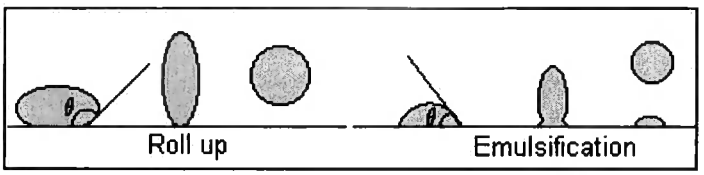

Roll-up usually occurs with hydrophilic materials, such as cotton, the surfactant coats the fabric and the soil is lifted from the surface of the fabric. In the emulsification process the fabric is generally hydrophobic such as polyester. The surfactant coats the soil which is usually an oily residue and changes the surface tension of the soil. The lowering of the surface tension causes an increase in the contact angle (θ) and may cause the dirt to spontaneously desorb from the surface. Young's equation can be used to determine whether the soil is likely to spontaneously desorb:

$$\cos\theta = \frac{\gamma_{ws} - \gamma_{os}}{\gamma_{ow}} \qquad \text{Equation 6.5}$$

γ_{ws} = surface tension between the surfactant solution and the solid substrate,

γ_{os} = surface tension between the soil and the solid substrate,

γ_{ow} = surface tension between the surfactant solution and the soil.

If cos $\theta \geq 90°$ then is it likely that the soil will spontaneously desorb.[16,19] During the washing process the fabric and surfactant solution are agitated and under constant motion. Under these conditions the interface is continually changing and is being constantly refreshed. It is therefore important to obtain a thorough understanding of the interface ageing process. In this chapter the technique of Brewster Angle Reflectivity (BAR) is described and a feasibility study carried out studying the ageing of liquid surfaces.

Temperature plays an important part in micelle stability, there is a point known as the Krafft point below which the surfactant becomes insoluble and drops out of solution forming crystals.[18] Below this temperature there is less energy for the counterions to distance themselves from the surfactant molecules. Therefore the headgroups become neutralised and are not affected by hydrophilic repulsion and the tailgroups are attracted to each other by van der Waals forces.

6 .2 MEASUREMENT OF THE CMC .

The CMC of a surfactant may be determined by monitoring any of the physical properties discussed in figure 6.1 above as a function of concentration. However these methods are invasive and the recorded value of the CMC depends on the method chosen and the purity of the surfactant, values vary by ± 50% and so a non invasive method is required to improve precision. Table 6.1 below shows a typical range of CMC values.

Table 6.1 CMC by varying techniques.[29]

Surfactant	Conductivity (mM)	Surface Tension (mM)
CTAB	0.9	0.8
TTAB	3.6	2.34
DTAB	16.8	14.45

CTAB Cetyltrimethylammonium bromide (shown in Figure 6.3),

TTAB Tetradecyltrimethylammonium bromide (alkyl chain length = 14 carbons)
DTAB Dodecyltrimethylammonium bromide (alkyl chain length = 12 carbons).

Some of the common experimental methods for determining the CMC are briefly described below.

6 .2.1 Conductivity

The molar conductivity of an ionic surfactant solution will decrease above the CMC as the relatively large size of the micelles reduce the mobility of the ions. The counter ions will also be attracted to the micelle and thus the number of ions available for charge carrying is reduced. A graph of conductivity versus concentration is plotted. The CMC is calculated by the change in the gradient, the change is often subtle and so it is difficult to get an accurate value by this method.

6 .2.2 Surface Tension

One of the most common methods to determine the static surface tension of a surfactant solution is by detachment methods. The most common method involves measuring the force required to remove a ring (usually platinum) from the surface. The ring method is attributed to Du Noüy and assumes that the force required to detach the ring from the solution is proportional to the surface tension multiplied by the circumference of the ring. A correction factor derived by Harkins and Jordan is required to account for the non-vertical direction of the tension forces when the ring is detached.[13,30]

The surface tension increases with increasing surfactant concentration up to the CMC. Above the CMC there is only a small change in the surface tension with concentration as the excess surfactant added goes to form micelles which are not surface active. The CMC is determined by a sharp change in the gradient of the plot of surface tension versus surfactant concentration. This technique cannot be used to probe the surface properties of surfactants above the CMC. The Du Noüy tensiometer (the ring method) was used to determine

the CMC of CTAB and the method is fully described in the experimental section 6.6.1.1.

6 .2.3 Spectrophotometry

Spectroscopic techniques are now commonly used to investigate a range of properties of micellar solutions.[17] The ability of micelles to solubilise a relatively large amount of water insoluble compounds (probes) means that the CMC can be determined by optical techniques. Adding a probe at low concentration ($<10^{-6}$ Mol dm^3) is not thought to perturb the system. However as the precise location of the probe within the surfactant system is unclear the results can be ambiguous.[31]

6 .2.3.1 UV-visible Spectroscopy

A chromophore that is absorbing in the UV visible portion of the spectrum and is water insoluble, such as an azo dye,[32] is included into the surfactant solution. The absorption of the solution is monitored with increasing surfactant solution. When the CMC is reached a sharp change in the optical signal is recorded as the chromophore is taken into the micelles and absorbs the incident UV signal.

6 .2.3.2 Fluorescence Spectroscopy

The luminescent properties of certain dye molecules, such as pyrene-3-carboxylate,[33] Rhodamine 6G and methyl orange[34] depend on their environment. Thus the fluorescence signal from a dye in aqueous solution differs from that in a micelle. A trace amount of a fluorescent probe is added to a surfactant solution and the emission spectrum monitored as a function of surfactant concentration. A distinct change in the intensity of the spectral peaks is observed as the surfactant forms micelles and the dye is solubilised. This technique is more sensitive than UV absorption and so less dye is used, hence the system is less perturbed.[17] Another method can be used if the

6.3 THE SURFACE EXCESS CONCENTRATION.

At an ideal interface between two phases such as vapour and a liquid phase the properties of phase α will end as phase β begins. However in reality the interface is not sharply defined and there is a region (τ) over which the properties of bulk α gradually change to those of bulk β, see Figure 6.7.

Figure 6.7. Surface Excess Concentration.

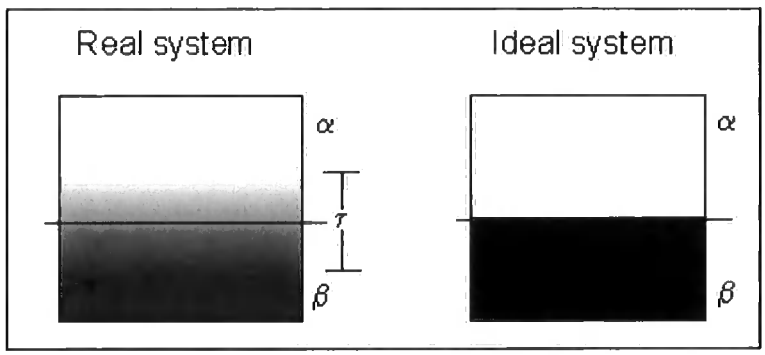

Mathematically this is treated by defining an arbitrary dividing surface (χ) to handle the properties of the bulk phases. The dividing surface may be positioned anywhere within τ and the bulk properties of α and β are taken to be constant up to the dividing surface (as in the ideal system). The actual values of α and β will then differ from the theoretical value by a value known as the surface excess, Γ. The surface excess may be positive or negative representing an excess or deficiency of that property at the surface.

When in equilibrium the two phases α and β can be described by the Gibbs adsorption Equation 6.6 which relates the surface tension (γ) to the amount of substance and the chemical potential of the components in a system for a constant surface area (A) at a constant temperature (T).

$$\sum_i n_i^s d\mu_i + A d\gamma = 0 \qquad \textbf{Equation 6.6}$$

Where:

n_i^s = The number of moles of component i at the surface (s), (mol),

μ_i = the chemical potential of component i, (J mol^{-1}),

γ = the surface tension, (Jm^{-2}),

A = the surface area of the solution, (m^2).

If α is a gaseous phase and the β phase is a 2 component system (e.g. component 1 is the solvent and component 2 is the solute), Equation 6.6 can be divided through by A and becomes

$$d\gamma = -\frac{n_1^s d\mu_1}{A_1} - \frac{n_2^s d\mu_2}{A_2} \qquad \textbf{Equation 6.7}$$

The surface excess of component i at the surface is defined as:

$$\Gamma_i = \frac{n_i^s}{A} \qquad \textbf{Equation 6.8}$$

Therefore using Equation 6.7 becomes:

$$-d\gamma = \Gamma_1 d\mu_1 + \Gamma_2 d\mu_2 \qquad \textbf{Equation 6.9}$$

As mentioned above the position of the dividing surface is arbitrary so it may be chosen so that Γ_2 goes to zero. Figure 6.8 shows the changing properties of the components across the interface and the position of the dividing surface (χ).

Figure 6.8. The dividing surface.

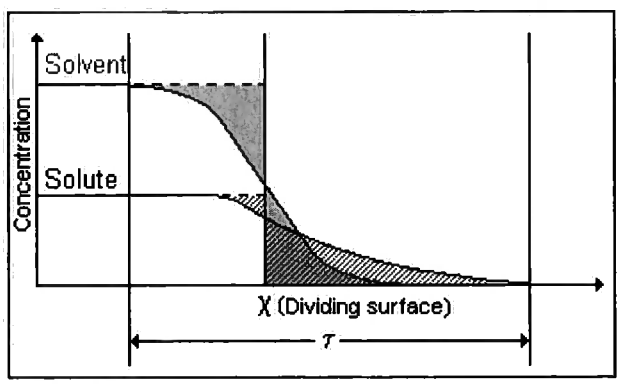

The number of moles of the solvent (n_1) is the usual property that is taken to go to zero, therefore referring to Figure 6.8 the dividing surface is positioned such

that the shaded areas of the solvent are equal about χ and so cancel but the solute has an overall surface excess. The general notation when using the number of moles of solvent is Γ_2^1, other properties such as the total number of moles (N) or total weight (W) may be selected as the property to go to zero and the surface excess would then be defined as Γ^N and Γ^W respectively.

In summary, two portions of the solution are taken, one at the surface and the other from the bulk. Both portions contain the same number of moles of solvent. The surface excess (Γ_2^1) is then defined as the number of moles of the solute in the bulk portion subtracted from the number of moles in the surface portion divided by the area of the surface [4,15]

Equation 6.7 is usually rewritten by replacing the chemical to give experimentally measurable quantities. The chemical potential is related to the activity by:

$$\mu_2 = \mu_2^0 + RT \ln a_2 \qquad \textbf{Equation 6.10}$$

Where:

R = the gas constant, (8.314 $JK^{-1}mol^{-1}$),

T = temperature, (K),

a_2 = the activity of the solute,

μ_2^0 = the chemical potential of the pure solute, ($Jmol^{-1}$),

μ_2 = the chemical potential of the solute in the solution, ($Jmol^{-1}$).

For dilute solutions the activity (a_2) is proportional to the concentration (c).[15,17] Combining Equation 6.9 and Equation 6.10 and differentiating with respect to constant temperature yields the Gibbs equation:

$$\Gamma_2^1 = \frac{-1}{RT}\frac{d\gamma}{d\ln c} \qquad \textbf{Equation 6.11}$$

Where:

Γ_2^1 = surface excess (mol m^{-2}),

R = gas constant, (8.314 J K^{-1} mol^{-1})

T = Temperature (K),

c = concentration of surfactant,

γ = surface tension (N m^{-1}).

The surface excess has units of mole m^{-2} and so the mean area occupied by the adsorbed molecules can be determined. This equation was shown to hold for nonionic surfactants by McBain in 1932.[36]

A plot of the surface tension versus the log of the concentration can then be plotted, the gradient $\left(\frac{d\gamma}{d\ln c}\right)$ is calculated and Equation 6.11 is then used to determine the surface excess concentration. The behaviour of a typical surfactant (CTAB) is shown in Figure 6.9 below.

Figure 6.9 Surface Excess Concentration Plot

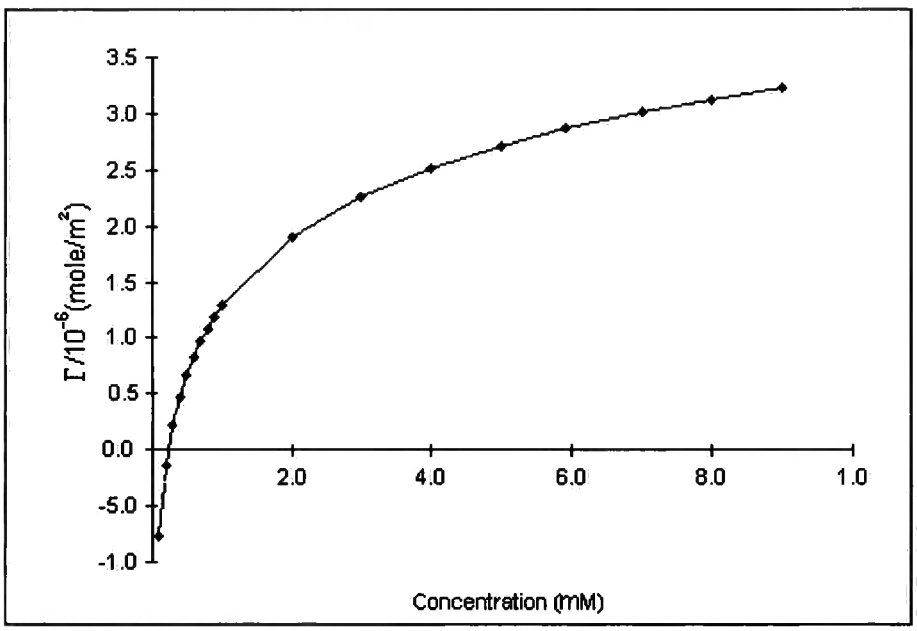

The plot was recorded using a Du Noüy ring tensiometer at Bristol University with the kind assistance of Dr Eastoe. The details of this experiment are described later in this chapter, section 6.5.3. The plot shown above shows a negative surface excess concentration at low surfactant concentration, this is due to the large errors associated with the experiment at low concentrations. It

is expected that the surface excess concentration should be zero at zero concentration.

Using the calculation method described above the CMC was determined to be 0.9 mM at 25°C.

The surface excess can only be accurately calculated up to the CMC using this method. Above the CMC the change in the surface tension with increasing concentration is much smaller, this change is greater than the precision of the instrument.[7] However information concerning the surface properties above the CMC is needed for systems such as detergency.

Haydon and co-workers suggest a modified form of the Gibbs equation for ionic surfactants to include the fact that counter ions adsorb at the interface to maintain an electrically neutral interface.[20] Thus a factor of 2 is included in to the denominator of Equation 6.11 for a 1:1 solution of ionic surfactants (unless there is excess inert electrolyte where shielding will apply). Tajima *et al.* have shown that this relationship holds for ionic surfactants (sodium dodecyl sulphate).[36] However other methods described below have been developed to directly determine surface excess which do not depend on the ideal behaviour of the surfactant solution.[16]

One of the first experiments to verify the Gibbs equation was by McBain *et al.* in 1932.[35] They used a microtome which consisted of a sharp blade that scooped up a thin layer of the surface for analysis. The results were within 10% of the Gibbs equation. Radiotracers have also been used to investigate the surface excess, the solute of interest was labelled with a radioisotope which was a weak beta emitter. The penetration into the surface of the β radiation (electrons) emitters was approximately 0.06 mm hence recording the intensity of the emitted radiation gives a direct measure of the surface concentration.[38] The technique of neutron reflection is also used to study the surface excess, this methods allows concentrations above and below the CMC to be studied.[39] A general introduction to neutron reflection is described in section 1.3.4 and excellent reviews of the technique have been written.[7,8] The area per molecule

of the surfactant at the air/water interface can be calculated from neutron reflectivity:[37]

$$A = \frac{\sum m_i b_i}{\rho\tau} \qquad \textbf{Equation 6.12}$$

Where:

A = area/molecule of the surfactant

m_i = number of species i,

b_i = the scattering length,

ρ = the scattering length density of the layer,

τ = the thickness of the layer.

The surface excess can be calculated from the area per molecule using Equation 6.8. Thomas and co-workers have measured the surface excess of TTAB above and below the CMC using neutron reflectivity and comparing the results with surface tension measurements (Pt-Ir ring).[22] The neutron reflectivity results showed that the surface excess increased above the CMC but the surface tension results were found to be inaccurate due to impurities and incomplete wetting of the ring. Therefore they were unable to verify the reflectivity results. More recently neutron reflectivity has been successfully used to investigate mixed surfactant solutions.[39,40]

6.4 THE DYNAMIC SURFACE EXCESS CONCENTRATION.

As far back as 1890 Lord Rayleigh showed that the surface tension of soap changed over time.[41] Most surfactants are used in dynamic systems, for example synthetic lung surfactants mentioned above. The lungs are continually expanding and collapsing and so the lung surfactants are undergoing a continual pressure change and the surface is constantly refreshed. The ageing of surfactants depends on its dynamic properties. However the properties of the dynamic surface tension (σ_{dyn}) and surface excess (Γ_{dyn}) may be different from their equilibrium values (σ_e and Γ_e respectively). The dynamic surface

tension may be measured directly (see below) but the dynamic surface excess is more difficult to measure. Until recently there was no experimental method to directly determine the dynamic surface excess, previously it was calculated from the dynamic surface tension.

An invasive but simple method of measuring the CMC is to use a Wilhelmy plate (WP), Bain and co-workers used both a filter paper and a platinum WP to measure σ_{dyn} for calibration curves to convert σ_{dyn} to Γ_{dyn}.[42] They found that the filter paper plate correlated well with neutron scattering results. However the data for the platinum plate was low at low surfactant concentration, this was attributed to incomplete wetting of the platinum plate.

To study surface relaxation on the microsecond time scale the oscillating jet method may be used. This consists of a jet emerging through a noncircular orifice, oscillations are observed in the jet and from these oscillations (of wavelength λ) the surface tension can be derived using Equation 6.13 derived by Lord Rayleigh and later by Bohr.[12]

$$\gamma_{app} = \frac{4\rho\upsilon^2(1+37b^2/24r^2)^2}{6r\lambda^2(1+5\pi^2r^2/3\lambda^2)} \qquad \textbf{Equation 6.13}$$

Where:

γ_{appl} = dynamic surface tension,

υ = volume velocity,

ρ = density of the solution,

r = sum of minimum and maximum half diameters of the jet,

b = the difference of the minimum, and maximum half diameters,

λ = wavelength of oscillation.

These parameters are measured optically and a first approximation is that the surface age at a given node is the distance form the jet orifice divided by the jet velocity. A typical jet will have a diameter of 0.03 cm, a velocity of 1 cm^2/s and a wavelength of oscillation of 0.5 cm.[12] Using this method the surface tension of water takes approximately 0.6 ms to reach equilibrium.

One of the most common current methods to determine the dynamic surface tension on the millisecond to second time scale is to use the maximum bubble pressure experiments.[4] The experiment consists of a capillary tube which is positioned below the surface of the surfactant solution of interest. Bubbles of an inert gas are blown through the capillary into the solution from a gas reservoir. The pressure required to create the maximum size bubble without causing bubble detachment is measured. Eastoe *et al.* have used the maximum bubble pressure experiment to determine the dynamic surface tensions of a range of nonionic surfactants.[43,44] They used the Ward and Tordai equations defined below:

$$\Gamma_{dyn(t\to 0)} = \gamma_0 - 2RTc\left(\frac{Dt}{\pi}\right)^{1/2} \qquad \textbf{Equation 6.14}$$

$$\Gamma_{dyn\,(t\to)} = \gamma_{eq} - \frac{2RT\Gamma^2}{2c}\left(\frac{\pi}{Dt}\right)^{1/2} \qquad \textbf{Equation 6.15}$$

Where:

c = the bulk concentration,

Γ = the surface excess,

γ_0 = the surface tension of the pure solvent,

γ_{eq}= the equilibrium surface tension of the surfactant.

Theoretical studies are presently being carried out to improve the calculation of the bubble lifetime to allow the investigation of short lifetimes ($<10^{-3}$ s).[45]

Non-invasive methods for determining the dynamic surface tension and excess have recently been developed by Bain *et al.* They used ellipsometry,[9] surface light scattering[42] and neutron reflectivity[9] to directly determine the dynamic surface properties of a solution of CTAB flowing through an overflowing cylinder (OFC). This OFC is a simple yet effective design by Bergink-Martens, Prins and co-workers, the flow is two-dimensional unlike the oscillating jet and the

flow is significantly more laminar than allowing the solution to flow down an inclined plane.[46] Measurements are recorded on the 0.1 - 1 second time scale. The OFC used by Bain and co-workers consists of two concentric stainless steel cylinders as shown in Figure 6.10.

Figure 6.10 The Over-flowing Cylinder.

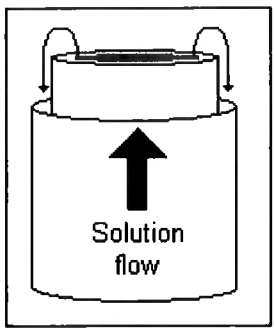

The solution is pumped up through the first cylinder to produce a large surface area (approximately 70 mm), although towards the edge of the cylinder the surface becomes curved and realignment of optics is required. When the solution reaches the surface it expands, this causes a change in the surface tension. Therefore across the surface of the solution there is a surface tension gradient, this gradient is balanced by shear stress and viscous stress. The changing surface tension accelerates the underlying liquid creating a hydrodynamic flow which in some cases is sufficiently strong that self-sustaining systems have been observed.[47] This effect is known as the Marangoni effect and results in a changing surface excess across the surface. The OFC offers a large flat surface of flowing surfactant solution to be investigated. A known concentration of surfactant is pumped through the OFC and the ellipticity can be measured from the centre to a radial distance of 10 mm allowing the study of the changing surface excess across the surface.

Ellipsometry and Wilhelmy plate measurements were used to determine the dynamic surface tension of CTAB using the OFC.[9] In this experiment the radial distance was fixed at 8 mm and a range of surfactant solutions were used in the OFC. The ellipticity as a function of concentration was recorded. Ellipsometry does not directly measure the surface tension, unlike WP measurements, however calibration curves were derived by relating the

ellipticity to static Wilhelmy plate results. The study of flowing systems by ellipsometry therefore relies on the assumption that the monolayer is in equilibrium with the bulk directly below the surface as ellipsometry only detects changes at the surface. There was good agreement between the ellipsometry and the WP results which indicates that the expanding surface of the OFC is near or at local equilibrium with the bulk. Ellipsometry was found to decrease in sensitivity towards the CMC, the ellipticity signal decreases as the amount of *p*-polarised light increases due to increasing surfactant concentration. The advantages of ellipsometry are that results can be recorded quickly, it has a small footprint (see below) and that it is laboratory based, errors are estimated to be < 1% for a monolayer.[9]

Using the technique of neutron reflectivity with the OFC Bain and co-workers were able to directly measure the dynamic surface excess.[10] This is the first direct measurement of Γ_{dyn} for an expanding surface. The experiments were carried out using the SURF reflectometer at ISIS using deuterated CTAB in null reflecting water (nrw). The neutron reflectivity results were compared to the ellipsometry results and there was good agreement. Again neutron reflectivity offers is a powerful technique which allows the direct measurement of surface properties either as a function of concentration or the variation of the surface excess with radial distance. The associated difficulties with the technique are with the alignment and the large footprint of the incident beam. Footprints of 20 x 20 mm, 30 x 30 mm and 40 x 40 mm were used. Although the cylinder is 70 mm in diameter the curvature of the surface becomes significant > 10 mm from the centre resulting in some of the reflected signal being deflected, thus reducing the collection efficiency and accuracy.

Attempts to image soluble surfactants using the BAM equipment were unsuccessful as the exchange of surfactant between the surface and bulk is on the order of microseconds[15] resulting in dynamic surface with small domains. The change in refractive index across the interface was insufficiently sharp i.e. there wasn't adequate contrast between the surface layer and that of the bulk and so no domains were detected by the camera. A change in intensity of the images was noted, as the surfactant concentration increases the images

appeared brighter indicating that the intensity of the reflected light was proportional to the surface concentration.

To investigate this phenomenon in further detail the Brewster Angle Microscopy apparatus was redesigned to measure the change in the reflected intensity of a solution with concentration. The camera was replaced by photo-detectors to increase the sensitivity of the system to monitor the reflectivity of the surface, this set-up is called Brewster angle reflectivity (BAR). The intensity of the reflected light is given by:[4]

$$R = \left[\frac{\tan(\theta_i - \theta_t)}{\tan(\theta_i + \theta_t)}\right]^2 \quad , \quad \theta_t = \sin^{-1}\left[\frac{n_1 \sin\theta_i}{n_2}\right] \qquad \textbf{Equation 6.16}$$

Where:

R = the intensity of the reflected light,

n_1 = the refractive index of the film,

n_2 = the refractive index of the subphase,

θ_1 = the angle of incidence (i.e. the Brewster angle)

θ_2 = the angle of refraction.

Equation 6.16 shows that the reflectivity depends on the refractive index of the solution at the interface, as the surface concentration of the surfactant increases so does the refractive index and hence the reflectivity. Above the CMC the surface excess levels off as the added surfactant goes to form micelles, the reflectivity of such a system should mimic this behaviour. The true value of the CMC can be then measured by this all-optical method as the experimental method does not interfere with the surfactant solution.

In this work BAR has been used the investigate the surface behaviour of several surfactant solutions. The experiments verify that the system was sufficiently sensitive to study the surface excess. Unfortunately time restraints prohibited the production of a flowing chamber and hence the study of flowing systems using BAR.

6.5 EXPERIMENTAL

6.5.1 Brewster Angle Reflectivity (BAR).

Brewster Angle Reflectivity (BAR) was developed in our lab as a non-invasive method to determine the surface excess of surfactant solutions, with a view to study the ageing of the air/liquid interface. As previously mentioned a change in the intensity of the reflected light with concentration had been observed. The first step was to determine whether this change in reflectivity could be quantified.

The measurements were recorded around the Brewster angle, as the reflectivity is much more sensitive to changes in surface concentration at this angle.[48] The BAM equipment was rearranged for this experiment and the camera was replaced by a more sensitive detector. A photodiode and a photomultiplier (PM) tube were investigated. The set-up is shown in Figure 6.11 below.

Figure 6.11 Top View of BAR Set-up.

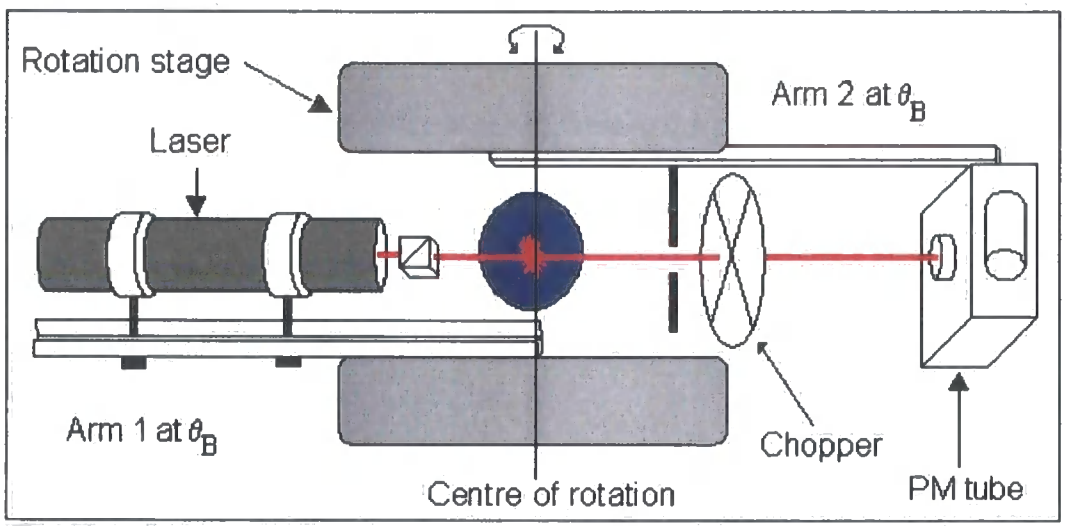

The beam expander was removed from the laser (He-Ne, Melles-Griot, 633 nm), this ensured that the area of the detector was greater than the diameter of the laser. The changes in the reflected signal were expected to be very small

therefore it was essential to collect all of the reflected signal. The reflected signal was detected by a PM tube (Hamatsu R928) and in a separate experiment by a photodiode (RS), which were each mounted in in-house built casings. A 633 nm interference filter was added to the front of the PM tube to reduce the effects of stray light and protect the equipment, all experiments were performed in the dark. A resistor, known as a terminating resistor, may be added to the detector to change its sensitivity, increasing the terminating resistance increases the sensitivity of the detector but reduces the response time of the detector. However if the resistor is chosen such that response time is faster than the chopper frequency a sharp square wave is recorded and the signal is not compromised. A 50 kΩ terminating resistor was used with the PM tube and a 100 kΩ was used with the diode.

The trough was exchanged for a small container so that the rotation stages could be positioned opposite each other. Two aluminium extension arms were made to mount the laser and detector, this set-up allowed motion of the laser and detector about the centre of rotation so they could be moved simultaneously and scanned around the Brewster angle without moving the sample. A pinhole and a chopper were mounted onto arm 2 with the diode/PM tube. The sample was mounted onto a labjack for crude height adjustments. The pinhole had an adjustable iris which was reduced to a minimum (d = 1 mm). This acted as a target for fine height adjustments. By adding small amounts of solution the height was adjusted until the laser was reflected from the surface straight though the pinhole to the detector, the pinhole was then opened (d = 30 mm) during the experiment.

Although experiments proved that the detectors were not sensitive to the position of the laser over the detecting surface, the diameter of the detecting surface was only 4 mm and so there was little room for movement away from the optical axis of the system. Therefore the alignment of the detector and the laser was critical, the beam had to go through the centre of rotation and move exactly in the vertical plane.

Virtually all of the light is transmitted into the subphase near the Brewster angle, this posed major problems as the transmitted light was scattered by the bottom of the container and a small but significant portion of this scattered light was co-linear with the reflected signal. A relatively intense source is needed as the signal is minimal at the Brewster angle and difficult to detect. However increasing the source intensity also increases the amount of light transmitted into the subphase and hence scattered by the container. Several containers were tested to find one that caused the least amount of scattered light, the container must be free from impurities that may affect the results. A glass dish was initially tested, this was selected as it could be cleaned thoroughly. To reduce scattering it was placed into the top of a matt black block of wood, an insert the size of the dish was drilled out. The block reduced the scattering and held the dish in the same position each time, as the reflected signal was sensitive to the position of the dish. Several experiments were carried out using the glass dish but during the experiments it was noted that some of the transmitted light scattered by the glass was being detected by the diode and reproducible values of the reflected signal could not be recorded. Many methods were tested to try and remove the scattered light by spatially filtering the collected beam using pinholes and tubes on the detection side of the set-up. These were not sufficient to remove the scattered signal but due to the amount of light scattered along the optical axis a different type of container had to be found.

A small Teflon trough with a well was tested but as the laser scanned around the Brewster angle the beam struck different regions of the top-hat during each run and this changed the background signal each time and so again scattering from the container interfered with the results which meant that this was not a suitable container.

A dark plastic beaker was finally used, although this was certainly not ideal as it could absorb ions or leach species into solution, it provided an excellent container as it was relatively deep and was dark enough to absorb the transmitted light. Experiments showed that the signal was independent of the position of the container and reproducible results could be obtained. As the background

scattering had been removed and more sensitive detector was chosen and the diode was replaced by the PM tube.

A lock-in amplifier (Stanford Research Systems, SR510) was used to gather the data from the diode, this was then sent via an RS232 cable to the PC. A BASIC program was written to control the rotation stages and to collect and average the data, saving it in ASCII format, (see appendix B). Using a water sample the reading on the lock-in amplifier was optimised (the maximum value) by scanning the phase of the lock-in. The Brewster angle was obtained by scanning the rotation stages until the signal from a water sample was at a minimum, fine adjustments of the polariser were then made, again until a minimum value of the reflectivity was reached.

Experiments were carried out at ambient temperature, 18-23°C. Initially surfactant concentrations of ¼ CMC, ½ CMC, CMC and 2 x CMC were used to test the relationship between the reflectivity and surface concentration. Each sample was placed into the container, the height of the solution was adjusted until the reflected light passed through the pinhole, the pinhole was then opened for the experiment. The rotation stages did not record the position of the laser and detector in real space only the relative positions from when the stages were either turned on or reset. At the beginning of the experiment the laser and diode were rotated so that they were horizontal (determined by using engineers spirit level) and the rotation stages were reset to 0° on the DPS display. The laser and detector were moved to approximately the Brewster angle, fine adjustments were then made until the reflectivity was at a minimum (i.e. the incident signal was at θ_B). The laser and detector were moved simultaneously by the BASIC program in steps of 0.05° over a range of 1° around the Brewster angle, these ranges could be determined by the operator. The data were recorded into the PC by the program, 50 readings were taken and averaged at each angle and the average values were saved and plotted (Microsoft Excel), this was referred to as a reflectivity scan. A typical set of curves recorded from reflectivity scans of CTAB at various concentrations are shown in Figure 6.12.

Figure 6.12 Reflectivity curves.

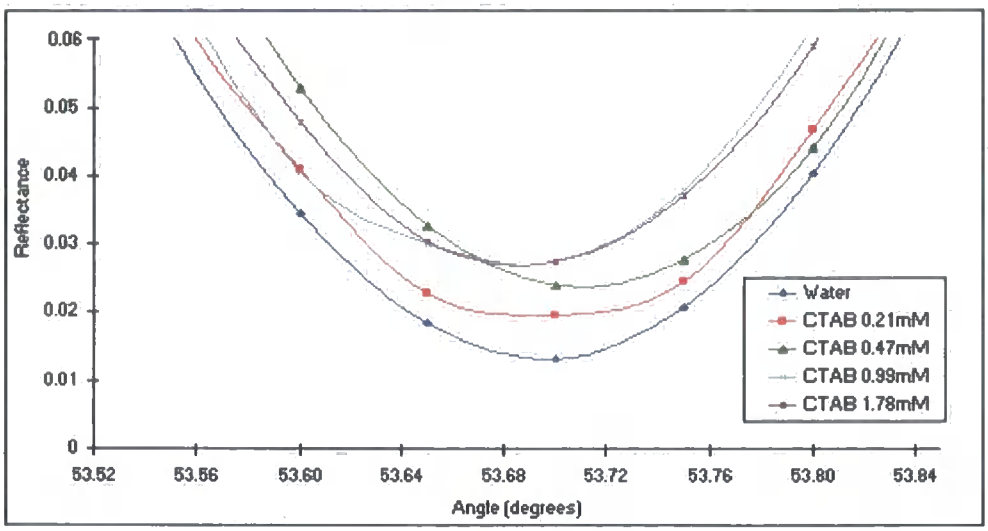

The minimum of the water curve was taken to be the Brewster angle, the intensity of the reflected signal was then read from the curve at this angle for each subsequent surfactant concentration. This intensity was then plotted against the corresponding concentration to give a reflectivity versus concentration plot, known as a BAR plot.

6.5.2 Determination of the CMC by Conductivity.

Conductivity measurements were carried out using a conductance meter (Jenway 4310). A range of eleven solutions 14 to 2 mM of the sodium perfluorononanoate were made up in de-ionised water and placed in a water bath at 23.5°C and allowed to reach thermal equilibrium. The probe was placed into each solution and the reading was recorded, it was rinsed with de-ionised water between readings. This whole procedure was repeated and the CMC was determined by the change in gradient of the graph of conductance versus concentration.

6.5.3 Determination of the CMC by Tensiometry

The tensiometry results were recorded at Bristol University with the help of Dr. Julian Eastoe and his group using a Kruss K10 tensiometer with a platinum du Noüy ring. A sample was placed into the dish and allowed to equilibrate, values were recorded at 298K. Spinning the ring in a blue bunsen flame for

approximately 5 seconds removed any surface impurities such as grease, care was taken to ensure that the metal was not allowed to get white hot as this would distort the shape of the ring invalidating the readings. The ring was then attached to the tensiometer and lowered until it was below the liquid surface. Once wetted the ring was raised until it was just covered by the solution and the tensiometer was started. The tensiometer raised the ring until the film between the ring and the solution ruptured, this was recorded as the surface tension of the film. This procedure was repeated five times for each solution and the values averaged, a range of solutions 4 mM to 0.01 mM was used for CTAB.

6.6 RESULTS AND DISCUSSION.

The n-alkyl trimethylammonium bromides were initially studied since their properties are well known and high purity samples can be easily obtained. The experimental conditions were optimised using these surfactants and was then applied to other common surfactants systems. The exact experimental method changed throughout these experiments as adjustments were made to improve the results, these changes are discussed within each results section.

6.6.1 Alkyl Trimethylammonium Bromides.

Cetyltrimethylammonium bromide (CTAB), tetradecyltrimethylammonium bromide (TTAB) and dodecyltrimethylammonium bromide (DTAB) were used for this experiment. The increase in the hydrocarbon tail length causes the molecule to become more hydrophobic and so the CMC decreases as the chain length increases, this trend is shown Table 6.2.

Table 6.2 CMC of Trimethylammonium bromides. [49,50]

Surfactant	CMC /mmol dm^{-3}
CTAB	14
TTAB	3.6
DTAB	0.9

The values for the CMC were also measured in our lab using the UV spectroscopy method using was methyl orange as the probe, see section 6.2.3.1.

CTAB (Avocado), TTAB (Sigma) and DTAB (99% pure Sigma) were initially used without further purification.

6.6.1.1 Tensiometry Results.

The surface tension experiments were recorded according to the method outlined above in section 6.5.2.

Figure 6.13 Surface Tension of CTAB.

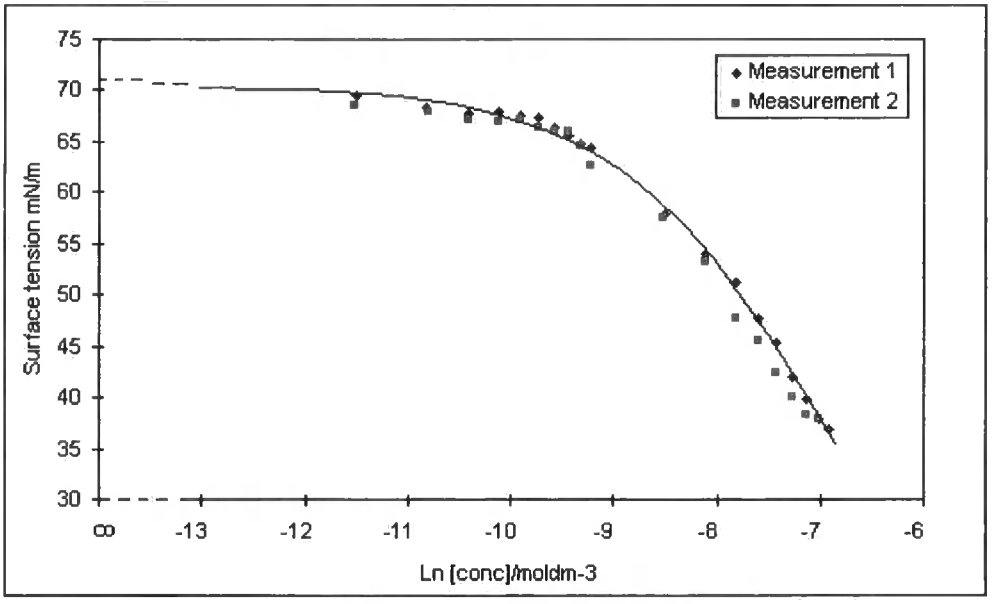

Using equation 6.11 the surface excess concentration for CTAB was calculated. This plot is shown in Figure 6.9 above.

6.6.1.2 Reflectivity Results.

The reflectivity of aqueous solution of ¼ CMC, ½ CMC, CMC and 2 x CMC of CTAB, TTAB and DTAB were studied. Solutions were prepared and placed into the glass container. The reflected light intensity was monitored using the

photodiode system which was fitted with a 100 kΩ terminator resistor for CTAB and DTAB. These are shown in Figure 6.14 below.

Figure 6.14 BAR plot of CTAB.

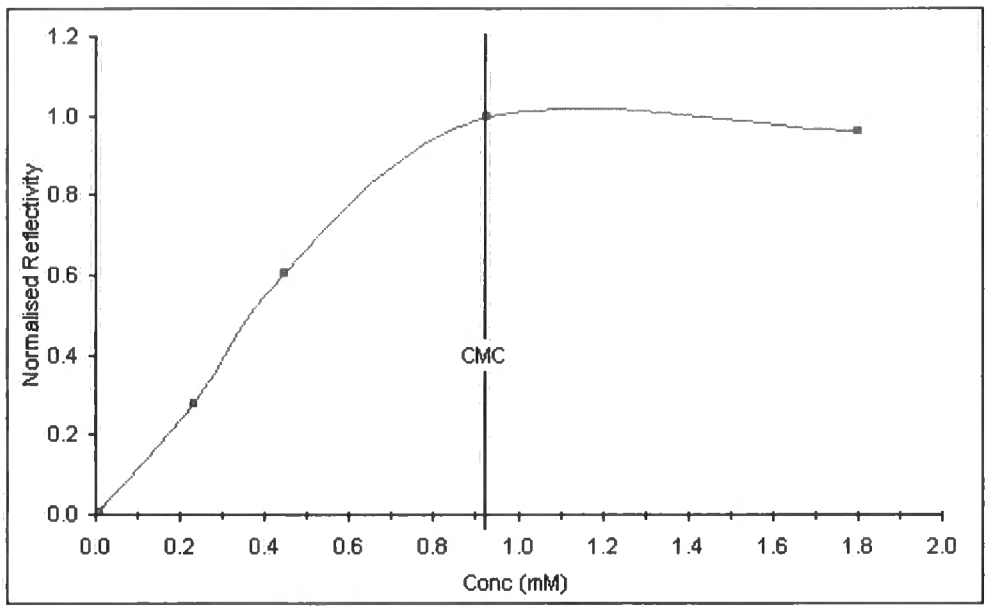

Figure 6.15 BAR plot of DTAB

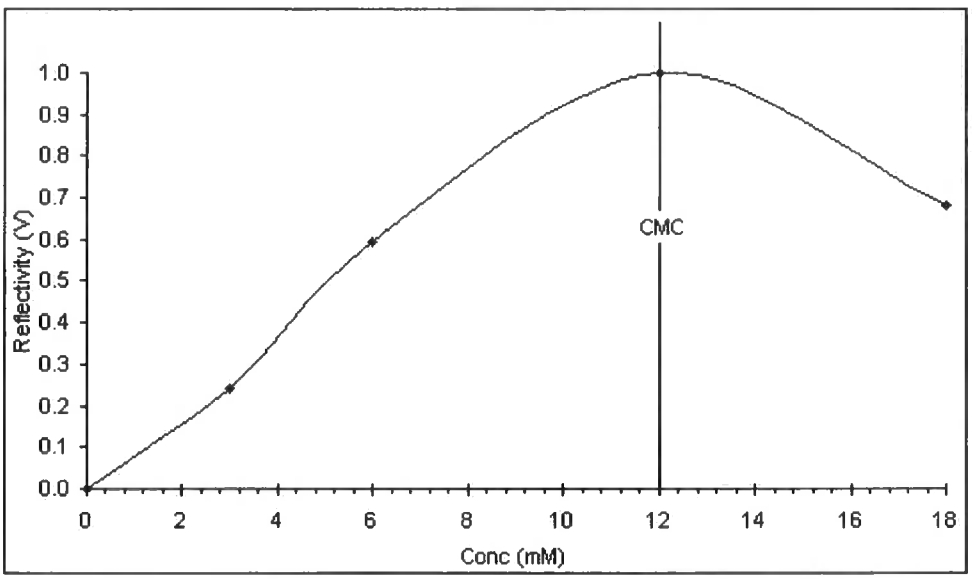

The decrease in the value of the DTAB above the CMC shown in Figure 6.15 above is most likely to be due to impurities. Nilsson recorded a similar shaped curve for the surface excess concentration of sodium dodecylsulphate which he attributed to lauryl alcohol.[51] Lauryl alcohol is surface active and acts as an impurity but after foam fractioning this peak in the plot was eliminated.[52,53]

Unfortunately there was not sufficient time to purify the material and repeat this experiment.

The CTAB results using BAR show a similar trend results of the Thomas group using neutron reflectivity.[7,36] They recorded a significant increase in reflected intensity with increasing surfactant concentration, this directly demonstrates that surface excess concentration increases with increasing concentration.

As mentioned above, initially no change of reflectivity with concentration could be detected for TTAB, this was unexpected as the properties of CTAB, TTAB and DTAB follow a trend and the technique worked for CTAB and DTAB. The initial failure to obtain BAR results with TTAB was put down to impurities such as tetradecyl bromide.[7]

During these experiments the general trend of the reflectivity scans was the same but a large shift in the baseline (the minimum value at the Brewster angle with a water sample) was noted. As discussed above this was found to be due to background scattering and so the glass dish was exchanged for the plastic beaker. The removal of the excess scattering impinging on the detector meant that the intensity of the signal was significantly reduced. The diode was not sensitive enough to detect such small changes in the signal and so it was replaced by the PM tube. An interference filter was attached to the front of the PM tube to reduce the effect of any ambient room light striking the tube, the experiments were performed with the room lights off. Initially a 10 kΩ terminator resistor was attached to the PM tube, this was replaced by a 50 kΩ terminator resistor to increase the sensitivity of the PM tube. Although the larger termination resistor reduces the response time of the detector this was not an issue as the response time of the system was greater than the chopper frequency. A lock-in amplifier was used to record the data and transfer the information to the PC.

The beaker required a relatively large amount of surfactant (~ 400ml). To reduce the amount of surfactant used the beaker was cut in half and the above CTAB

solutions were used to ensure that the background scattering recorded by the PM tube did not increase due to the height reduction.

Using a water sample the signal on the lock-in amplifier was minimised. This was performed by scanning the phase of the lock-in until the signal was at a maximum. The experimental parameters were set, see Table 6.3.

Table 6.3 Experimental conditions for the BAR of TTAB

Parameter	Value
Gain	100μV
Phase	100.2°
Chopper frequency	75 Hz

TTAB was recrystallised using analar acetone, solutions of 1mM, 2 mM, 3 mM, 4 mM were prepared and the BAR plot was recorded. Initial results indicated that the solution was sufficiently purified and so solutions of 0.5 mM, 1.5 mM, 2.5 mM, 3.5 mM were also prepared. The resulting plot with all the concentrations is shown in Figure 6.16 below:

Figure 6.16 BAR plot of TTAB.

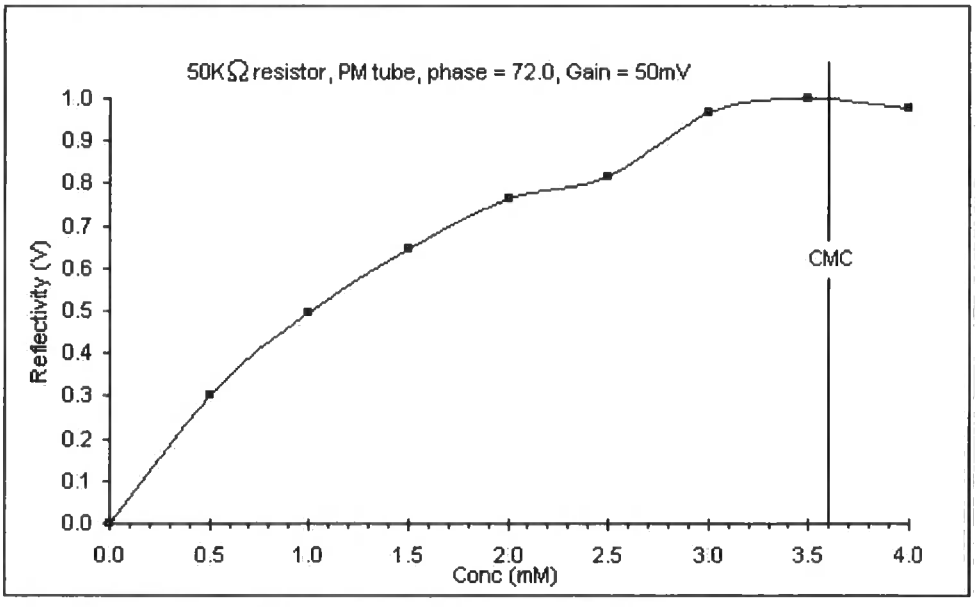

Figure 6.17 below shows a comparison between the Du Noüy ring and BAR results. Such a plot can be used to calibrate the BAR technique allowing the surface excess concentration to be measured using BAR. This in turn would allow dynamic systems to be investigated using BAR.

Figure 6.17 Comparing Ring and BAR Methods for CTAB

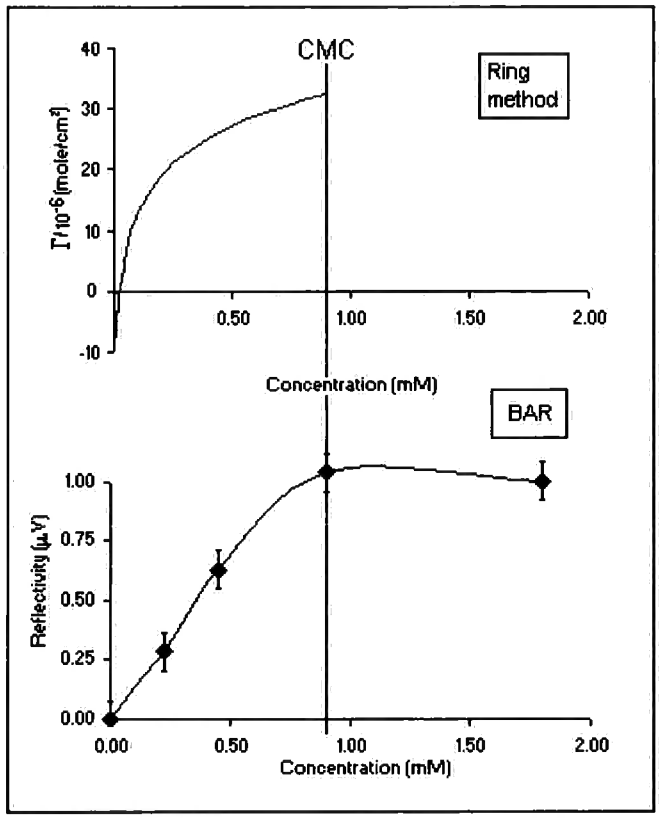

Once the CMC of the trimethylammonium bromides could be consistently determined by the BAR other surfactants were tested.

6.6.1.3 Sodium Dodecylbenzenesulfonate

Literature values for the CMC of sodium dodecylbenzenesulfonate (NaDBS) give a range of 1.2 - 2.1 mM using the conductivity method.[54] The CMC of NaDBS (Aldrich) was recorded to be 0.55 mM in our lab using UV spectroscopy (methyl orange). Samples of ¼ CMC (0.3 mM), ½ CMC (0.6 mM), CMC (1.2 mM) and 2 x

CMC (2.4 mM) were used as an initial test. The parameters used are shown in Table 6.4.

Table 6.4 Experimental conditions for the BAR of SDS.

Parameter	Value
Gain	100μV
Phase	82.5°
Chopper frequency	66 Hz

For each concentration a reflectivity scan was recorded, this was over 0.8 in steps of 0.05. Fifty points were taken an averaged at each point and 4 reflectivity scans were taken at each concentration value. The scans were then converted to a BAR plot, see Figure 6.18. The CMC is determined by a change in gradient of the BAR plot, above the CMC is plot is observed to plateau. In the plot below (Figure 6.18) the CMC is determined to be between 0.4 and 0.5 mM.

Figure 6.18 BAR Plot of NaDBS

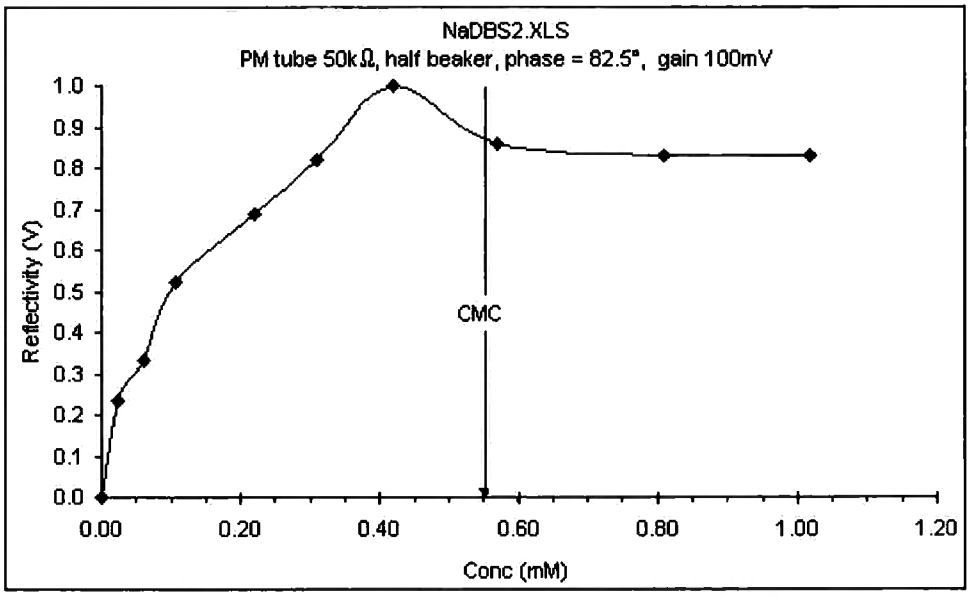

The CMC measured by the reflectivity method is consistent with the value measured by the dye method (0.55 mM). The values of the CMC and above were found to decrease. Similar results were observed with the DTAB reflectivity plot, again this lowering is thought to be due to surface active impurities which are taken into the micelles above the CMC. A simple purification method was not found and lack of time prohibited any further investigation.

6.7 CONCLUSIONS

The new technique of Brewster Angle Reflectivity developed in this work offers a simple non-invasive, non-perturbing method of determining the CMC of surfactant solutions. BAR may then be used to measure the surface excess of a surfactant solution if suitably calibrated. It is postulated that this technique would work on flowing solutions if the flow was sufficiently laminar and the scattering at a minimum. The BAR experimental set-up is similar to that of ellipsometry, however ellipsometry measurements require detailed calculations of the reflected signal. The sensitivity has shown to decrease near to the CMC[9] whereas BAR is particularly sensitive to the surface concentration in the region of the CMC.

---

1. Prud'homme, R. K. and Khan, S. A. Ed. *Foams, Theory, Measurement and Applications.* Surfactants Science Series **57**. Marcel Dekker, N. Y. (1996).
2. Cutler, W.G. and Davis, R. C. Ed. *Detergency and Test Methods, part II.* Surfactants Science Series **5**. Marcel Dekker, N. Y. (1975).
3. Morrow, N. R. *Interfacial Phenomena in Petroleum Recovery.* Surfactants Science Series **36**. Marcel Dekker, N. Y. (1991).
4. Adamson, A. W. and Gast, A. P. *Physical Chemsitry of Surfaces*, 6th edit. John Wiley & Sons. USA. (1997).
5. Lipp, M. M., Lee, K. Y. C., Zasadzinski, J. A. and Waring A. J. *Chemtech*, **27**, 42 (1997).

6. Kurnaz, M. L. and Schwartz, D. K. *Phys. Rev. E.* **56**, 3378 (1997).
7. Simister, E., Thomas, R. K., Penfold, J., Aveyard, R., Binks, B. P., Fletcher, P. D. I., Lu, J. R. and Sokolowski , A. *J. Phys. Chem.* **96**, 1383 (1992).
8. Penfold, J., Richardson, R, M., Zarbakhsh, A., Webster, J. R. P., Bucknall, D. G., Rennie, A. R., Jones, R. A. L., Cosgrove, T., Thomas, R. K., Higgins, J. S., Fletcher, P. D. I., Dickinson, E., Roser, S. J., McLure, I. A., Hillman, A. R., Richards, R. W., Staples E. J., Burgess, A. N., Simister, E. and White, J. W. *J. Chem. Soc., Faraday Trans.* **93,** 1 (1997).
9. Manning-Benson, S., Bain, C. D. and Parker, S. R. W. *J. Colloid Interface Sci.* **189**, 109 (1997).
10. Manning-Benson, S., Parker, S. R. W. and Bain C. D. *Langmuir* **14**, 990 (1998).
    McBain, J. W. *Trans. Faraday Soc.* **9**, 99 (1913).
11. Adamson, A. W. *Physical Chemistry of Surfaces.* 5th Edition, John Wiley & Sons. USA. (1990).
12. Hartley, C. S. *Aqueous Solutions of Paraffin Chains Salts,* Hermann and Cie, Paris. (1936).
13. Shaw, D. J. *Colloid and Interface Science.* 4th edition. Butterworth Heinemann. (1996).
14. Debye, P. *J. Phys. Colloid Chem.* **51**, 18 (1947).
15. Heimenz, P. C. and Rajagopalan, R. *Principles of Colloid and Surface Chemistry.* 3rd edition. Marcel Dekker Inc., New York. (1997).
16. Hunter, R. J. Foundations of Colloid and Interface Science, Volume 1. Oxford University Press, UK (1992).
17. *Surfactant Dictionary and Encyclopedia.* Lomax, E. Ed. Specitality Training Limited, Warwickshire, UK. (1992).
18. Porter, M. R. *Handbook of Surfactants.* 2nd edit. Blackie, London. (1994).
19. Fredell, D. L. *Cationic Surfactants, Analytical and Biological Evaluation.* Ed. Cross, J. and Singer, E. J. Marcel Dekker Inc. (1994).
20. Tanford, C. *The Hydrophobic Effect: Formation of Micelles and Biological Membranes.* 2nd edition, John Wiley and Sons, USA (1980).
21. Simister, E. A., Thomas, R. K., Penfold, J., Aveyard, R., Binks, B. P., Cooper, P., Fletcher, P. D. I., Lu, J. R. and Sokolowski, A. *J. Phys. Chem.* **96**, 1383 (1992).

22. Danielli, J. F. and Davson, H. *J. Cell. Comp. Physiol.* **5**, 495 (1934).
23. Birdi, K. S. *Lipid and Bipolymer Monolayers at Liquid Interfaces.* Plenum Press, New York. (1989).
24. Colin and Bangham. *Prog. Respir. Res.* **15**, 188 (1981).
25. Weidemann, G. Vollhardt, D. *Thin Solid Films*, **264**, 94 (1995).
26. Robertson, B. and Halliday, H. L. *Biochemica et Biophysica Acta - Molecular Basis of Disease*, **1408**, 346 (1998).
27. Miller, C. A., Raney, K. H. *Colloid Surfaces A.*, **74**, 169 (1993).
28. Moulik, S. P., Haque, E., Jana, P. K. and Das, A. R. *J. Phys. Chem.* **100**, 701 (1996).
29. Harkins, W. D. and Jordan, H. F. *J. Am. Chem. Soc.* 52, 1751 (1930).
30. Buwalda, R. T., Jonker, J. M. and Engberts, J. B. F. N. *Langmuir*, **15** 1083 (1999).
31. Winnik, F. M., Regismond, S. T. A. *Colloid. Surfaces A.* **118**, 1 (1996).
32. Stubicar, N, Stubicar, M. and Zadro, K. *Colloid. Surfaces A.* **135**, 245 (1998).
33. Ruiz, C. C. *Colloid Surfaces A.* **147**, 349 (1999).
34. Moroi, Y. *Micelles, Theoretical and Applied Aspects.* Plenum Press, New York. (1992).
35. McBain, J. W. and Humphreys, C. W. *J. Phys. Chem.* **36**, 300 (1932).
36. Tajima, K., Muramatsu, M. and Sasaki, T. *Bull. Chem. Soc. Japan* **43**, 1991 (1970).
37. Lu, J. R., Simister, E. A., Thomas, R. K. and Penfold, J. *J. Phys. Chem.* **97**, 13907 (1993).
38. Lu, J. R., Hromadova, M., Simister, E., Thomas, R. K. and Penfold, J. *Physica B* 198, 120 (1994).
39. Griffiths, P. C., Whatton, M. L., Abbott, R. J., Kwan, W., Pitt, A. R., Howe, A. M., King, S. M. and Heenan, R. K. *J. Colloid Interface. Sci.* **215**, 114 (1999).
40. Penfold, J., Staples, E., Thompson, L., Tucker, I., Hines, J., Thomas, R. K., Lu, J. R. and Warren, N. *J. Phys. Chem. B.* **103**, 5204 (1999).
41. Molliet, J. L. and Collie, J. *Surface Activity.* E & F. N. Span Ltd, London (1951).

42. Manning-Benson, S., Bain, C. D. Private communication.
43. Eastoe, J., Dalton, J. S., Rogueda, P. G. A., Crooks, E., Pitt, A. R. and Simister, E. A. *J. Colloid Interface Sci.* **188**, 423 (1997).
44. Eastoe, J., Dalton, J. S., Rogueda, P. G. A. and Griffiths, P. C. *Langmuir*, **14** 979 (1998).
45. Koval'chuk, V. I., Dukhin, S. S., Fainerman, V. B. and Miller, R. *J. Colloid Interface Sci.* **197**, 383 (1998).
46. Bergink-Martins, D. J. M. *Food Colloids and Polymers: Stability and Mechanical Properties.* Dickenson, E. and Walstra, P. Ed. Royal Society of Cambridge, Cambridge. UK (1993).
47. Bain, C. D., Burnett-Hall, G. D. and Montgomerie, R. R. *Nature*, **372**, 414 (1994).
48. Azzam, R. M. A. and Bashara, N. M. *Ellipsometry and Polarised light.* North-Holland, Netherlands. (1977).
49. James, A. M. and Lord, M. P. *Macmillan's Chemical and Physical Data.* Macmillan, London. (1992).
50. Lei, X. G., Tand, X. D., Lie, Y. C. and Turro, N. J. *Langmuir*, **7**, 2872. (1991).
51. Nilsson, G. J. *Phys. Chem.*, **61**, 1135 (1957).
52. Miles, G. D. *J. Phys. Chem.*, **49**, 71 (1945).
53. Brady, A. P. *J. Phys. Colloid Chem.* **52**, 56 (1949).
54. Van Os, N. M., Haak, J. R. and Rupert, L. A. M. *Physiochemical Properties of Selected Anionic, Cationic and Nonionic Surfactants.* Elsevier, N. Y. (1993).

APPENDIX A FALSE COLOURING OF BAM IMAGES.

The intensity of the reflected light from the surface is proportional the film thickness. Therefore qualitative information concerning the film thickness can be ascertained from the intensity range across the image. It is difficult for the human eye to distinguish between greyscale levels so to aid the interpretation of the images a Turbo Pascal 3.0 program was written to convert greyscale images to colour images. The BAM images are saved in the Tiff format. Using Paint Shop Pro these were converted and saved in binary format (portable pixel map (.ppm)). The program reads each pixel and converts it from a greyscale value to a colour value and then re-plots the pixels on the screen.

```
program colourit;
uses Crt, Graph, Dos;
var
  pic, picfile                    : string;
  f                               : text;
  ans, sise                       : char;
  GraphDriver, GraphMode          : integer;
  pix, numo, scrsize              : integer;
  x, y, wide, col, ints           : integer;
  Color                           : word;
  Palette                         : PaletteType;

begin
 repeat
 GraphDriver := Detect;
 InitGraph(GraphDriver, GraphMode,'');
 Randomize;

  wide  := 0;
  x     := 0;
  y     := 15;
  numo  := 0;
  ints  := 0;
     OutText('What is the name of the file? ');
     Readln(pic);
     picfile := 'C:\temp\' + pic;
     assign(f, picfile);
```

```
  reset(f);
  GetPalette(Palette);

   while (numo <= 1) do
   begin
      Read(f, sise);
      if (sise = 'o') then numo := numo + 1;
   end;

   Read(f, scrsize);

while not eof(f) do
begin
    while wide < scrsize do
      begin
        while (ints < 2) do
          begin
          Read(f, pix);
          ints := ints + 1;
      end;

   Read(f, pix);
     case pix of
        241..256        : col := 15;
        225..240        : col := 4;
        209..224        : col := 12;
        193..208        : col := 5;
        177..192        : col := 13;
        161..176        : col := 14;
        145..160        : col := 2;
        129..144        : col := 10;
        113..128        : col := 3;
        97..112         : col := 11;
        81..96          : col := 1;
        65..80          : col := 9;
        49..64          : col := 6;
        33..48          : col := 8;
        17..32          : col := 7;
        0..16           : col := 0;
     end;
    ints := 0;
    PutPixel(x, y, col);
```

```
        x := x + 1;
        wide := wide + 1;
       end;
    y    := y+1;
    wide := 0;
    x    := 0;
    end;

    outtextXY(400, 0, 'Again? ');

    readln(ans);
   until(ans = 'n');
   close(f);
end.
```

APPENDIX B AUTOMATION OF THE REFLECTIVITY EXPERIMENT

This program was used to run the Brewster Angle Reflectivity experiments and to move the laser and/or the detector. For each surfactant sample the laser and detector scan a small range of angles and the intensity of the reflected signal is recorded via a lock-in amplifier to the PC.

```
DECLARE SUB movit1 ()
CLS
COLOR 13, 0, 6
PRINT "                Welcome to WigTech"
PRINT "             Please press space to start"
DO
LOOP UNTIL INKEY$ = " "

OPEN "COM1:2400,N,8,1,CS,DS,CD" FOR RANDOM AS #1
OPEN "COM2:9600,N,8,2,CS,DS,CD" FOR RANDOM AS #3

 PRINT #3, "   "
 PRINT #3, "Z"
 FOR I = 1 TO 9000: NEXT I
 PRINT #3, "G 12"
 FOR I = 1 TO 9000: NEXT I
 PRINT #3, "P 71.3"

ans$ = "y"
DO WHILE LCASE$(ans$) = "y"

 INPUT "Run progam or move stages? R or M "; exp$
 IF LCASE$(exp$) = "m" THEN GOTO subroot
 INPUT "What filename"; name$
 file$ = "C:\scattie\expdat\" + name$
 OPEN file$ FOR OUTPUT AS #2

 INPUT "How many degrees to rotate"; deg$
   DO WHILE VAL(deg$) <= 0
    PRINT "Invalid input"
    GOTO redoit
```

```
   LOOP

INPUT "What step size (in degrees)"; step$
nos = VAL(deg$) / VAL(step$)
angle = 4000 * (VAL(step$))
INPUT "Up (u) or down (d) "; way$
IF LCASE$(way$) = "u" THEN a = -angle ELSE a = angle

num = 0
DO WHILE num <= nos
 total = 0

   FOR X% = 1 TO 50
     PRINT #3, "Q"
     INPUT #3, v1
     total = total + v1
   NEXT X%

   PRINT #2, (total * 1) / 50
   PRINT "Average value ="; ((total * 1) / 50)

   IF num < nos THEN PRINT #1, "*1mr" + LTRIM$(STR$(a)); ",2mr" + LTRIM$(STR$(a))
   FOR b = 1 TO 159999 * VAL(deg$): NEXT b

   num = num + 1
 LOOP

CLOSE #2

redoit: INPUT "Again y or n"; ans$
LOOP
GOTO last
subroot: movit1
GOTO redoit
last: END
END

SUB movit1
INPUT "Both (b), Laser (l), diode (d)"; equip$
INPUT "How many degrees to rotate"; rot$
angle = 4000 * (VAL(rot$))
```

```
INPUT "Up (u) or down (d)"; dir$
IF LCASE$(dir$) = "u" THEN c = -1 ELSE c = 1

SELECT CASE LCASE$(equip$)

 CASE "b"
 PRINT #1, "*1mr" + LTRIM$(STR$(c * angle)); ",2mr" + LTRIM$(STR$(c * angle))
 CASE "l"
 PRINT #1, "*2mr" + LTRIM$(STR$(c * angle))
 CASE "d"
 PRINT #1, "*1mr" + LTRIM$(STR$(c * angle))

END SELECT
END SUB
```

UNIVERSITY OF DURHAM

Board of Studies in Chemistry

POST GRADUATE COLLOQUIA, LECTURES AND SEMINARS FROM INVITED SPEAKERS

1995 - 1996

Prof. P. Lugar, Frei Univ Berlin, FRG.
Low Temperature Crystallography.

Dr. D. M. Davies, University of Northumbria.
Chemical reactions in organised systems.

Prof. Brian Robinson UEA, Norwich.
New Reactions for Organic Synthesis.

Prof. I Soutar, Lancaster University.
A Water of Glass? Luminescence Studies of Water-Soluble Polymers.

ProfJ. Saykally, Univeristy of California, Berkley.
Terahertz Laser Spectroscopy of water clusters; towards a genuine molecular model of liquids.

Prof. J. W. Emsley , Southampton University.
Liquid Crystals: More than Meets the Eye.

Dr J. Penfold, Rutherford Appleton Laboratory.
Soft Soap and Surfaces.

Prof. E. W. Randall, Queen Mary & Westfield College.

New Perspectives in NMR Imaging

Dr. Garry Rumbles, Imperial College London.

Laser Cooling in the Condensed Phase: the tale of a novel observation.

Prof. R. J. Donovan, University of Edinburgh.
Laser ionisation, from fundamentals to wealth creation.

1996 - 1997

Professor B. J. Tighe, Department of Molecular Sciences and Chemistry, University of Aston.
Making Polymers for Biomedical Application - can we meet Nature's Challenge?

Professor H. Ringsdorf (Perkin Centenary Lecture), Johannes Gutenberg-Universitat, Mainz, Germany.
Function Based on Organisation.

Professor D. M. Knight, Department of Philosophy, University of Durham.
The Purpose of Experiment - A Look at Davy and Faraday.

Prof. G. Olah, Loker Hydrocarbon Research, USA.
Crossing conventional Lines in my Chemistry of the Elements.

Professor J. Earnshaw, Deptartment of Physics, Belfast.
Surface Light Scattering: Ripples and Relaxation.

Dr Richard Templer, Imperial College, London.
Molecular Tubes and Sponges

Professor David Phillips, Imperial College, London.
A Little Light Relief.

Professor K. Muller-Dethlefs, York University
Chemical Applications of Very High Resolution ZEKE Photoelectron Spectroscopy.

Dr Julian Clarke, UMIST

What can we learn about polymers and biopolymers from computer-generated nanosecond movie-clips?

Prof. Sir James Black, Imperial College, London.
What I learned as a Medicinal Chemist.

Professor Brian Hayden, University of Southampton
The Dynamics of Dissociation at Surfaces and Fuel Cell Catalysts

Dr J. Staunton FRS, Cambridge University
Tinkering with biosynthesis: towards a new generation of antibiotics

Prof. J. Reihl, Michigan Technology University, USA.
The Enantioselectivity of Lanthanides.

Dr A. D. Taylor, ISIS Facility, Rutherford Appleton Laboratory
Expanding the Frontiers of Neutron Scattering

Dr Katharine Reid, University of Nottingham
Probing Dynamical Processes with Photoelectrons

Prof. M. Harrington, Caltech, USA.
Polymers both enable and limit the discovery of protein alterations in studies ranging from gene regulation to mad cow disease.

Prof. R.H. Grubbs., Caltech, USA.
Olefin Metathesis using Ruthenium Based Complexes.

Prof. Hyuk Yu. University of Wisconsin-Madison
Dynamics of Macromolecular Monolayers.

1997 - 1998

Prof. A P de Silva, The Queen's University, Belfast

Luminescent Signalling Systems.

Prof. Vernon Gibson, Imperial College, London.
Metallocene Polymerisation.

Dr Jeremy Frey, Department of Chemistry, Southampton University.
Spectroscopy of Liquid Interfaces: from bio-organic chemistry to atmospheric chemistry.

Prof. Randall W. Richards, University of Durham, Inaugural Lecture.
A Random Walk in Polymer Science.

Prof. David Andrews, University of East Anglia.
Energy Transfer and Optical Harmonics in Molecular Systems.

Prof. David Cardin, University of Reading.
Aspects of Metal and Carbon Cluster Chemistry.

Dr Steve Rannard, Courtaulds Coatings (Coventry).
The Synthesis of Dendrimers using Highly Selective Chemical Reactions.

Prof. P. Fowler, Department of Chemistry, Exeter University.
Classical and Non-classical Fullerenes.

Prof. Gus Hancock, University Oxford.
Surprises in the Photochemistry of Tropospheric Ozone.

Prof. R. Denning, University of Oxford.
The Design and Evaluation of 2nd Order Non-Linear Optic Materials.

Dr John Evans, Oxford University.
Materials which contract on heating (from shrinking ceramics to bullet proof vests.

Prof. George Wilson, University of Kansas.

The Applications of Microbiosensors to Continuous in-vivo Monitoring.

Prof. D. Batchelder, University of Leeds.
Raman Microscopy of Molecular Materials: confocal, direct imaging and scanning near field.

CONFERENCES ATTENDED.

North East Graduate Colloquia. University of Sunderland. 1996

European Conference on Organised Films (ECOF). Sheffield University, September, 1996.

Langmuir-Blodgett 8. Asilomar, California, August 1997. Poster Presentation:
Observation of Complex Formation at the Air/Water Interface by Brewster Angle Microscopy. A. J. Wigman and A. Beeby.